NASA CR-166649

DEVELOPMENT OF THE COASTAL ZONE COLOR SCANNER FOR NIMBUS 7

VOLUME 2 - Test and Performance Data

Ball Aerospace Systems Division
P. O. Box 1062
Boulder, CO 80306

May, 1979

FINAL REPORT F78-11, Rev. A

Prepared For

NATIONAL AERONAUTICS AND SPACE ADMINISTRATION
Goddard Space Flight Center
Greenbelt, Maryland 29771

Rev. A

TECHNICAL REPORT STANDARD TITLE PAGE

1. Report No.	2. Government Accession No.	3. Recipient's Catalog No.
F78-11		

4. Title and Subtitle	5. Report Date
Development of the Coastal Zone Color Scanner for NIMBUS 7 Volume 2 - Test and Performance Data	May, 1979
	6. Performing Organization Code
7. Author(s)	8. Performing Organization Report No.
9. Performing Organization Name and Address Ball Aerospace Systems Division P.O. Box 1062 Boulder, CO 80306	10. Work Unit No.
	11. Contract or Grant No. NAS5-20900
12. Sponsoring Agency Name and Address National Aeronautics and Space Administration Goddard Space Flight Center Greenbelt, Maryland 20771	13. Type of Report and Period Covered Type III Final Report
	14. Sponsoring Agency Code

15. Supplementary Notes

16. Abstract

This is the second of two volumes reporting on the development of the Coastal Zone Color Scanner for NIMBUS 7. This volume covers test results on the proto-flight unit, analysis of these test results and in-orbit performance data.

17. Key Words (Selected by Author(s))	18. Distribution Statement
Tests, Spectral Response, Signal to Noise, radiance, MTF, Co-registration, Field-of-view	

19. Security Classif. (of this report)	20. Security Classif.	21. No. of Pages	22. Price*

*For sale by the Clearinghouse for Federal Scientific and Technical Information, Springfield, Virginia 22151

PREFACE

The Coastal Zone Color Scanner (CZCS) is a 6-channel earth scanning radiometer for the measurement from orbit of chlorophyll and sediment in coastal waters. It was successfully launched on the NIMBUS 7 spacecraft in October 1978. This Volume 2 of the Final Report covers the results of the prelaunch tests performed on the Protoflight Model and its performance in space.

TABLE OF CONTENTS

LIST OF ILLUSTRATIONS

TABLE OF CONTENTS (Continued)

TABLE OF CONTENTS (Continued)

Section 1
INTRODUCTION

This is Volume 2 of the Final Report for the Coastal Zone Color Scanner (CZCS), the first satellite-based remote sensing system for the measurement of water color. This report covers the period from the start of the hardware development in January, 1975 through the successful launch of NIMBUS 7 in October, 1978. It covers the design, assembly and test of the CZCS Protoflight Model. The development of this model included design, breadboard and engineering model phases which led up to the assembly and test of the Protoflight Model. The results of the previous phases of work are reflected in the design and test results included in this report.

Volume 1 of this final report covers the following topics:

- A brief description of the CZCS mission objectives and an overview of the instrument developed to meet the mission objectives. This section is less technical in nature than the remaining sections.
- Important system design features are described.
- Design details and test results for each subsystem are covered.
- Appendix A presents additional science background related to the mission objectives.

Volume 2 of this Final Report covers the following topics:

- Prelaunch test results
- In-orbit performance data

Section 2
PRELAUNCH TEST RESULTS

The CZCS models have undergone extensive testing prior to delivery. The purposes of these tests are to verify that specified requirements are met and to obtain repetitive test data on various instrument parameters. All delivered CZCS instruments have had more than 300 hours of test time. The repetitive test data is used to establish performance trends which could indicate a deteriorating situation. The results of the CZCS Protoflight tests are examined with detail in Section 2.1 while some of the test results are evaluated with respect to expected performance in Section 2.2.

2.1 PROTOFLIGHT TESTS

The sequence and type of Protoflight tests are illustrated by Figure 2-1. At the system level, there are two types of performance tests in addition to the environmental tests. All of the tests have been performed to well thought out, well reviewed and very explicit procedures. Post Assembly Confidence Tests (PACT) are performed immediately after subsystem integration and alignment to verify instrument performance to specified operational requirements. The Orbital Sequence Tests (OST) are performed repetitively throughout the test sequence to determine performance changes with respect to established baselines. During an OST, the instrument is operated by command in a sequence identical to that to be used in orbit. Measurements are made of telemetry outputs, channel radiance and MTF responses, scan drive velocity jitter and electrical gains. The OST's are performed prior to and after EMI, Vibration and Thermal-Vacuum tests and during the Thermal-Vacuum test. Short Orbital Sequence Tests (SOST) are performed when the scanner mechanism launch lock (cage) is activated and the scan cannot be tilted. These are used prior to Thermal-Vacuum and between axes of vibration. After shipment to General Electric, the CZCS Protoflight underwent additional OST sequences as a part of the Bench Acceptance Test (BAT). In all, the Protoflight has experienced 117 Orbital Sequence Tests.

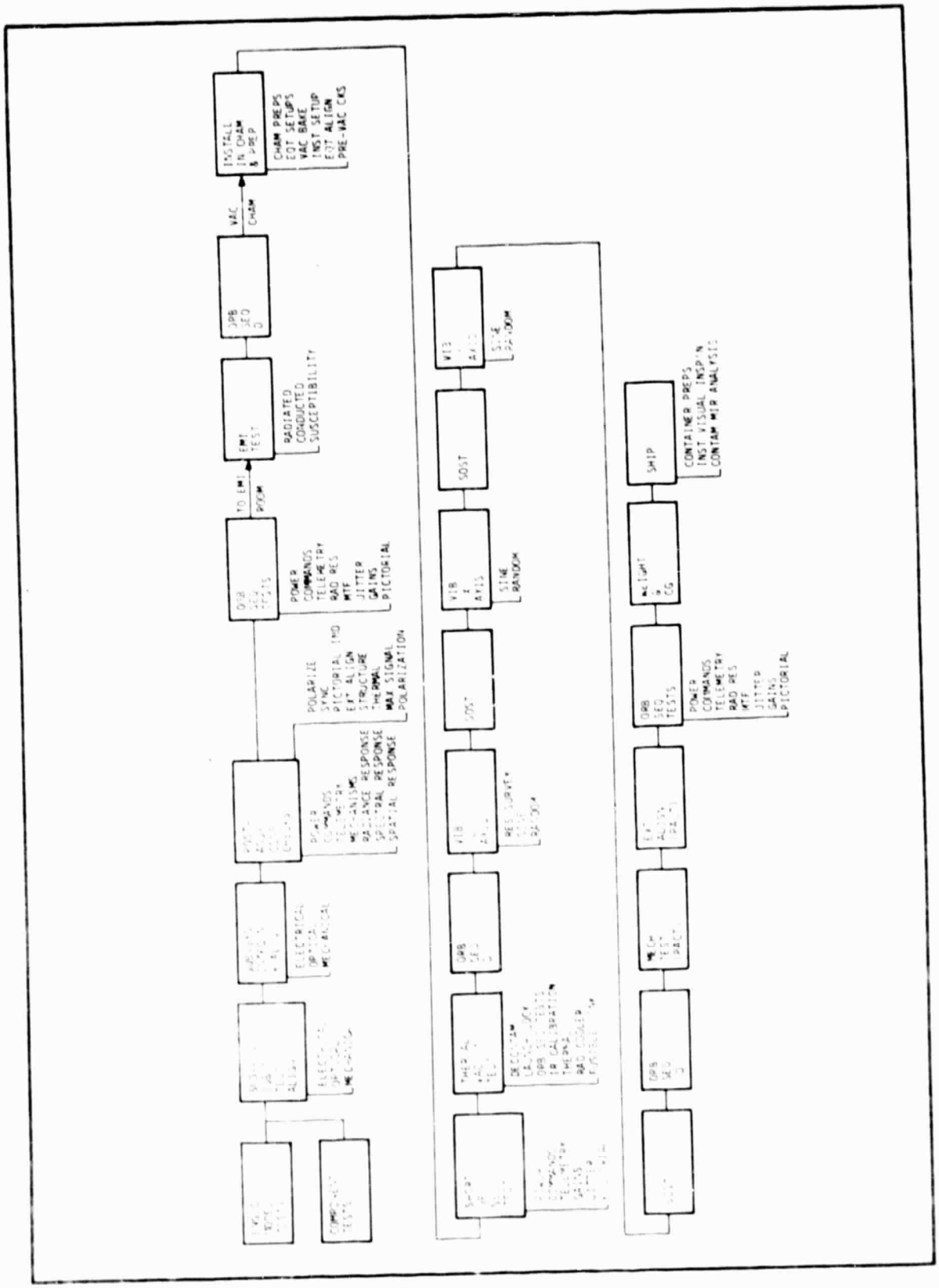

Figure 2-1 PROTOFLIGHT AND FLIGHT MODEL TEST FLOW

2.1.1 Spectral Response

The spectral responses of channels 1 through 5 were run as a part of the Post Assembly Confidence Test (PACT) in March, 1977. The spectral response of channel 6 was measured during April, 1977 as a part of PACT. Due to a noise problem, it was necessary to remove the channel 4 detector/preamplifier/ exit slit assembly and the spectral responses of channels 1-5 were remeasured in May, 1977. A problem with the visible calibration assembly was brought on by vibration tests making it necessary to remove the spectrometer from the optical subsystem for disassembly. Rework of the spectrometer due to the calibration assembly problem was the apparent reason for a shift in the spectral responses of channels 1-4. The spectrometer was readjusted in July, 1977 and the spectral responses remeasured at that time are shown in Figures 2-2 through 2-6. Retest after the subsequent revibration revealed no change as a result of vibration. Figure 2-7 is the spectral response of channel 6 as measured in April, 1977.

2.1.2 Signal to Noise

The signal to noise ratio is measured as a function of radiance input on channels 1 through 5 using a computer routine of the BCU called up by software. The integrating sphere supplied by GSFC is the source or target for those measurements. The BCU computes the average and standard deviation of 100 samples at each radiance level and then computes the ratio of the average to the standard deviation to determine the signal to noise ratio. This is done for each channel. Figures 2-8 through 2-12 are plots of the signal to noise ratios for channels 1-5 as a function of radiance. Each channel exceeds, by a comfortable margin, the specified signal to noise ratio indicated in the figures. These results are from measurements made after readjustments in July, 1977. The readjustments were the result of the spectrometer disassembly discussed in Section 2.1.1. Measurements made after realigning the spectrometer showed increases in the responses of channels 1-3 requiring gain reductions. Indications were that the original alignment was marginal, resulting in the vignetting of energy by the exit slits.

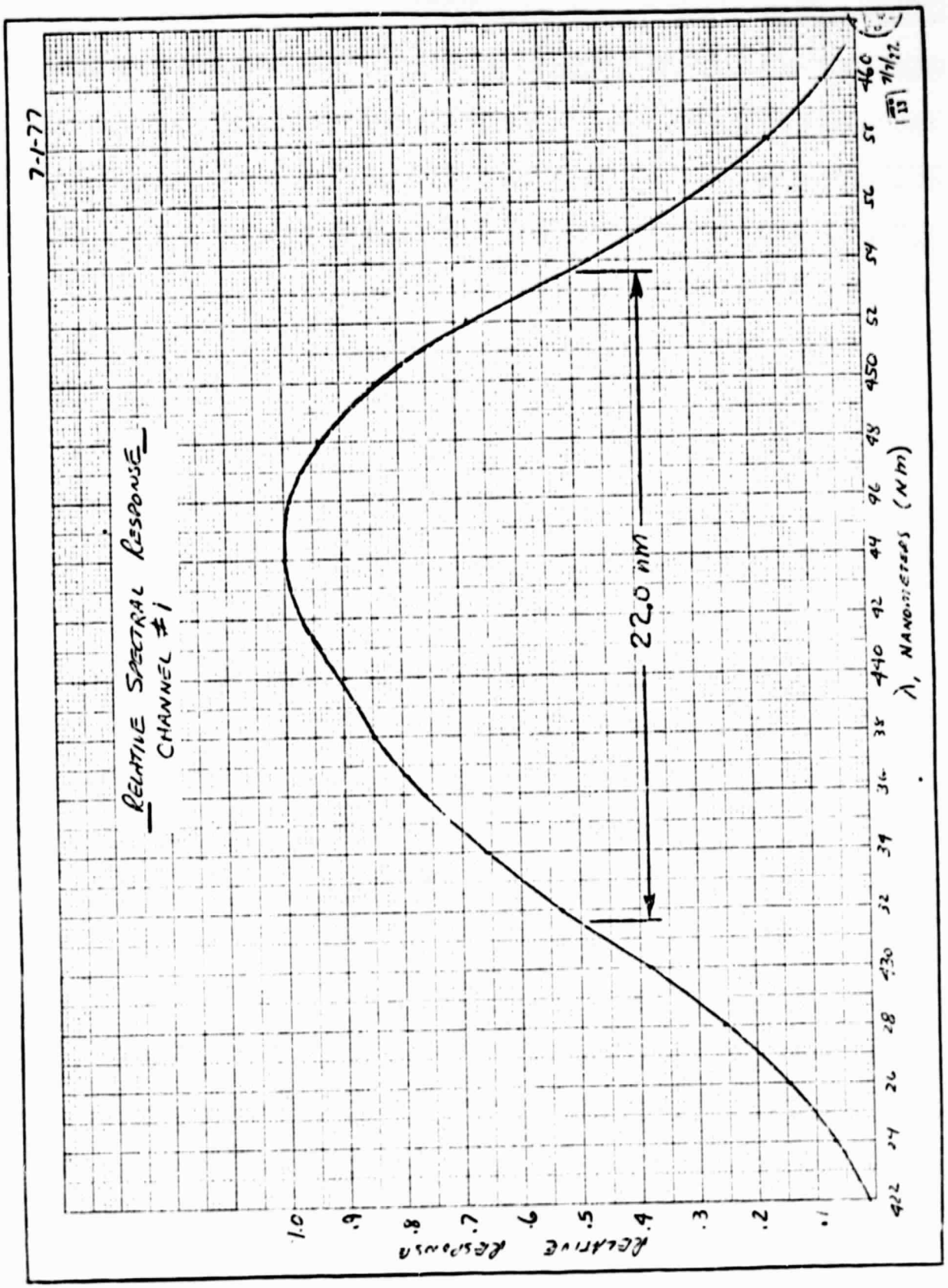

Figure 2-2 RELATIVE SPECTRAL RESPONSE--CHANNEL #1

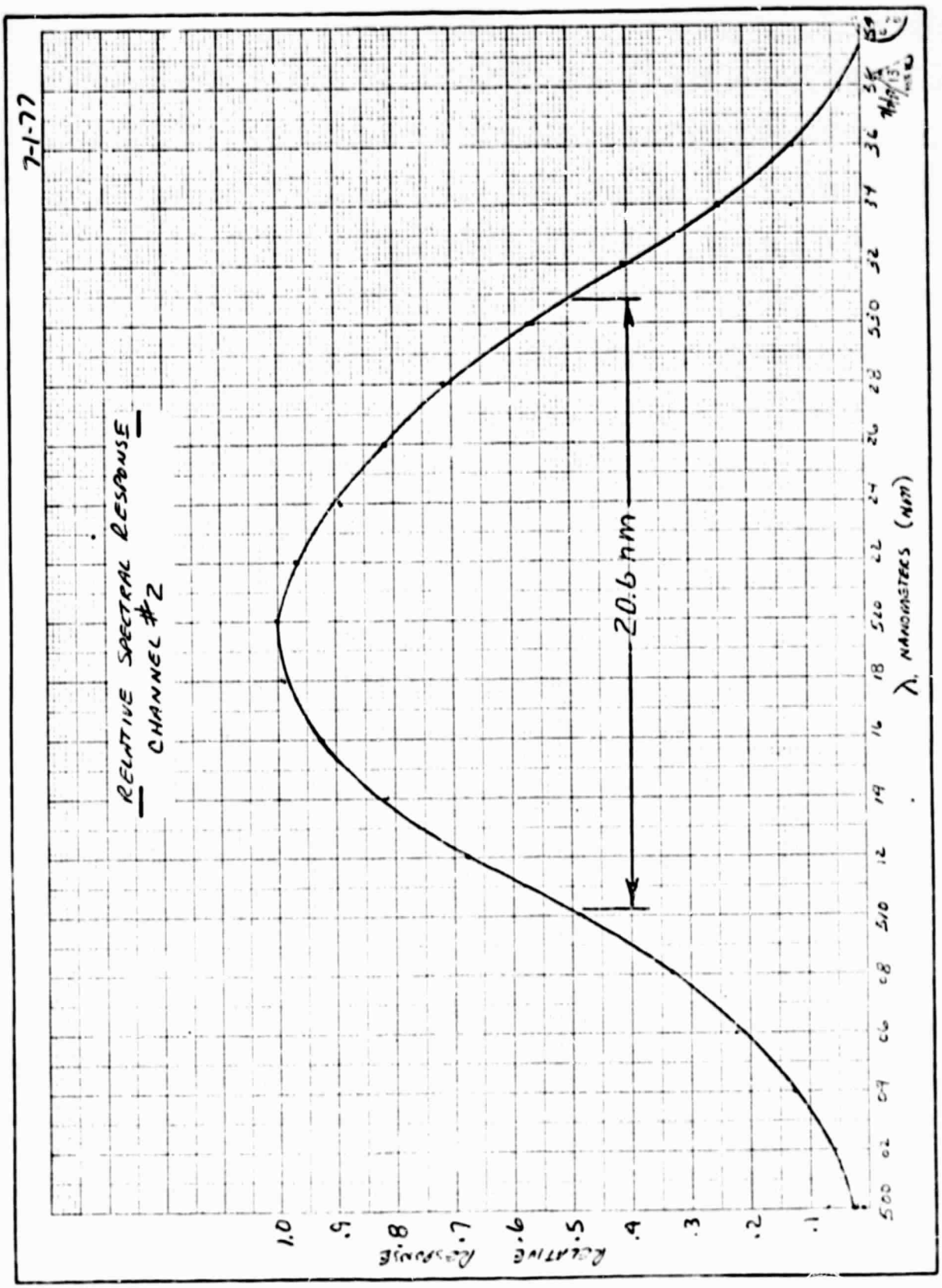

Figure 2-3 RELATIVE SPECTRAL RESPONSE--CHANNEL #2

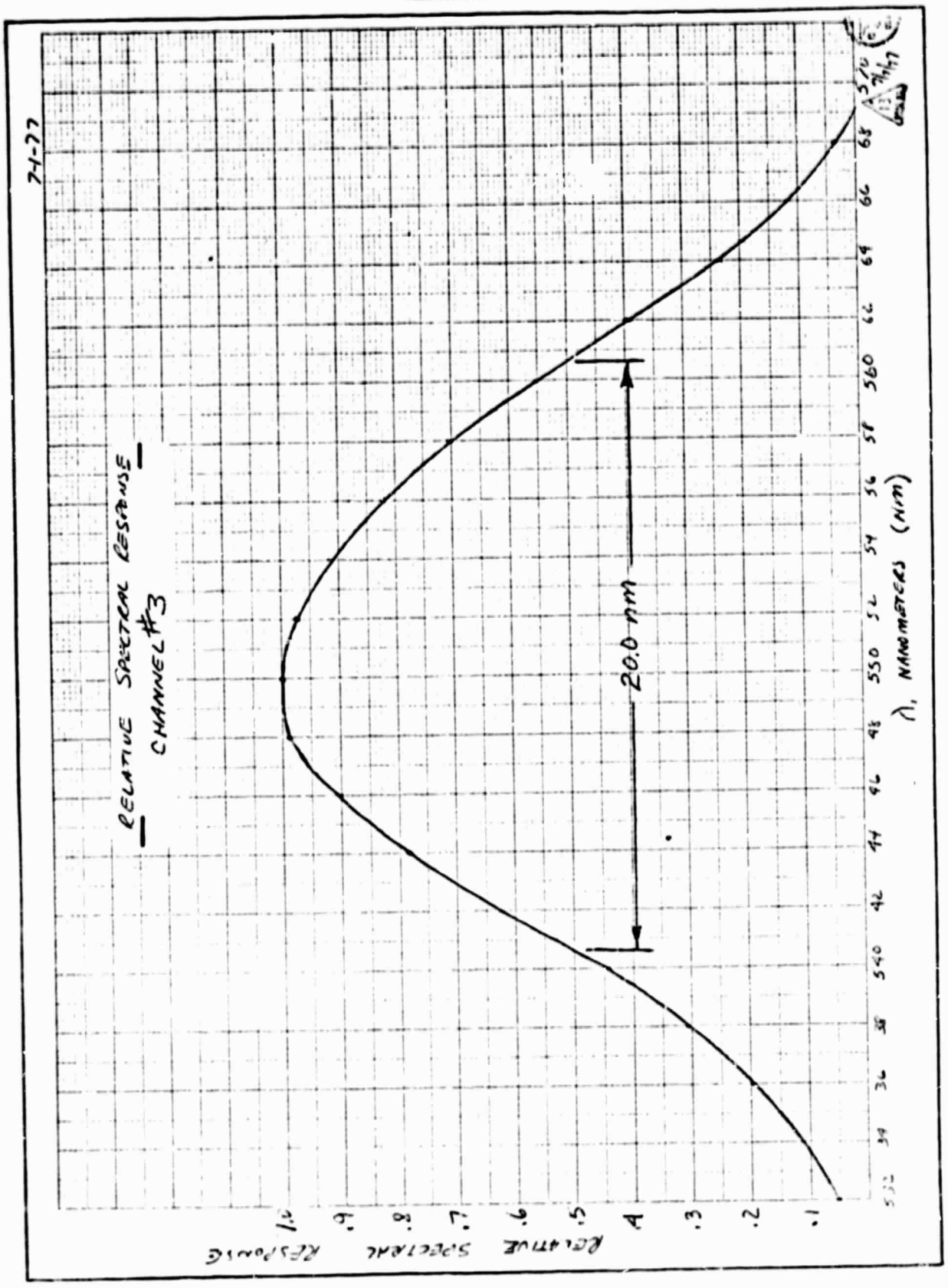

Figure 2-4 RELATIVE SPECTRAL RESPONSE--CHANNEL #3

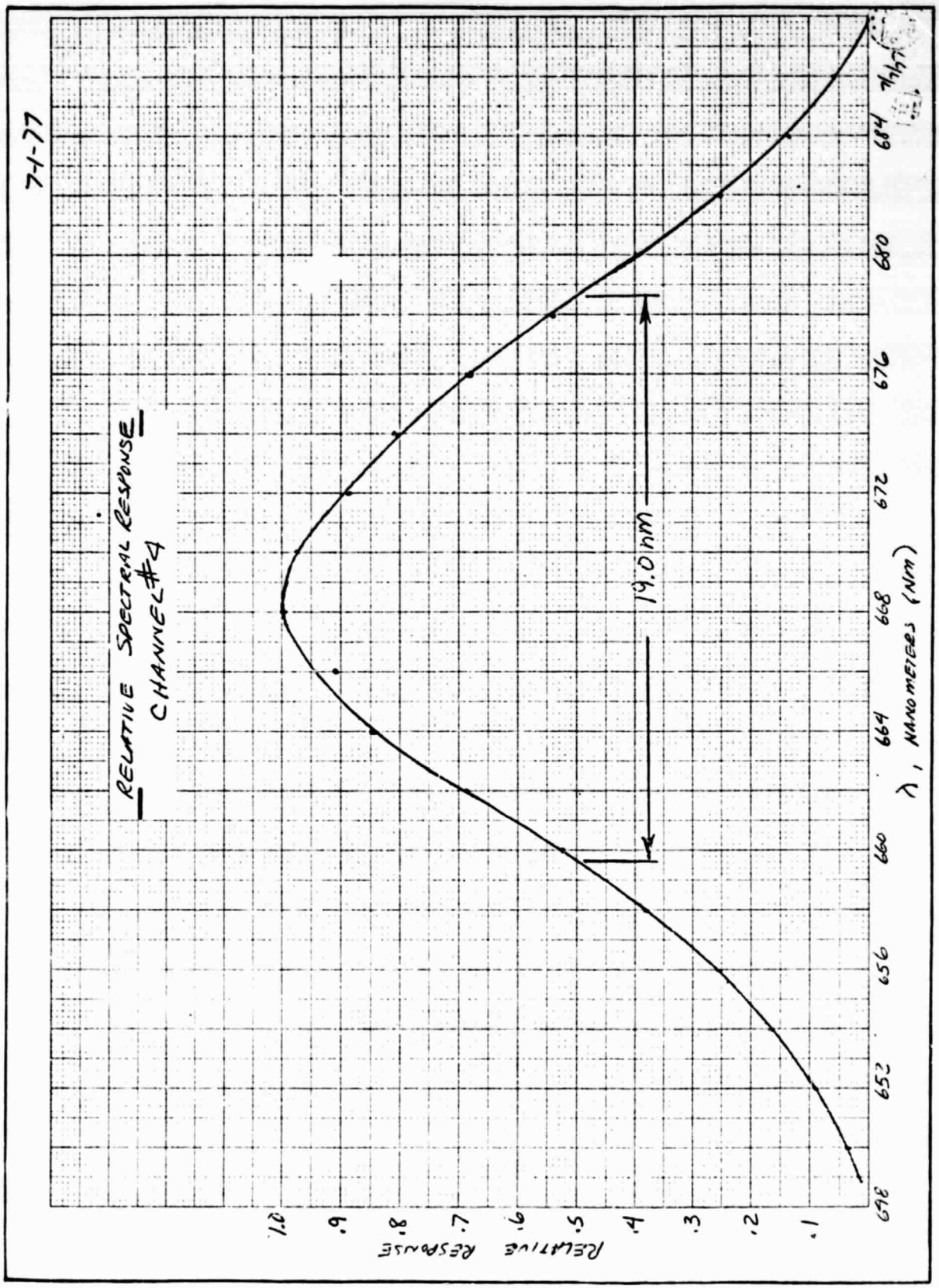

Figure 2-5 RELATIVE SPECTRAL RESPONSE--CHANNEL #4

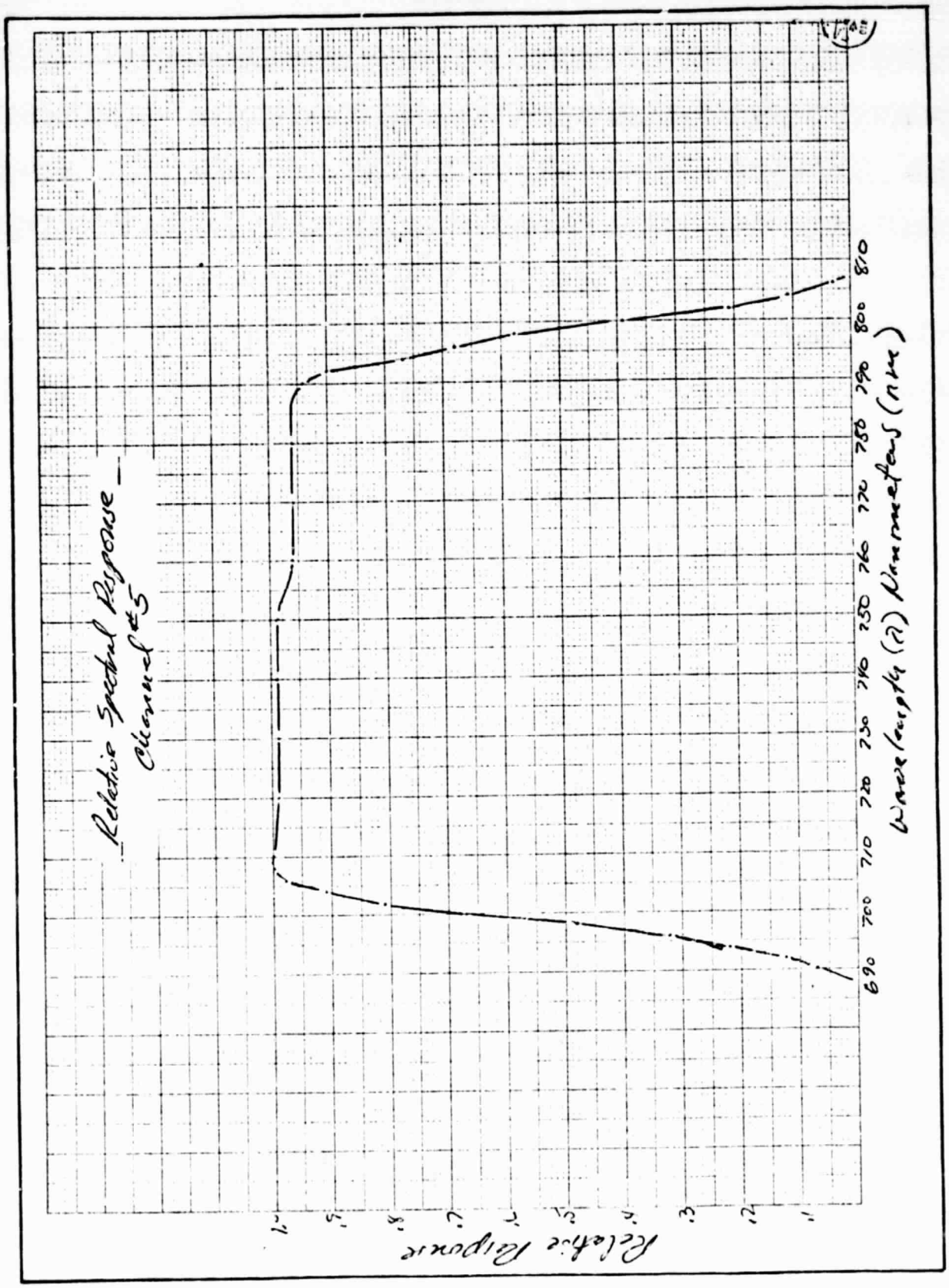

Figure 2-6 RELATIVE SPECTRAL RESPONSE--CHANNEL #5

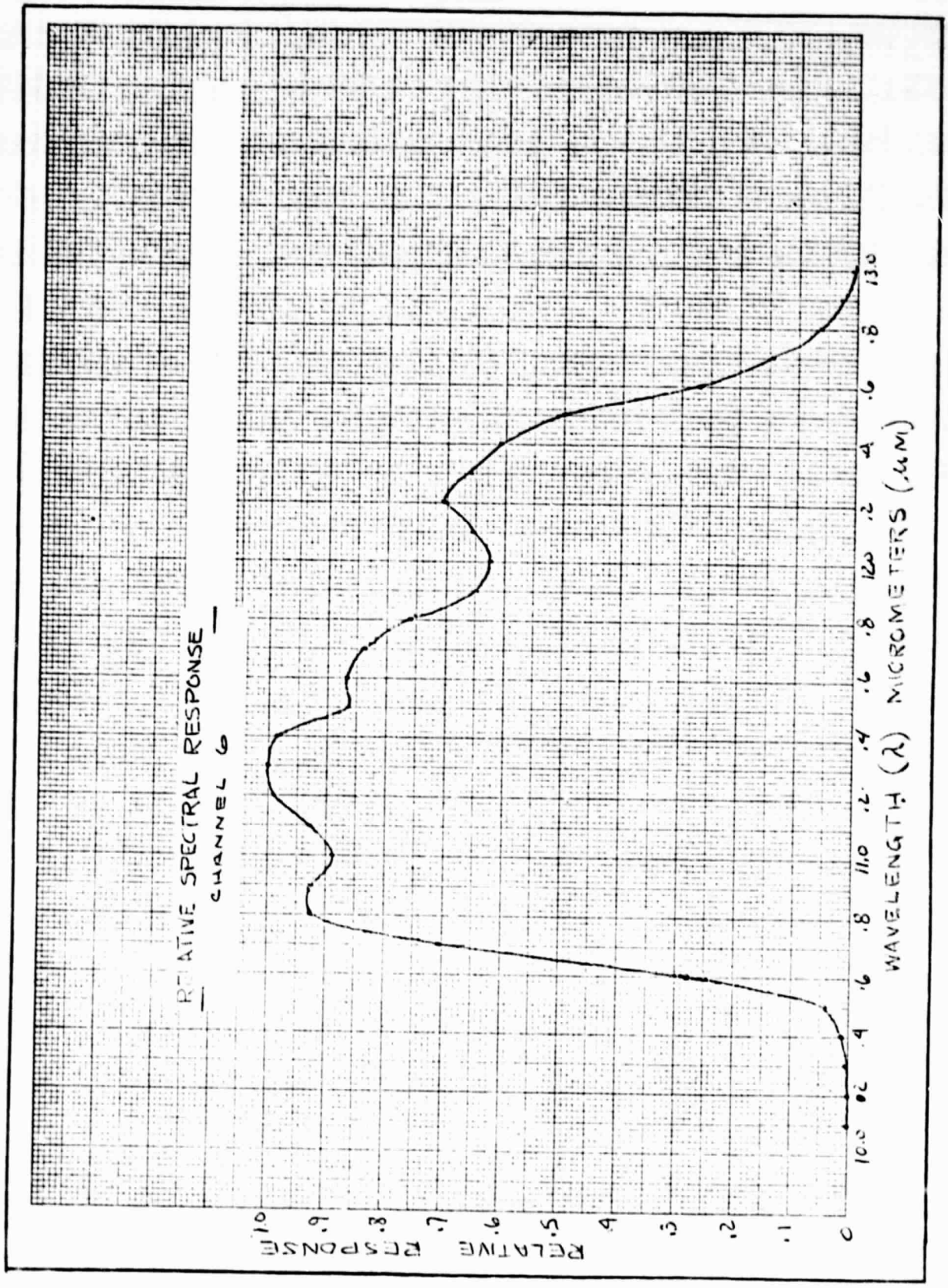

Figure 2-7 RELATIVE SPECTRAL RESPONSE--CHANNEL #6

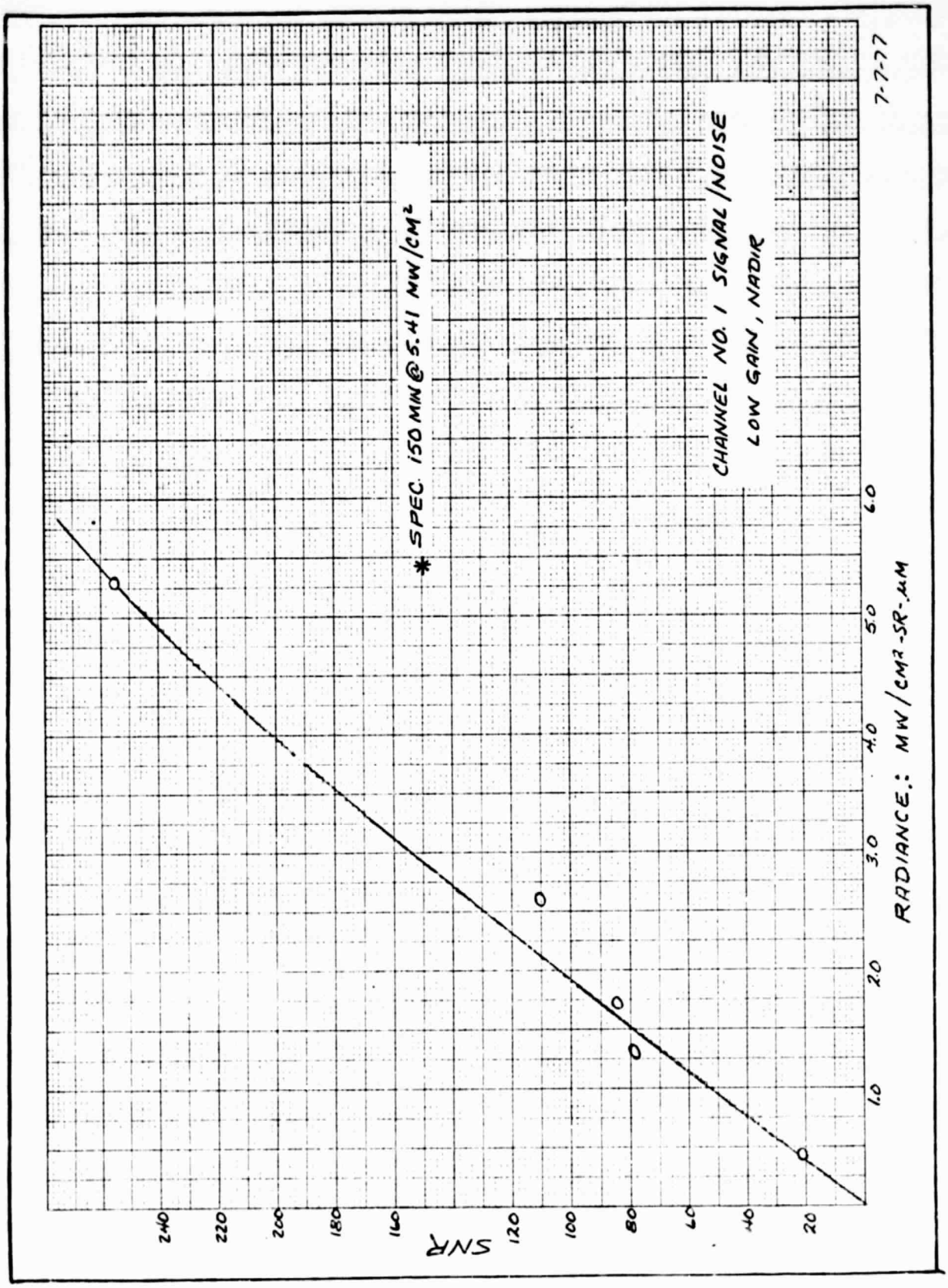

Figure 2-8 CHANNEL NO. 1 SIGNAL/NOISE LOW GAIN, NADIR

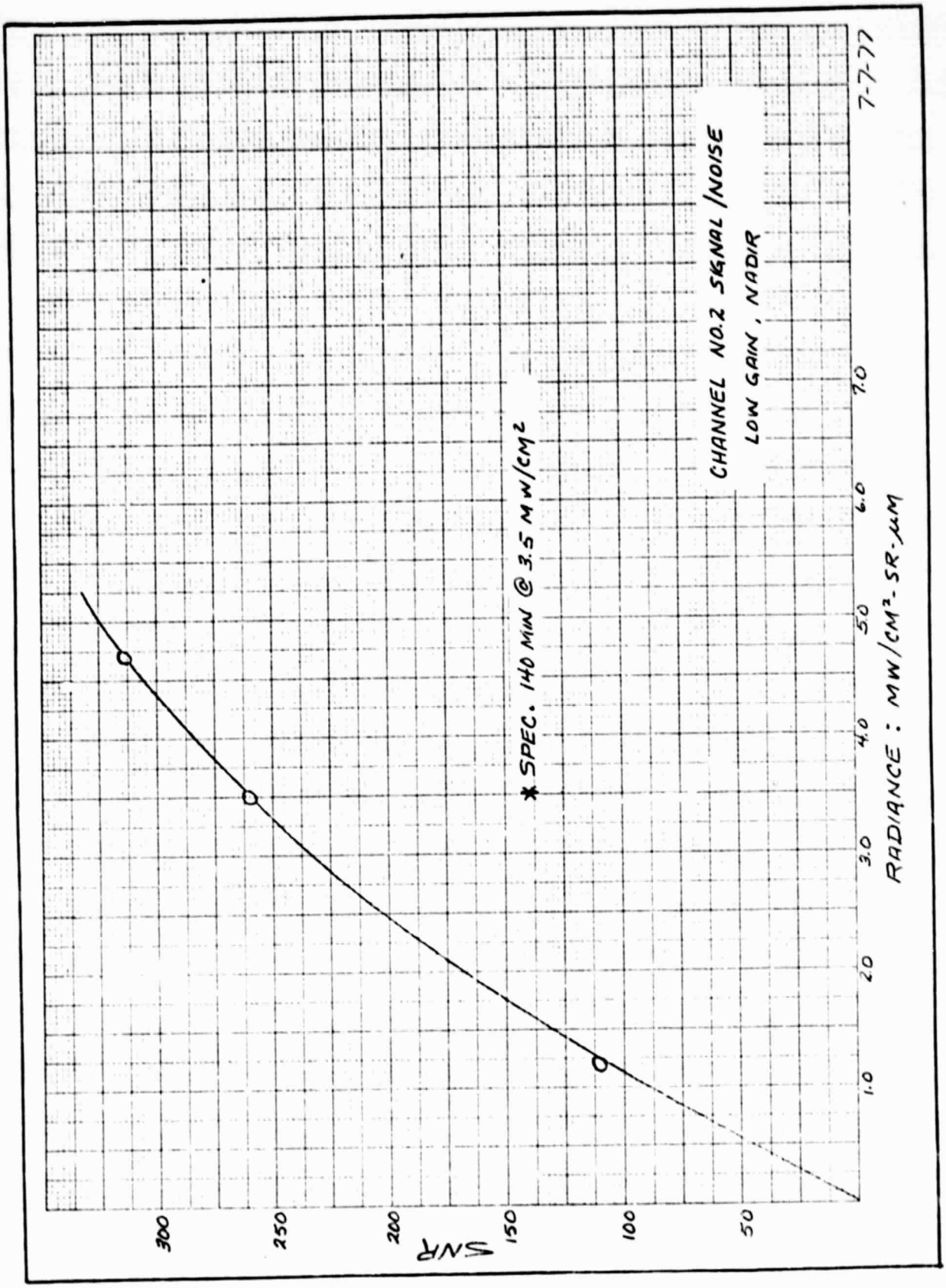

Figure 2-9 CHANNEL NO. 2 SIGNAL/NOISE LOW GAIN, NADIR

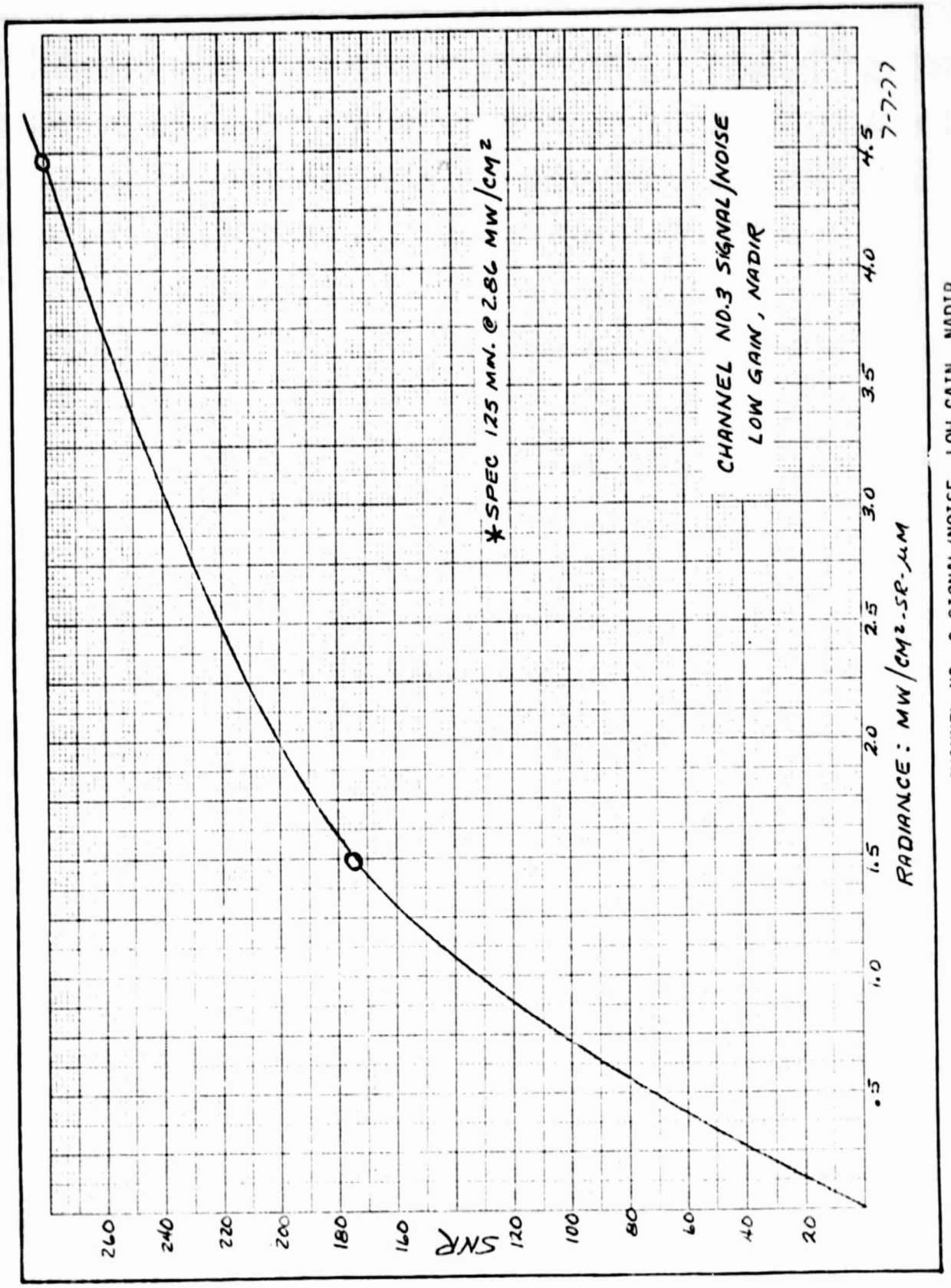

Figure 2-10 CHANNEL NO. 3 SIGNAL/NOISE LOW GAIN, NADIR

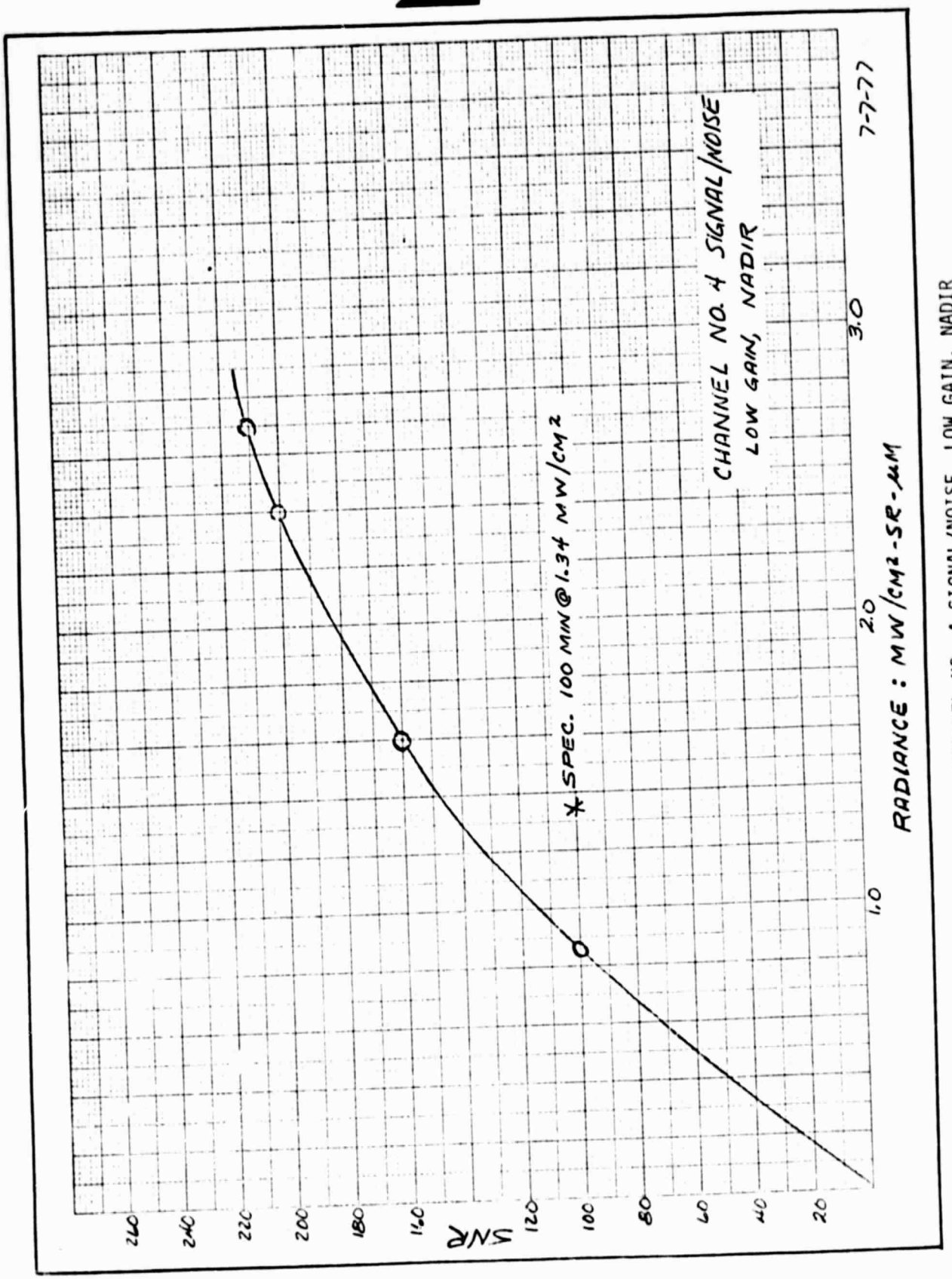

Figure 2-11 CHANNEL NO. 4 SIGNAL/NOISE LOW GAIN, NADIR

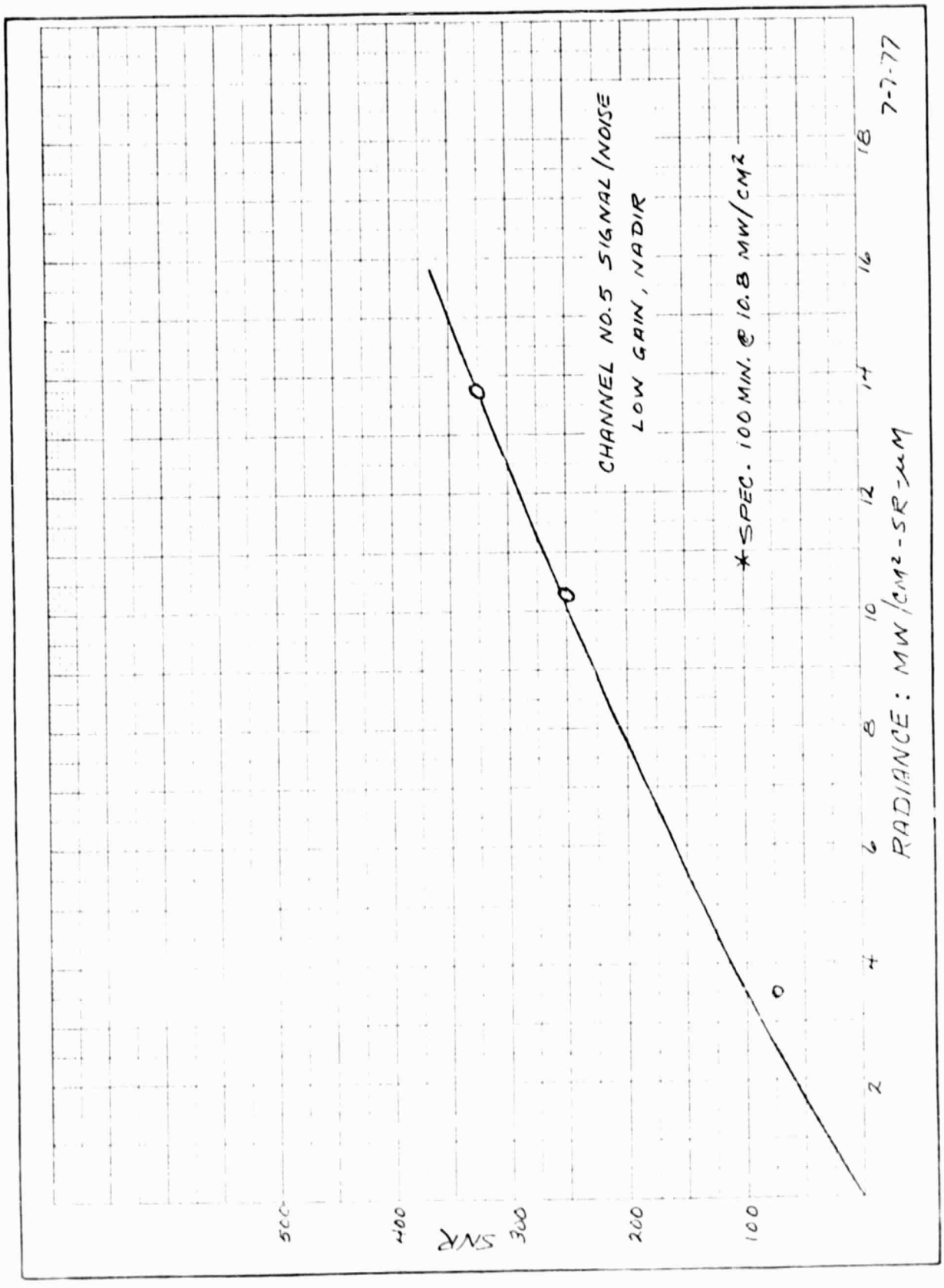

Figure 2-12 CHANNEL NO. 5 SIGNAL/NOISE LOW GAIN, NADIR

2.1.3 Radiance Response

Radiance response measurements were made during PACT on all channels. The integrating sphere supplied by GSFC was the "standard" source used for determining the responses of channels 1-5. This has provided a very stable and repeatable reference for response checks made after PACT. Figures 2-13 through 2-17 represent the responses of channels 1-5 using the integrating sphere. Measurements of channel responses performed as a part of the repetitive OST's used a collimator source designed for use in the Multi-Spectral Scanner (MSS) for Landsat. Due to a disparity in the secondary mirror obscurations (i.e., the collimator secondary mirror is larger than the CZCS secondary mirror), the coalignment between the CZCS and the collimator is extremely critical for repetitive readings. The MSS collimator is the source used for the signal to noise ratio and response measurements which make up the histograms of Section 2.1.6.

The response of channel 6 was also measured during PACT utilizing the bench cooler for detector cooling and black body targets for the space look and the earth scene. The radiance difference between the two targets was the basis for determination of the channel response. Gradients caused by convection limited the accuracy of these measurements. The measurements were repeated as a part of the Thermal Vacuum tests using a liquid nitrogen cooled space target and a thermoelectrically controlled earth scene target referred to as the Full Aperture Infrared (FAIR) target. Figure 2-18 shows channel 6 response as a function of scene radiance for instrument (mounting feet) temperatures of 10, 25, and 35°C in vacuum.

Table 2-1 is a compilation of slope and intercept data for each channel's radiance response equation. In channels 1-4, where there are four gain settings and a commandable threshold, data are included for all possible command conditions.

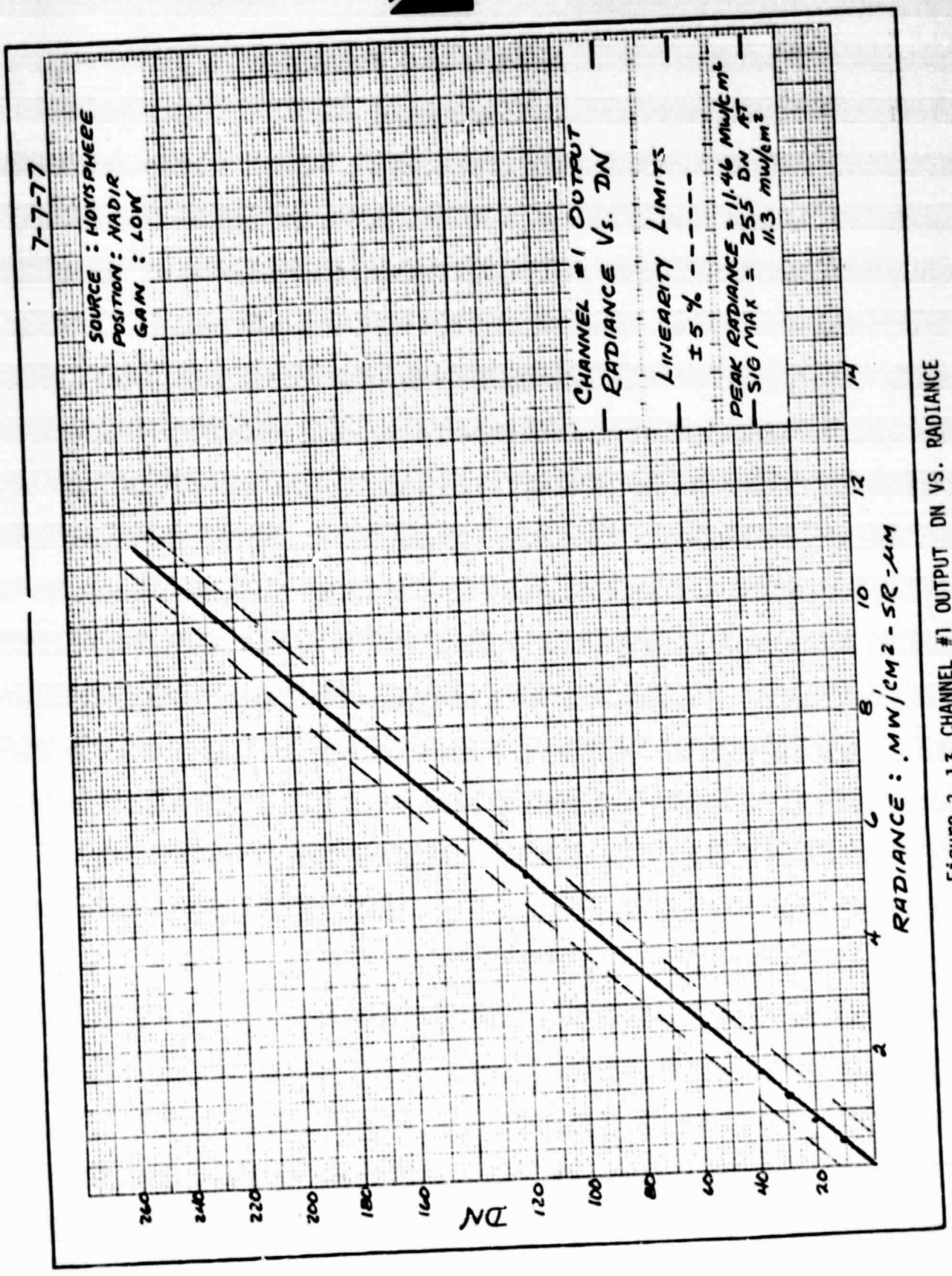

Figure 2-13 CHANNEL #1 OUTPUT DN VS. RADIANCE

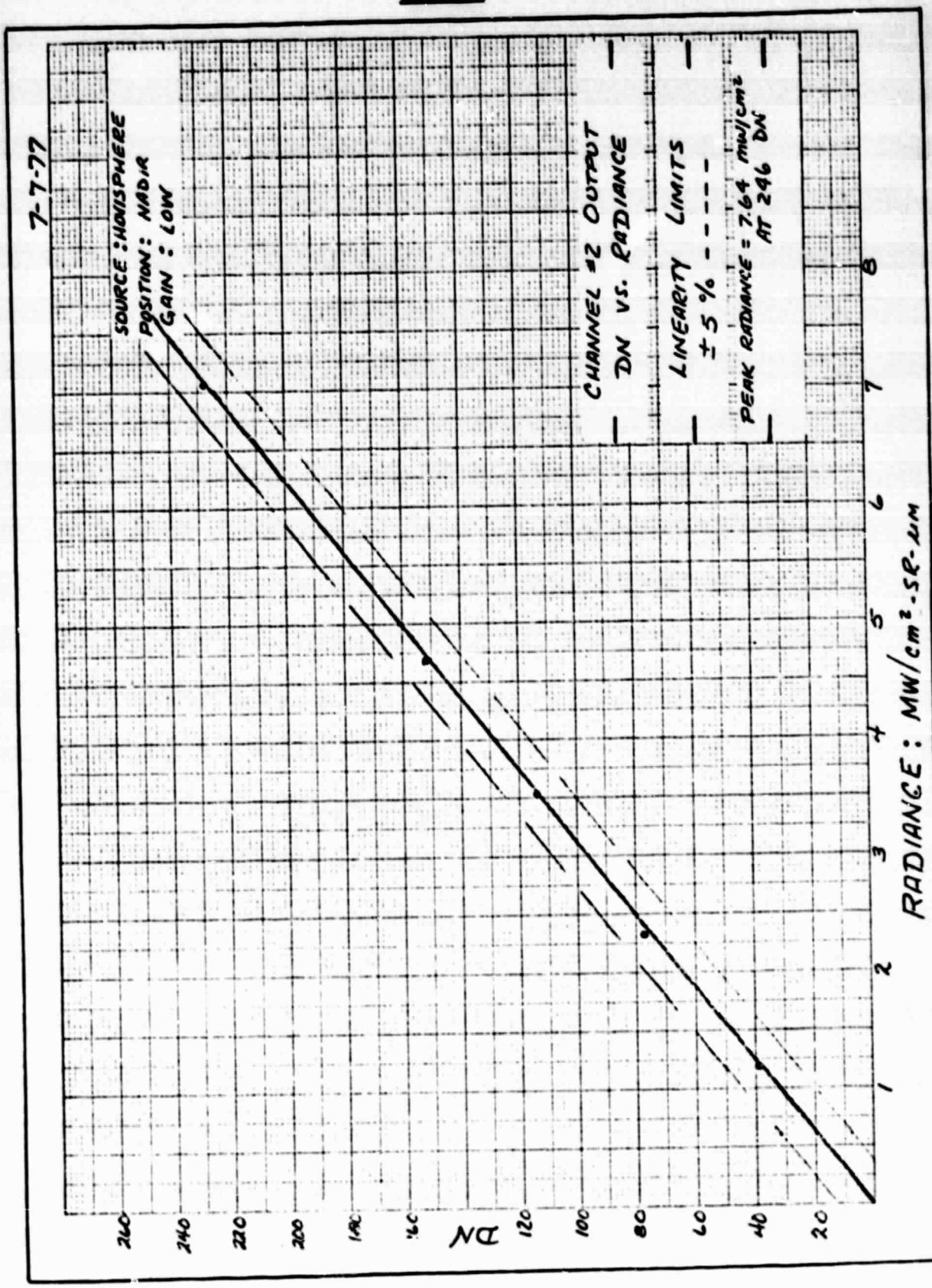

Figure 2-11 CHANNEL #2 OUTPUT DN VS. RADIANCE

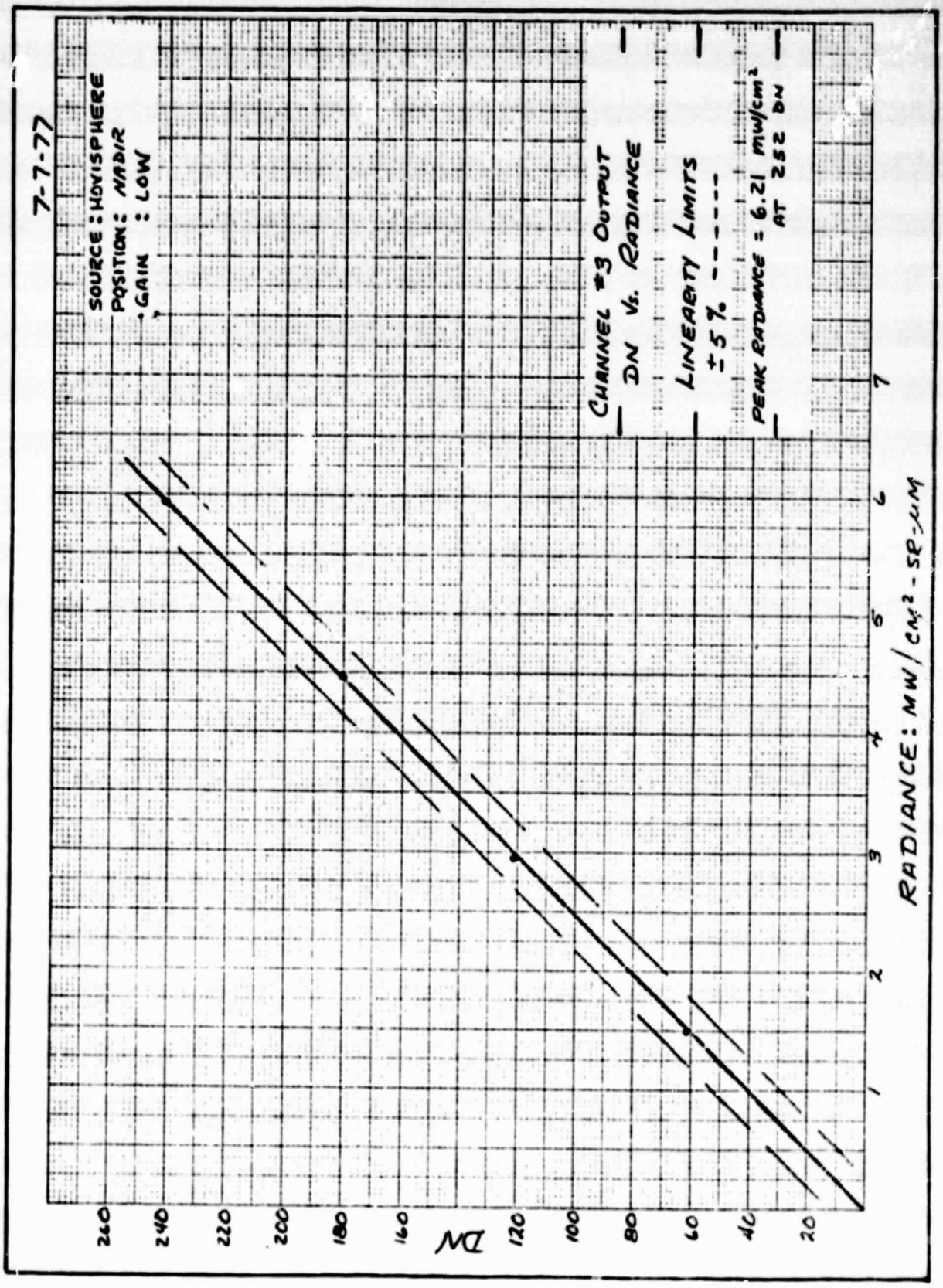

Figure 2-15 CHANNEL #3 OUTPUT DN VS. RADIANCE

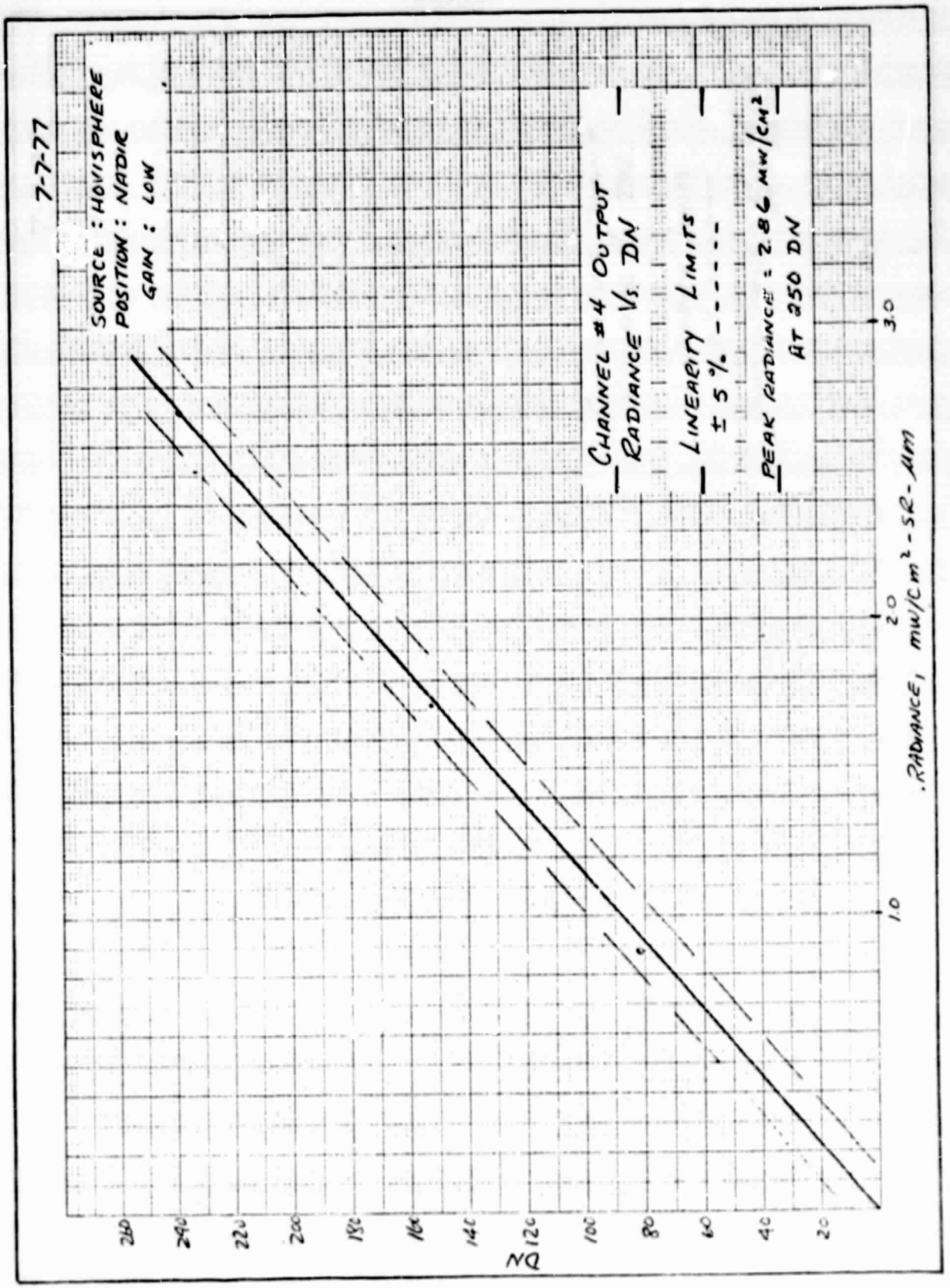

Figure 2-16 CHANNEL #4 OUTPUT DN VS. RADIANCE

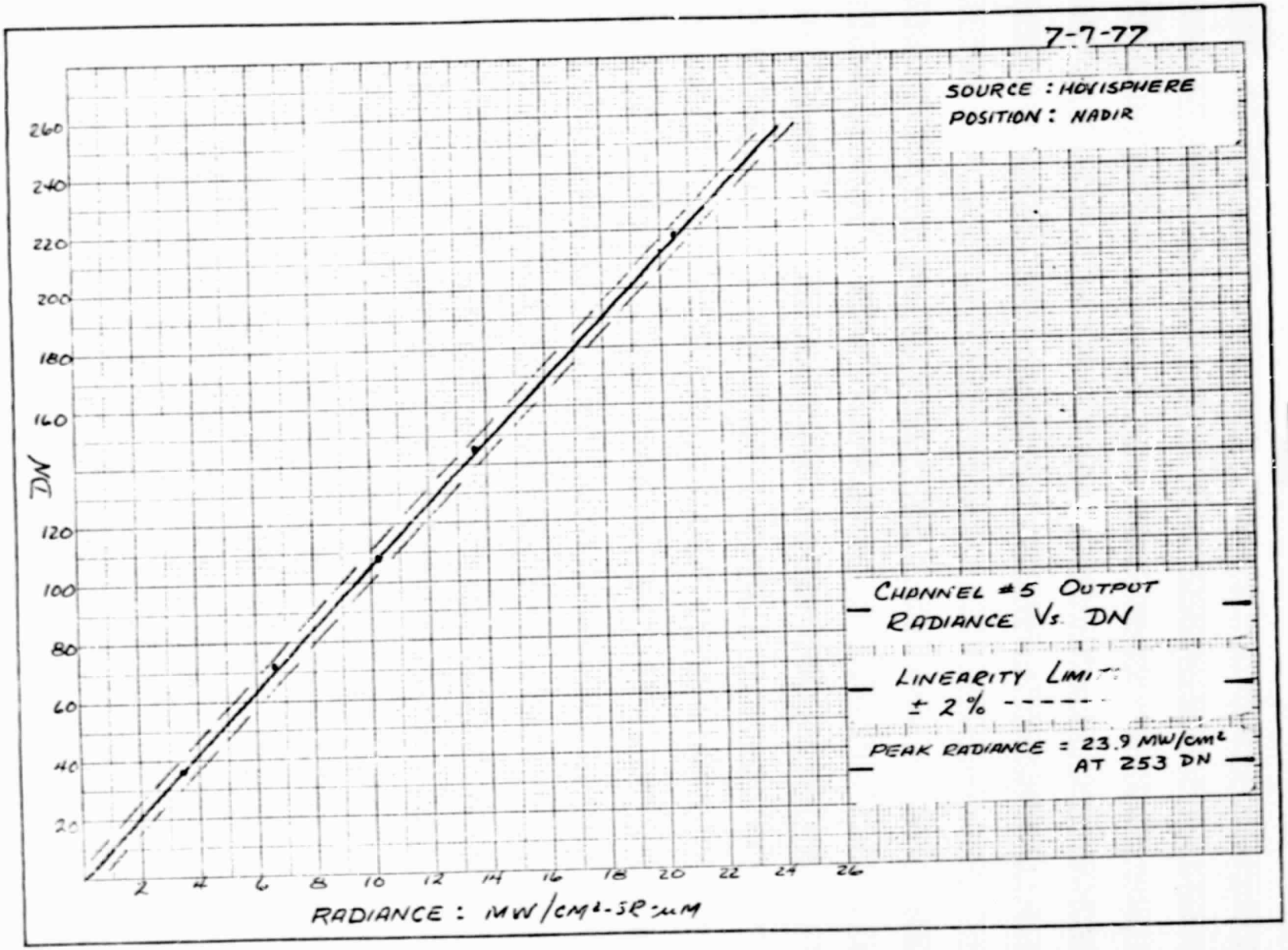

Figure 2-17 CHANNEL #5 OUTPUT DN VS. RADIANCE

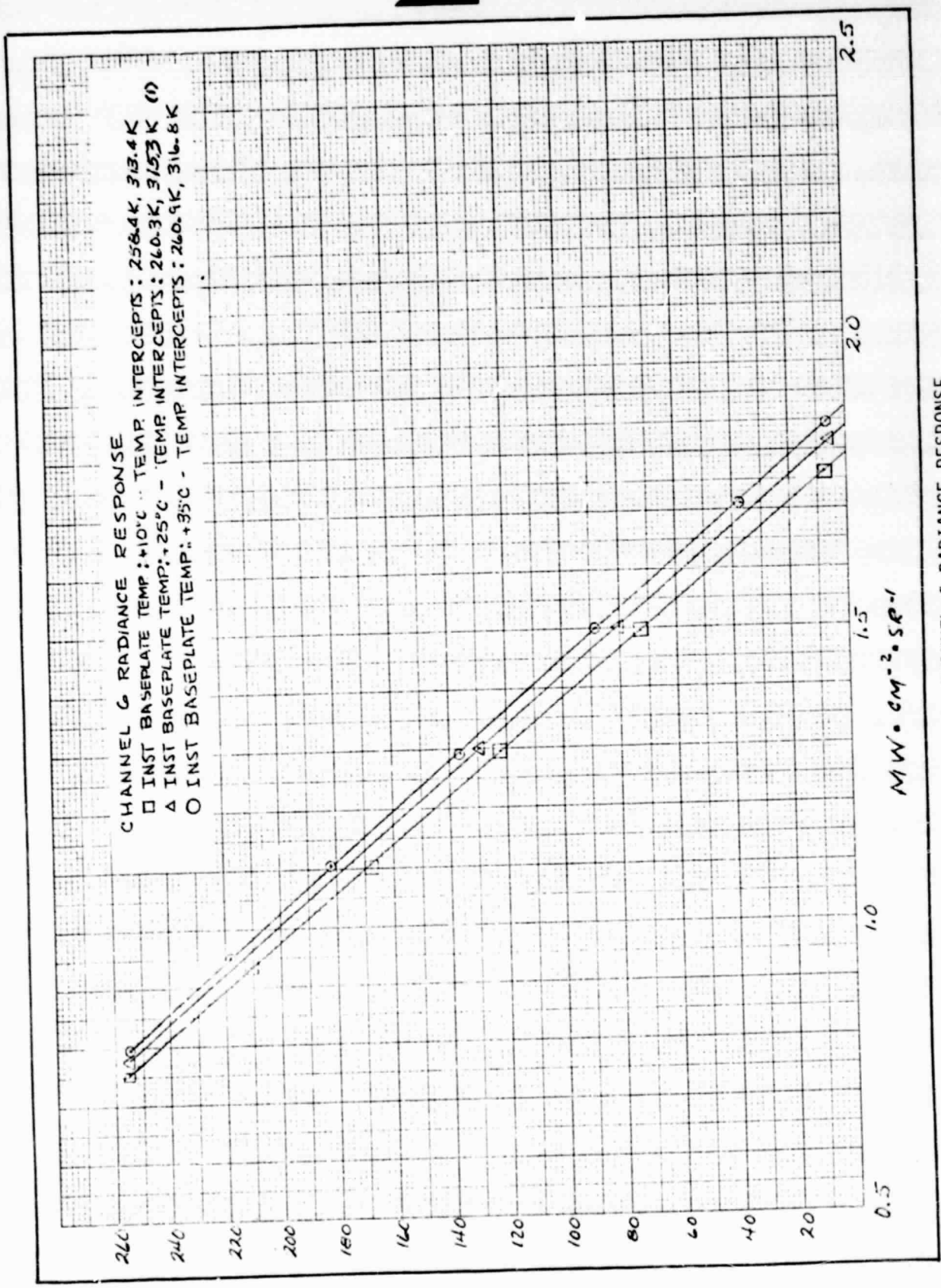

Figure 2-18 CHANNEL 6 RADIANCE RESPONSE

MODE	CHANNEL 1	CHANNEL 2	CHANNEL 3	CHANNEL 4	CHANNEL 5	CHANNEL 6****
Low Gain (00) Threshold OFF	a = 22.46 b = -0.89	a = 32.23 b = -2.05	a = 40.54 b = -3.24	a = 88.0 b = -1.0	a = 10.62 b = +0.30	a = -245.9* b = +440.9* a = -242.1** b = +444.8** a = -235.9*** b = +441.7***
Gain 1 Threshold OFF	a = 27.86 b = -1.47	a = 40.11 b = -3.54	a = 49.62 b = -3.1	a = 111.5 b = -4.0		
Gain 2 Threshold OFF	a = 33.69 b = -0.97	a = 49.22 b = -4.8	a = 60.88 b = -4.0	a = 135.0 b = -4.0		
High Gain (3) Threshold OFF	a = 47.33 b = -1.59	a = 67.29 b = -3.8	a = 84.7 b = -4.0	a = 187.0 b = -3.0		
Low Gain (00) Threshold ON	a = 78.8 b = -623.0	a = 119.0 b = -684.0	a = 154.0 b = -690.0	a = 308.8 b = -630.0		
Gain 1 Threshold ON	a = 104.0 b = -634.0	a = 136.5 b = -630.0	a = 178.0 b = -650.0	a = 363.0 b = -599.0		
Gain 2 Threshold ON	a = 112.8 b = -590.0	a = 173.3 b = -664.0	a = 230.0 b = -621.0	a = 427.0 b = -576.0		
High Gain (3) Threshold ON	a = 172.0 b = -648.0	a = 240.0 b = -667.0	a = 276.0 b = -593.0	a = 650.0 b = -637.0		

S = aN + b

S = Digital Number at Radiometer Output (0 to 255)

N = Radiance into Radiometer in mw/cm^2-sr-μm

*Instrument Baseplate at +10°C

**Instrument Baseplate at +25°C

***Instrument Baseplate at +35°C

****Channel 6 Radiance in mw/cm^2-sr

TABLE 2-1 RADIANCE RESPONSE EQUATIONS

2.1.4 Modulation Transfer Function

The system Modulation Transfer Function (MTF) was measured for each channel during PACT in such a way that the complete system response including sampling was included. The MSS collimator was used for channels 1-5 but, due to background problems, a 100 inch focal length collimator was provided by BASD for the channel 6 measurements. Even with a special test setup, channel 6 measurements were difficult to make properly. Because of this, OST's included only channel 1-5 MTF measurements except during Thermal Vacuum tests. The limited field available in either collimator allowed the use of a target which provided 3 cycles at 578 cycles per radian (c/r), 2 cycles at 385 c/r and 1.5 cycles at 289 c/r. The target is black with openings cut at the proper frequencies and is backlit by the collimator lamp. The instrument scans across the openings responding to the target radiance. A BCU computer routine, called up by software, allows the printout of the 16 consecutive pixels prior to, during and after the target for examination and computation of the MTF. At 478 c/r there are three maximum and three minimum sample points; at 385 c/r, 2 maximum and 2 minimum; and at 289 c/r, 2 maximum and 1 minimum. The average of the maximum samples and the minimum samples are determined and the MTF computed from the ratio of the maximum minus the minimum to the maximum plus the minimum. This is relativized by division by the MTF obtained at a low frequency, i.e., from the MTF of the completely open and closed aperture.

The channel 6 MTF is performed identically except a uniform black body source is the target background. Non-uniformity of the background target and heating of the aperture target make measurements in this channel difficult. Figures 2-19 through 2-24 show the MTF's of channels 1-6 as compared with the desired MTF's. In all cases the CZCS exceeded the desired values.

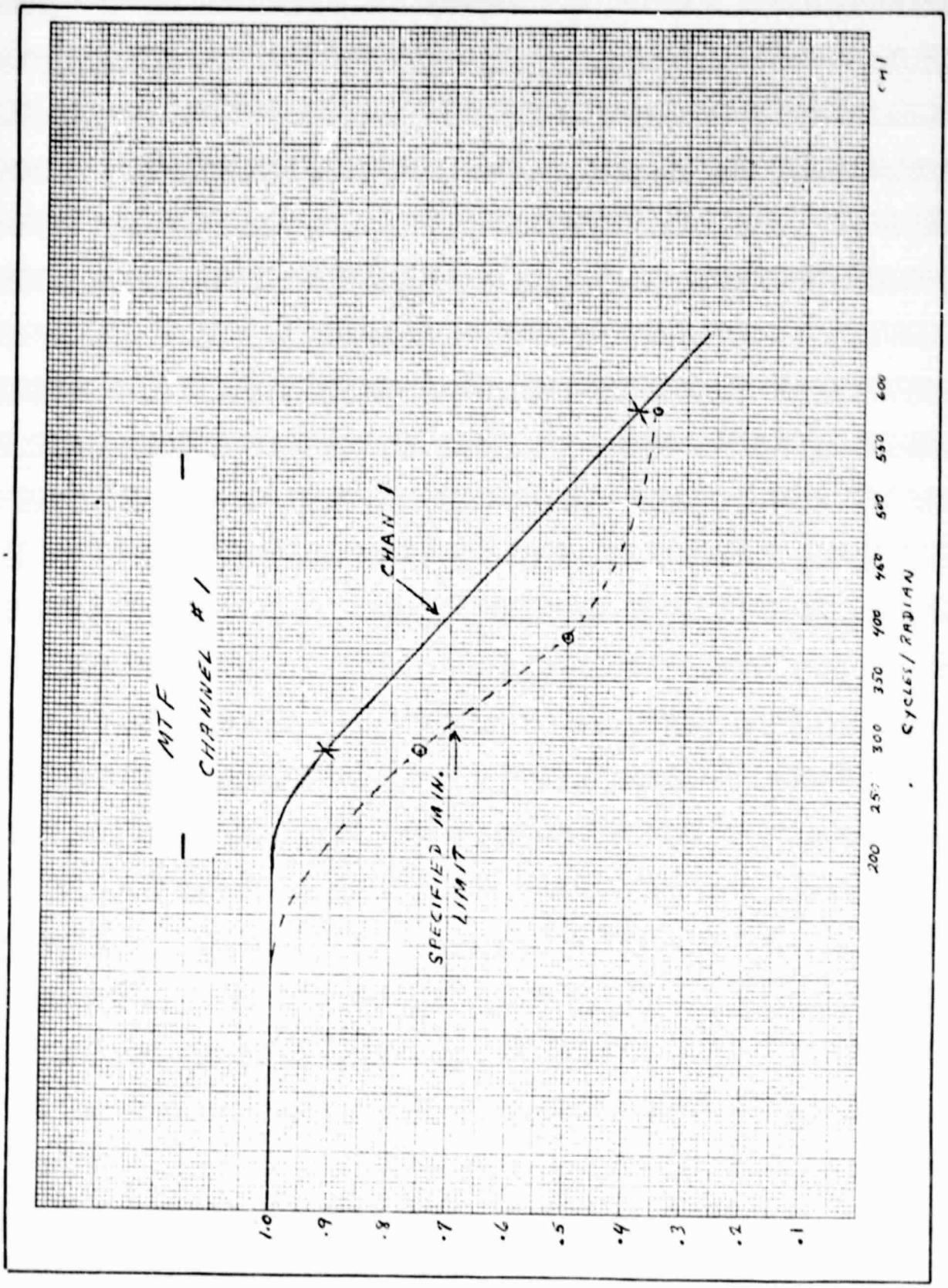

Figure 2-19 MTF CHANNEL #1

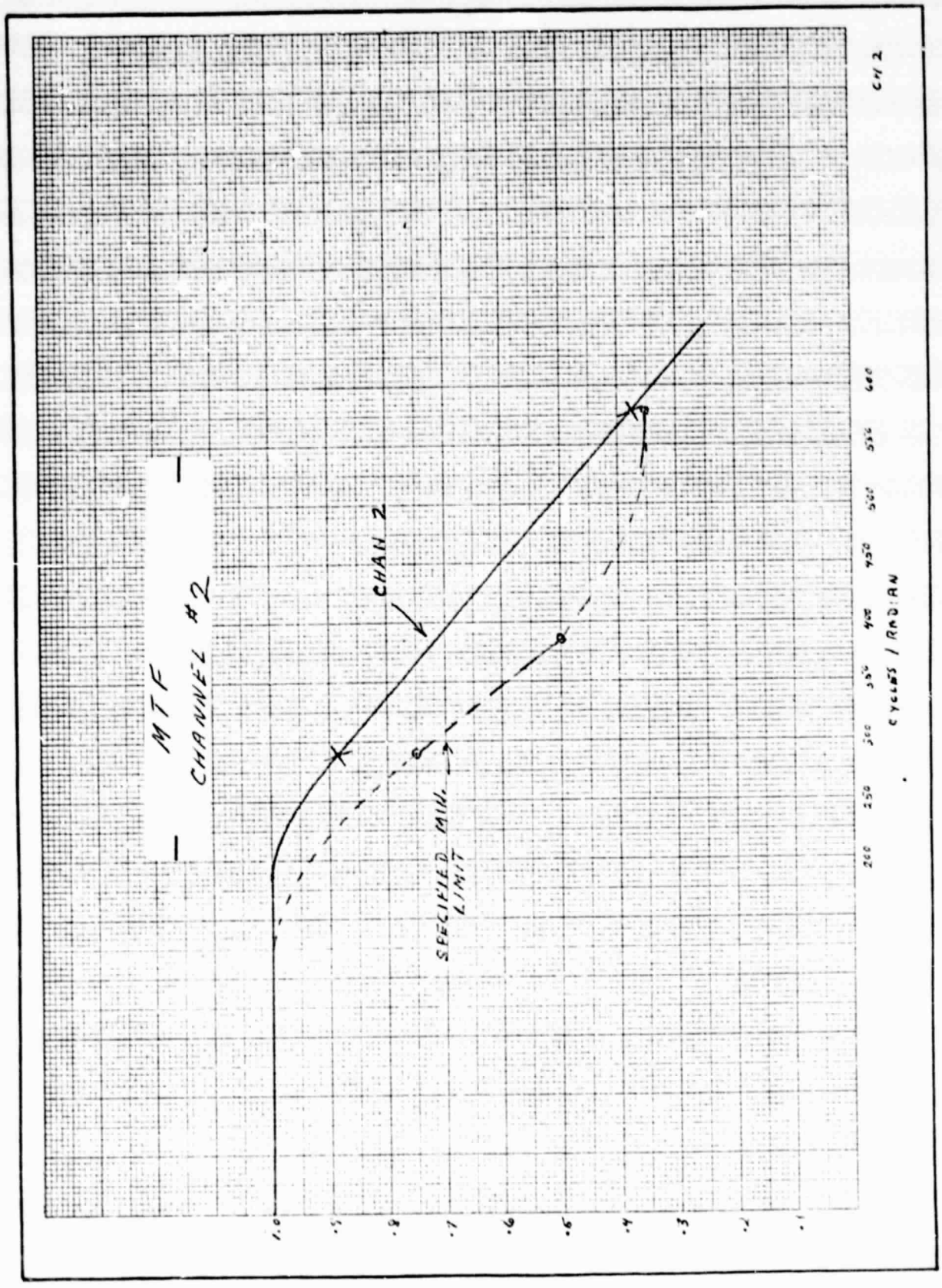

Figure 2-20 MTF CHANNEL #2

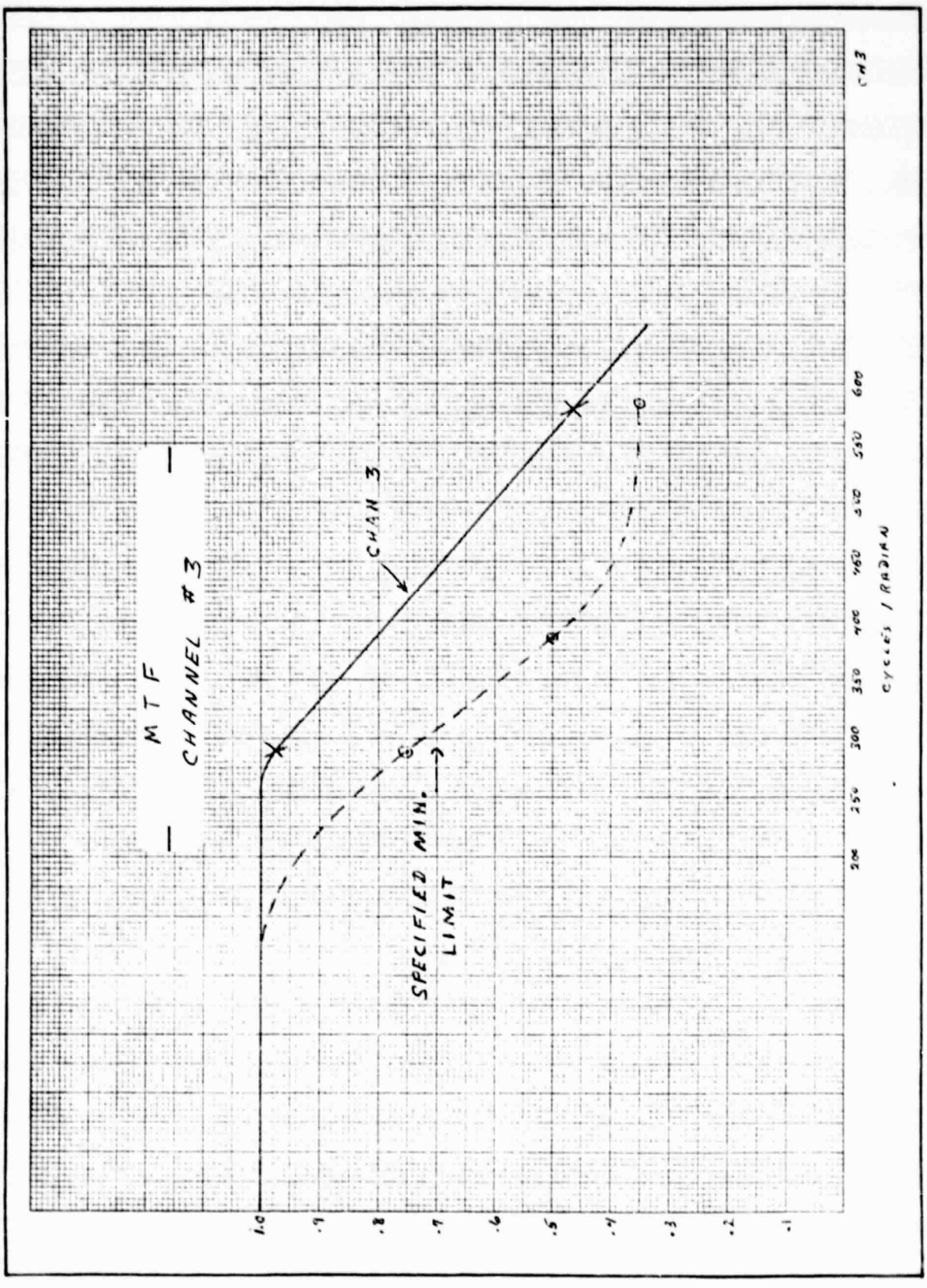

Figure 2-21 MTF CHANNEL #3

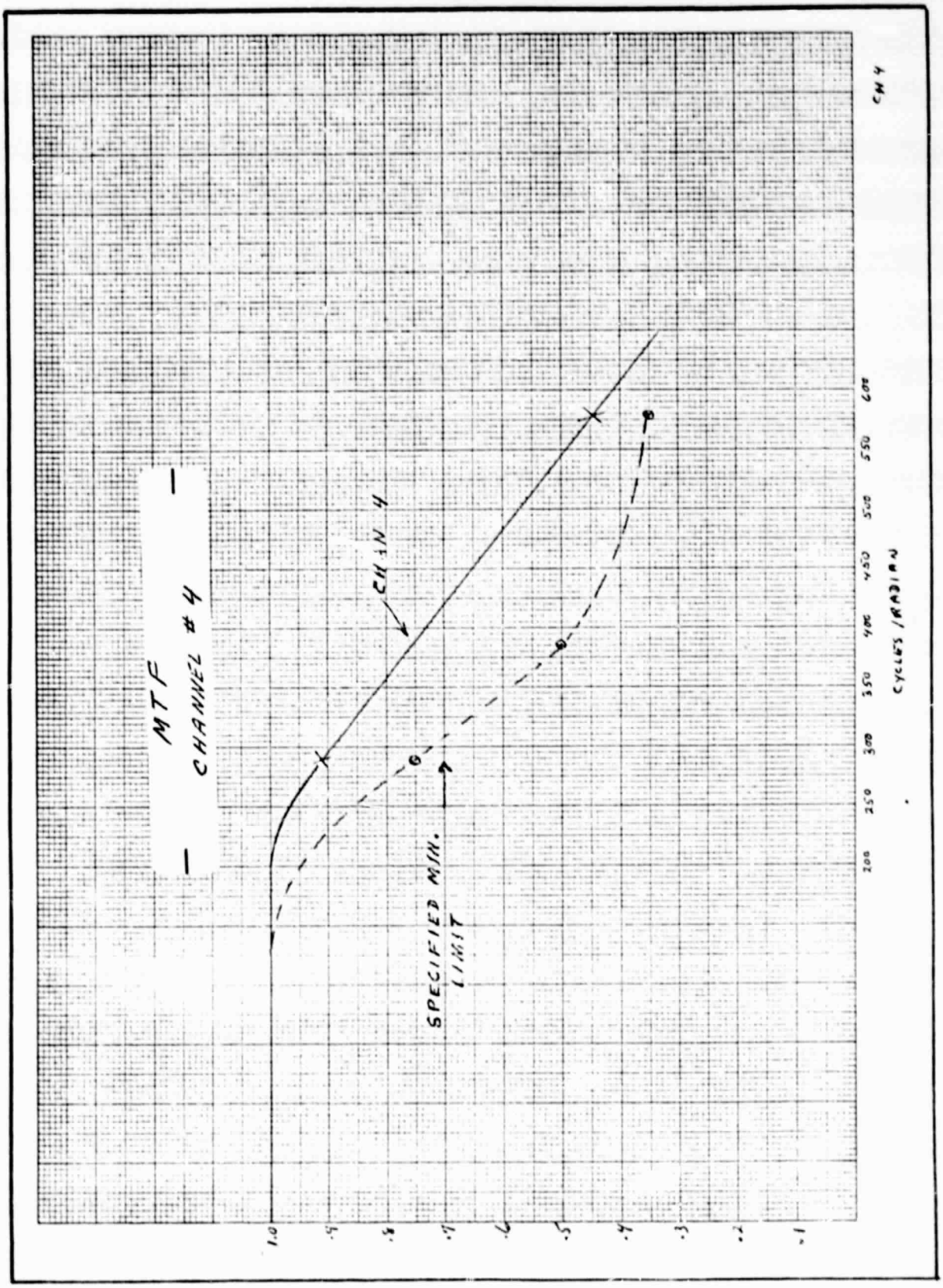

Figure 2-22 MTF CHANNEL #4

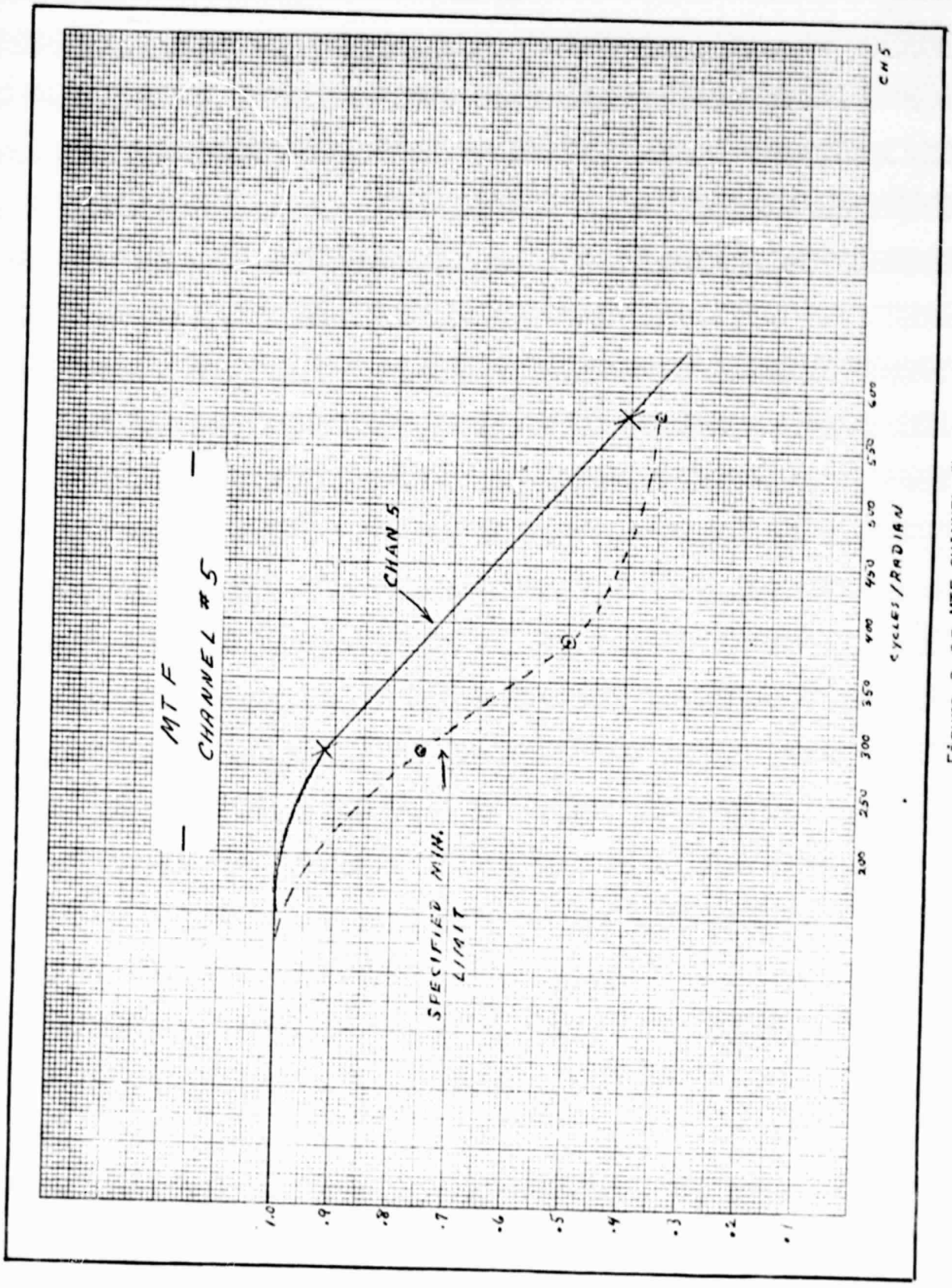

Figure 2-23 MTF CHANNEL #5

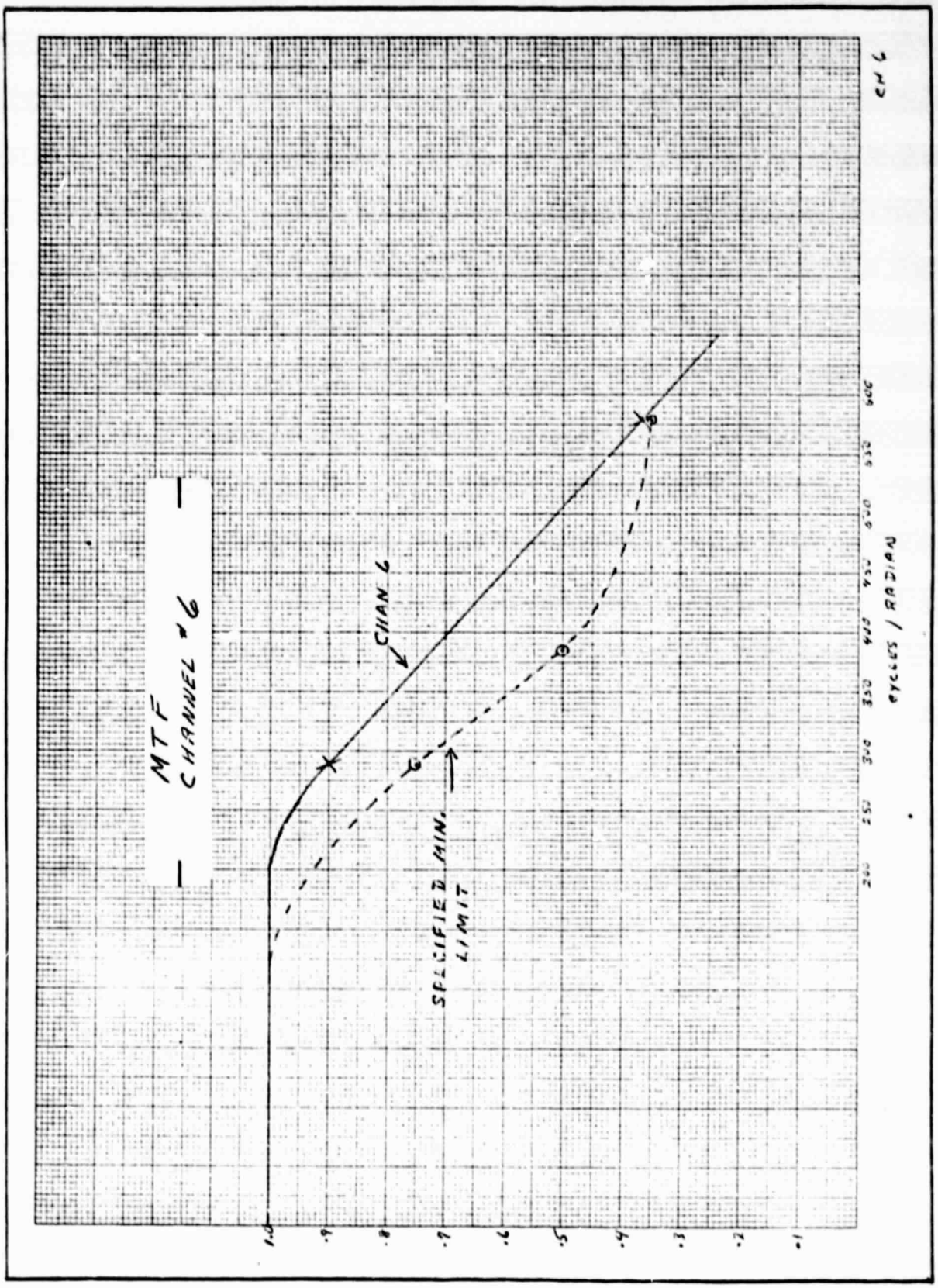

Figure 2-24 MTF CHANNEL #6

2.1.5 Optical Co-Registration and Field of View

The fields of view for channels 1-5 are set by the field stop. Since these channels share a common field stop, co-registration between these channels is inherently "perfect." Measurements of the fields of view and co-registration of channels 1-5 show that, within the bounds of measurement accuracy, this is true. To measure the field of view (FOV), the scan mirror is fixed and non-rotating, and a slit corresponding to 1/10 of the FOV, imaged by a collimator, back-lighted, and chopped for stability, is incrementally moved across the field image of the instrument. The slit is moved at the focal plane of the collimator by micrometer adjustment in 0.1 milliradian steps. Simultaneous readings are then made in all channels at each position of the slit. Since the lamp brightness could not be adjusted for optimum signal to noise ratio in all channels without saturation of channel 4, channel 1 and, particularly, channel 5 suffered from poor signal to noise ratios. Noise and positional ambiguity caused by the size of the slit are the probable sources of error in these measurements. Nevertheless, the half-amplitude widths of the FOVs for channels 1-5 were within 0.02 milliradians in the direction of scan and 0.025 milliradian in the cross scan direction. Co-registration of these half amplitude points were perfect except for channel 1, which was 0.02 milliradians off in the direction of scan. Figures 2-25 through 2-28 are plots of the along scan (direction of scan) fields of view for channels 1, 2, 3 and 5. The cross scan plots for the same channels are provided by Figures 2-29 through 2-32. Bi-directional co-registration between channels 1 and 5 and channels 2 and 3 are illustrated by Figures 2-33 through 2-36.

The FOV of channel 6 is set by the focal length of that channel and the detector size as the detector is the channel 6 field stop. Alignment between channel 6 and the other channels is adjusted principally by mirror M-5 (see Volume 1). The source used to back-light the slit is a Nernst Glower, which provides sufficient signal strength for co-registration measurements with channel 4. The field of view of channel 6 is slightly larger than the others, being 0.927 milliradians in the direction of scan and 0.88 milliradians in the cross scan direction. It co-registers with channel 4 to within 0.08 milliradians in both channels. Figures 2-37 and 2-38 depict the FOV and co-registration measurements of channels 4 and 6.

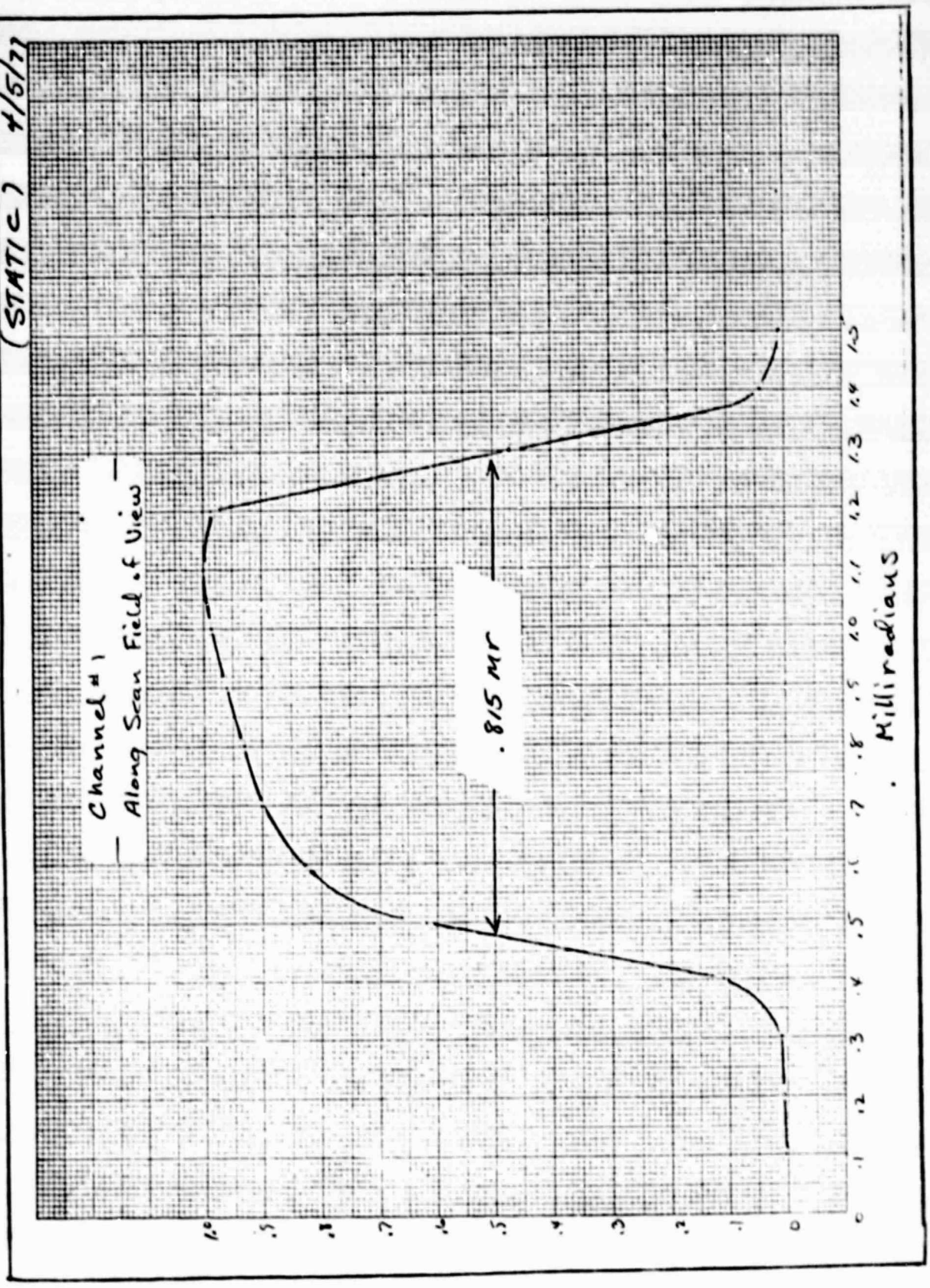

Figure 2-25 CHANNEL #1 ALONG SCAN FIELD OF VIEW

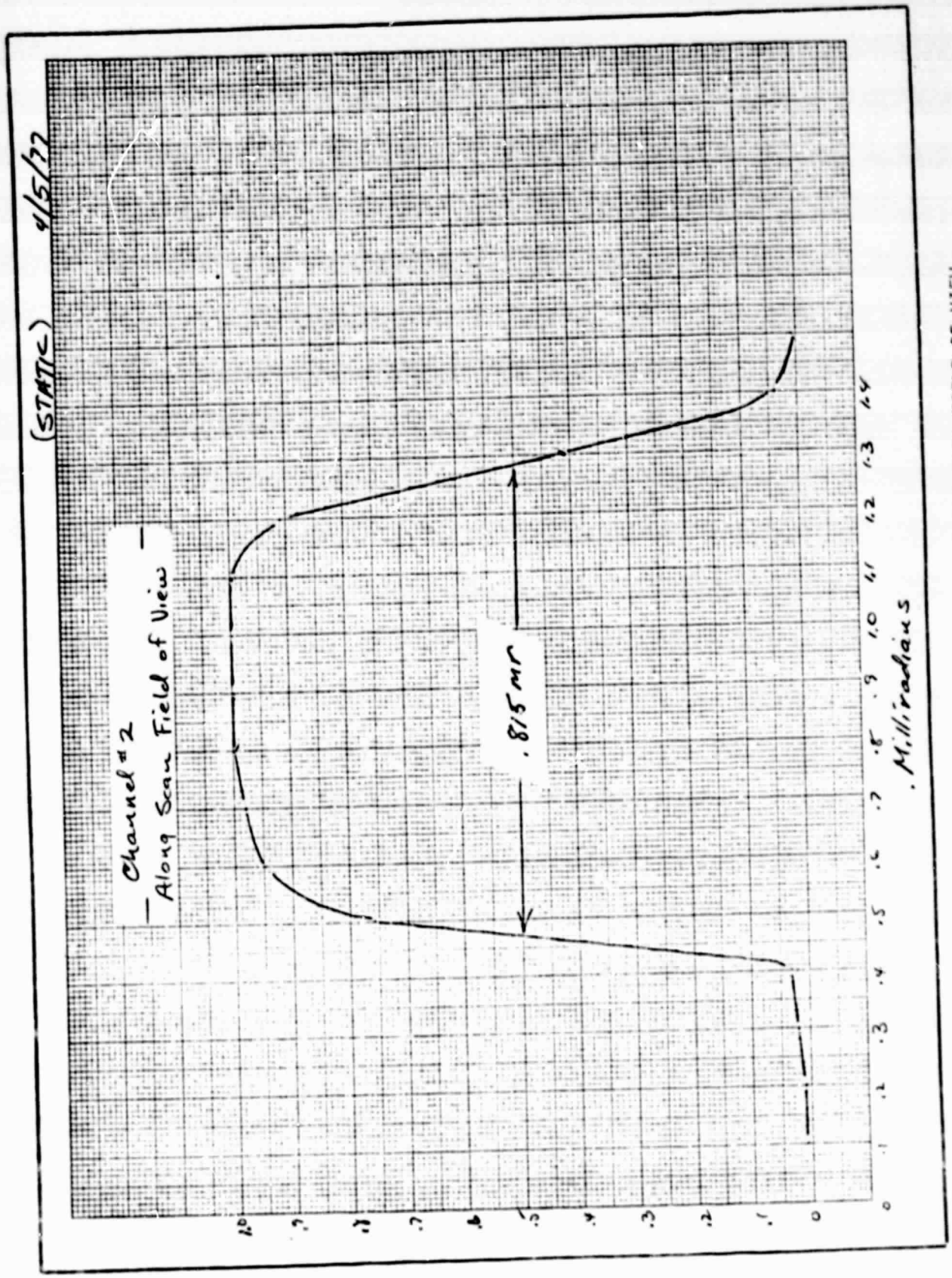

Figure 2-26 CHANNEL #2 ALONG SCAN FIELD OF VIEW

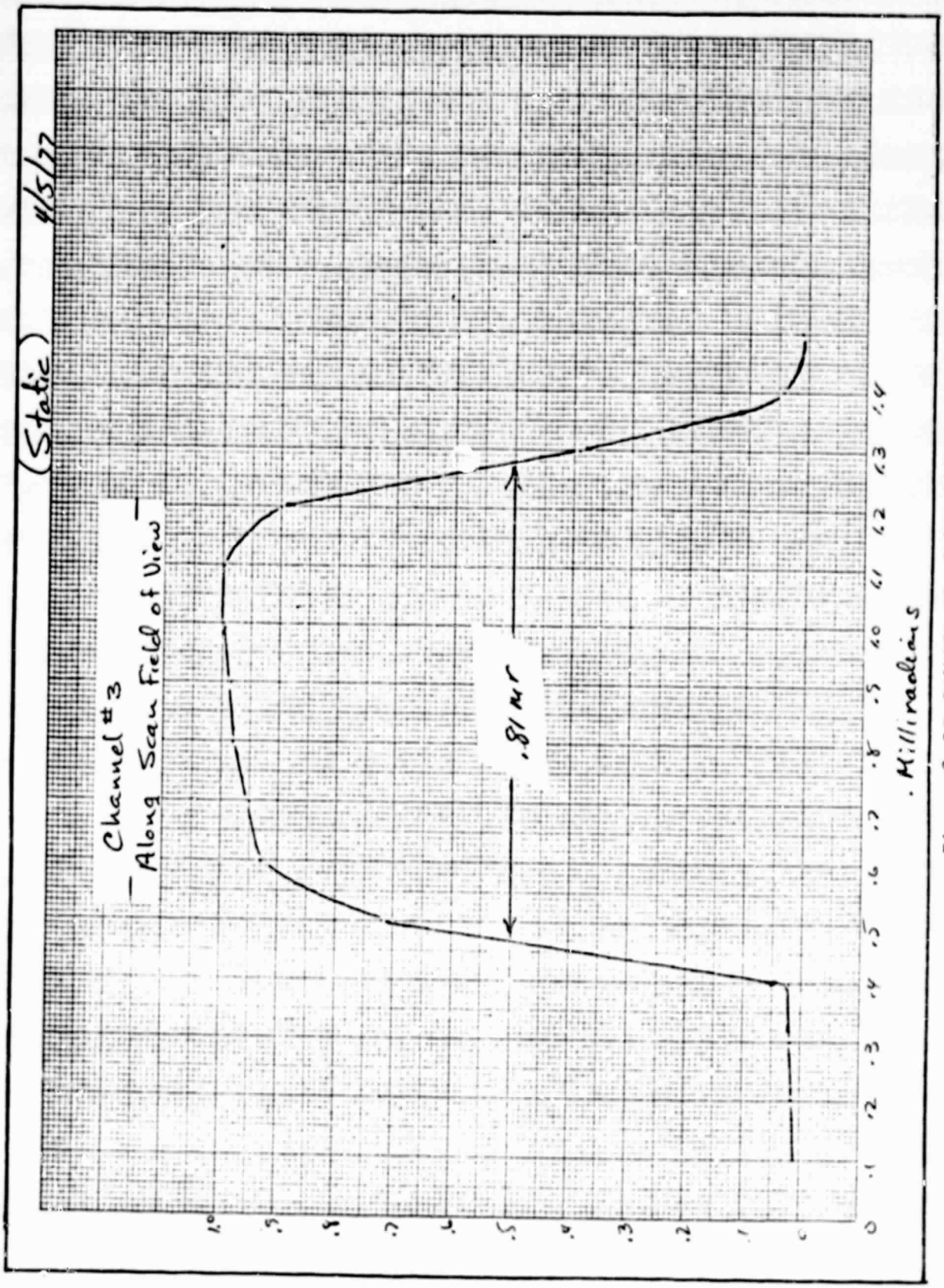

Figure 2-27 CHANNEL #3 ALONG SCAN FIELD OF VIEW

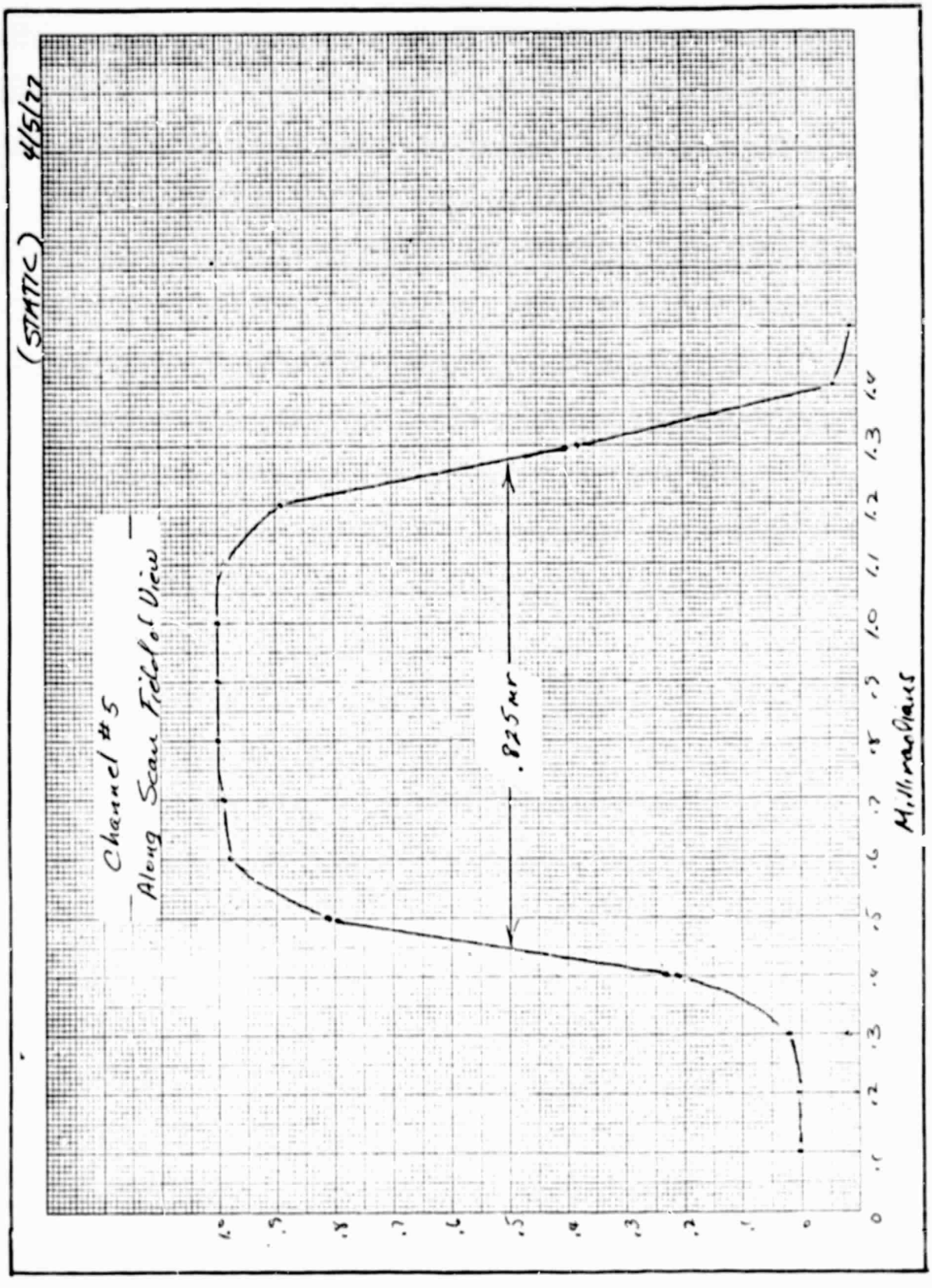

Figure 2-28 CHANNEL #5 ALONG SCAN FIELD OF VIEW

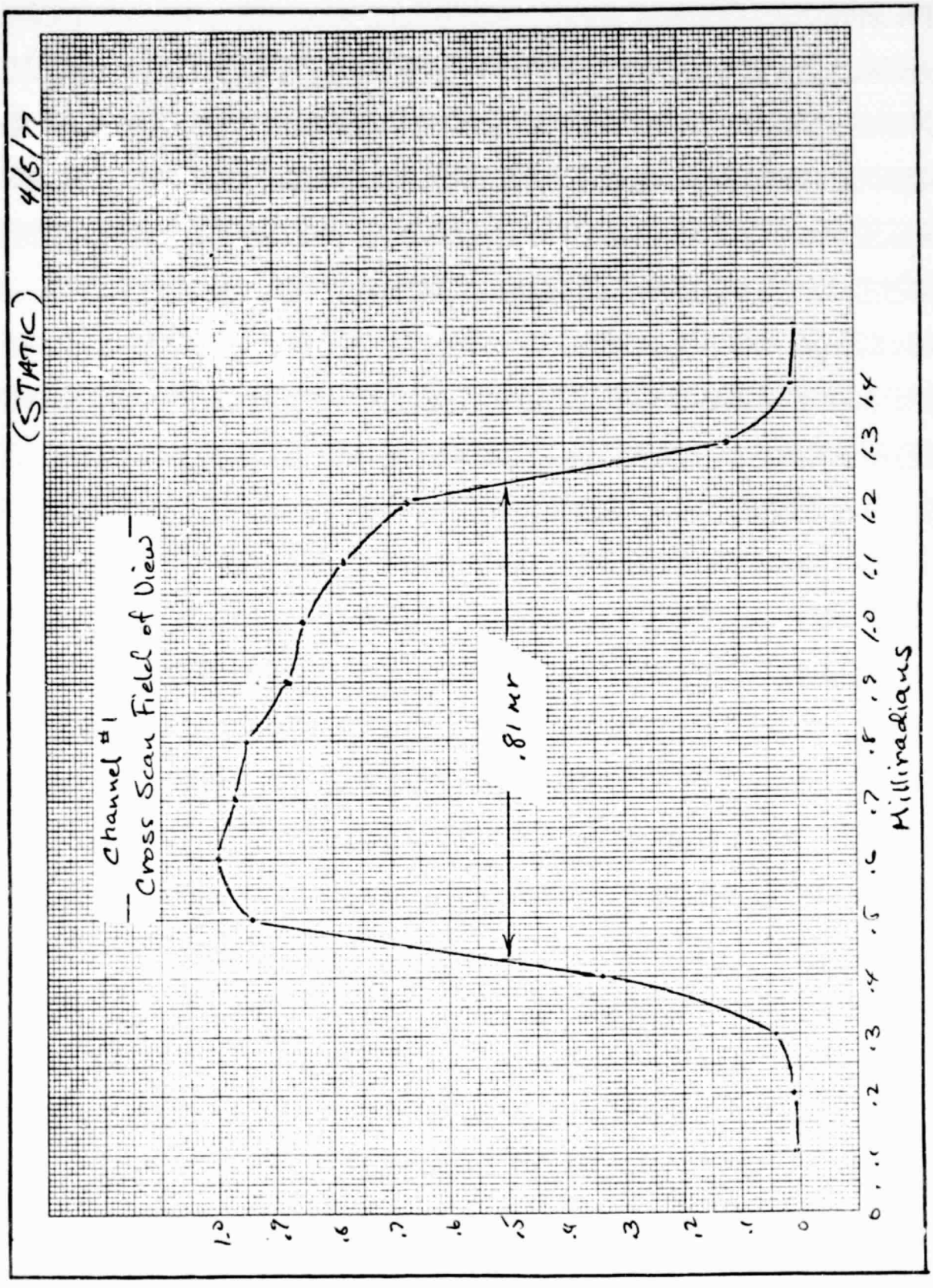

Figure 2-29 CHANNEL #1 CROSS SCAN FIELD OF VIEW

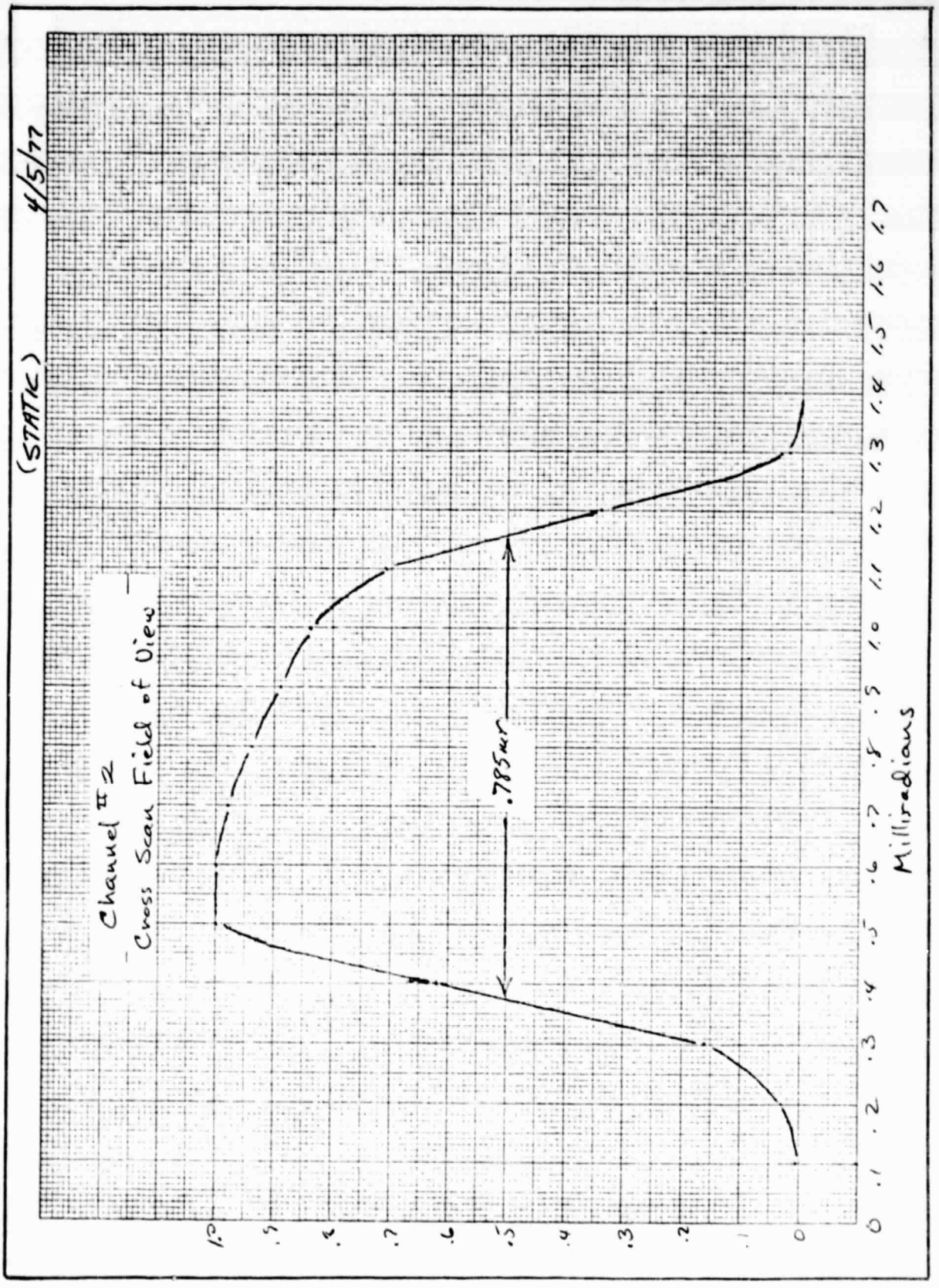

Figure 2-30 CHANNEL #2 CROSS SCAN FIELD OF VIEW

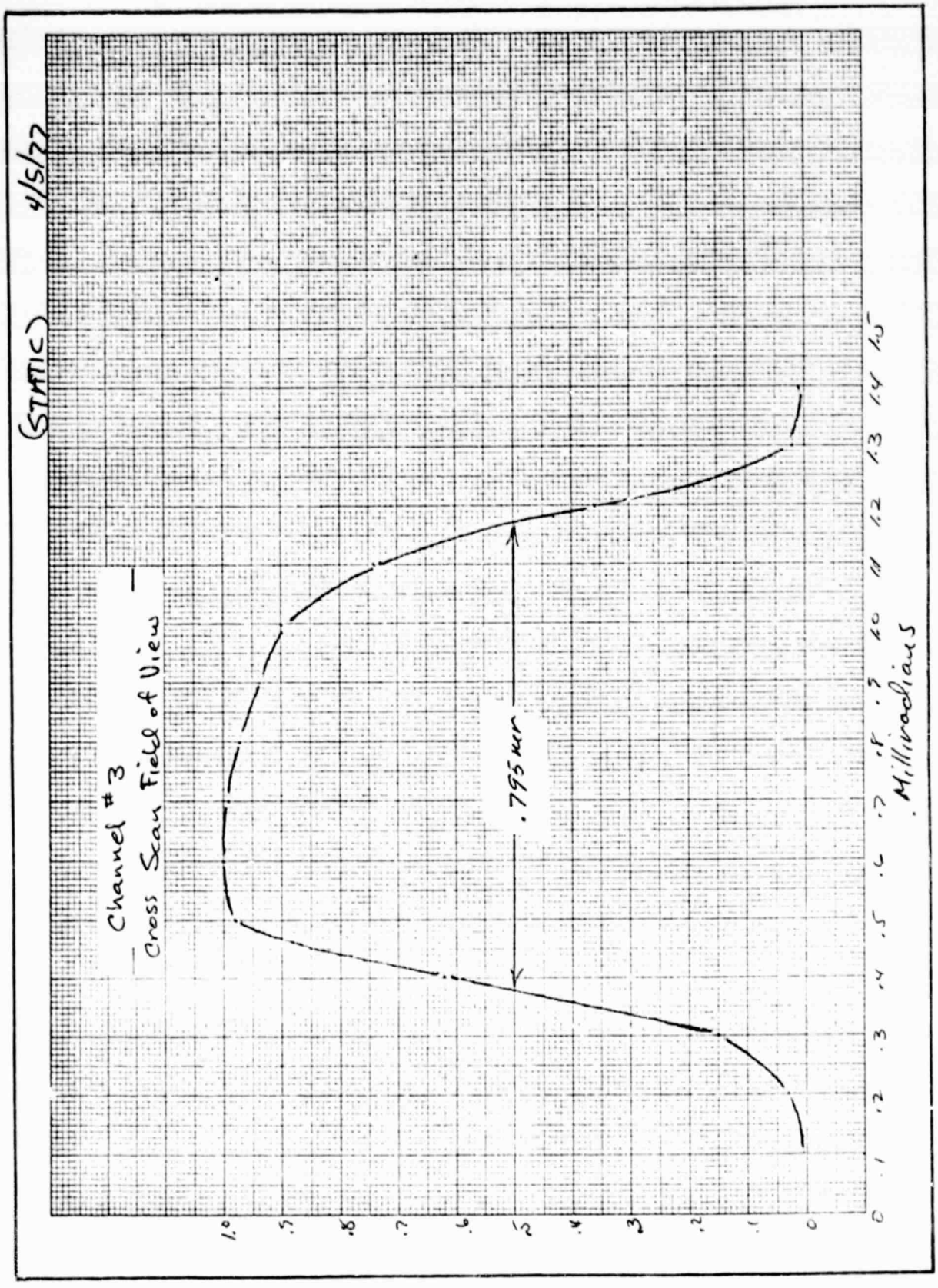

Figure 2-31 CHANNEL #3 CROSS SCAN FIELD OF VIEW

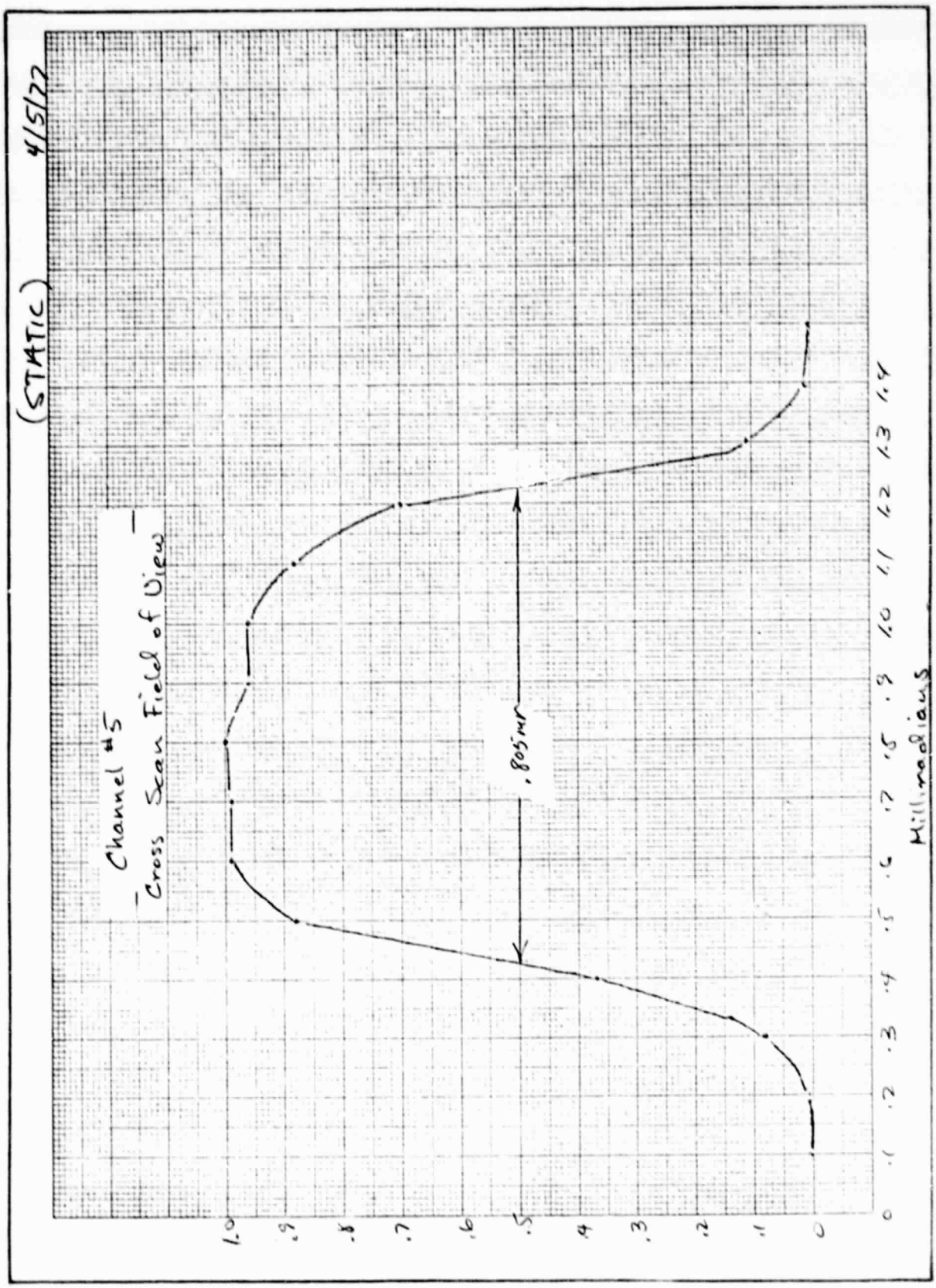

Figure 2-32 CHANNEL #5 CROSS SCAN FIELD OF VIEW

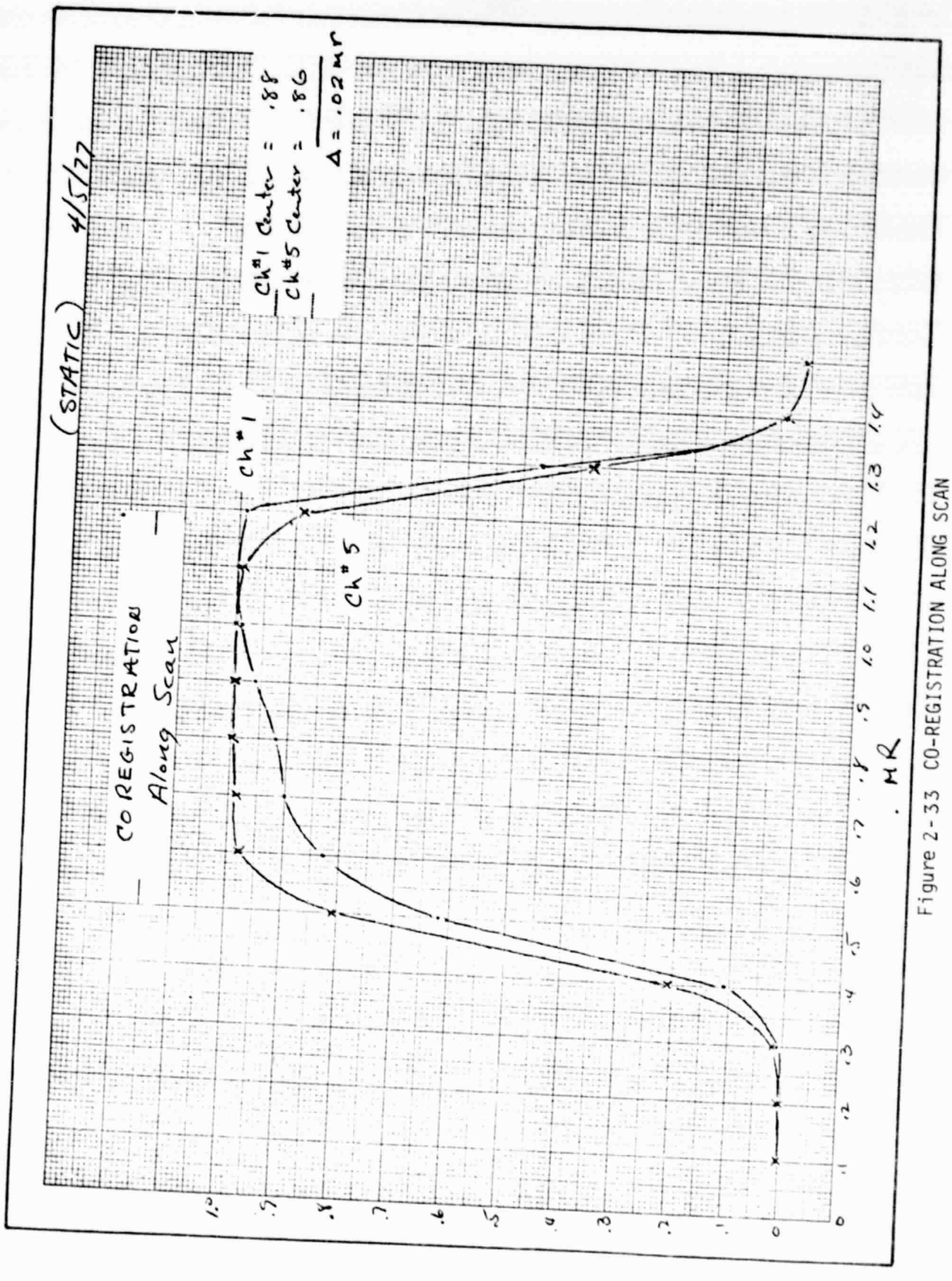

Figure 2-33 CO-REGISTRATION ALONG SCAN

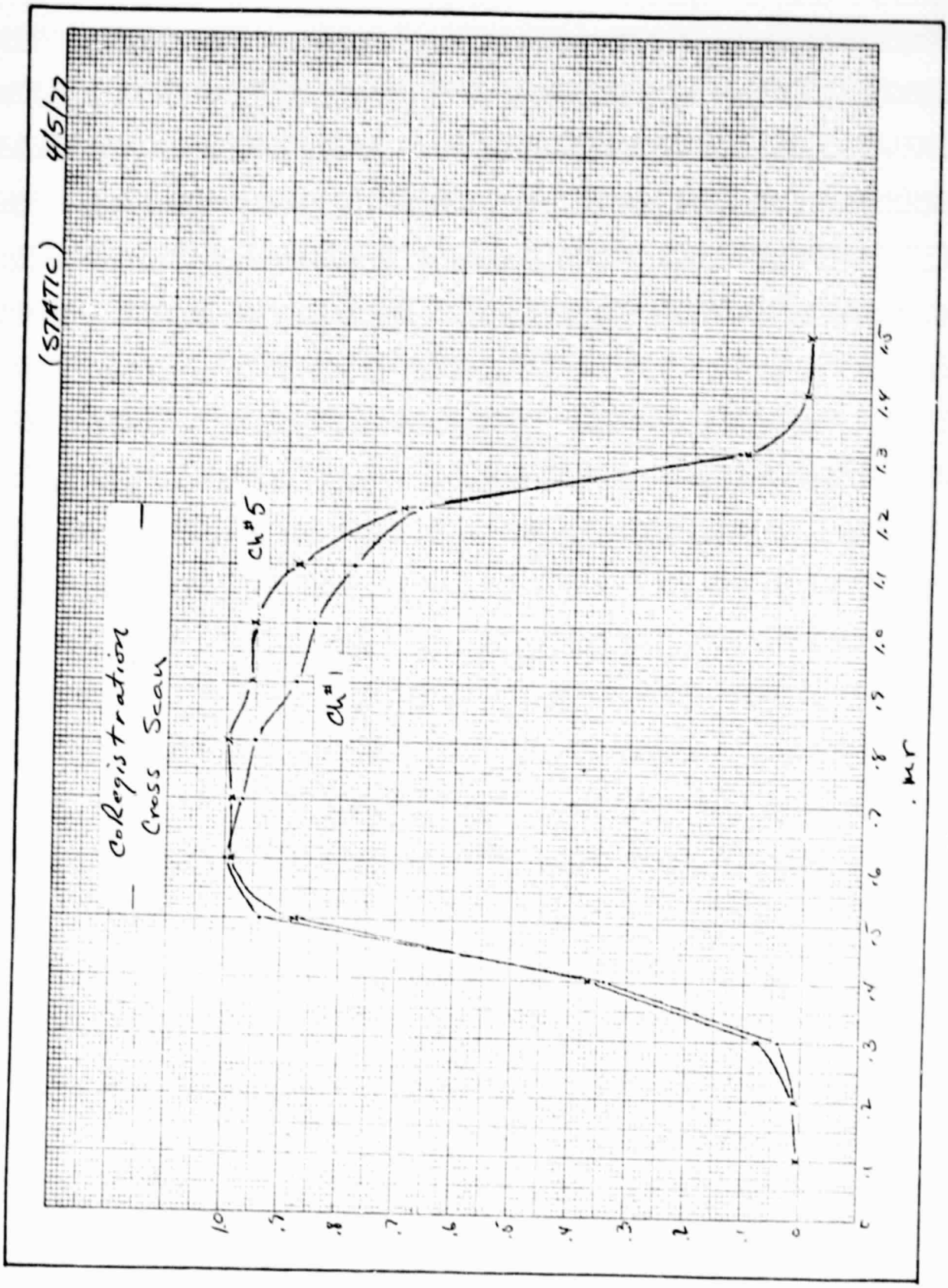

Figure 2-34 CO-REGISTRATION CROSS SCAN

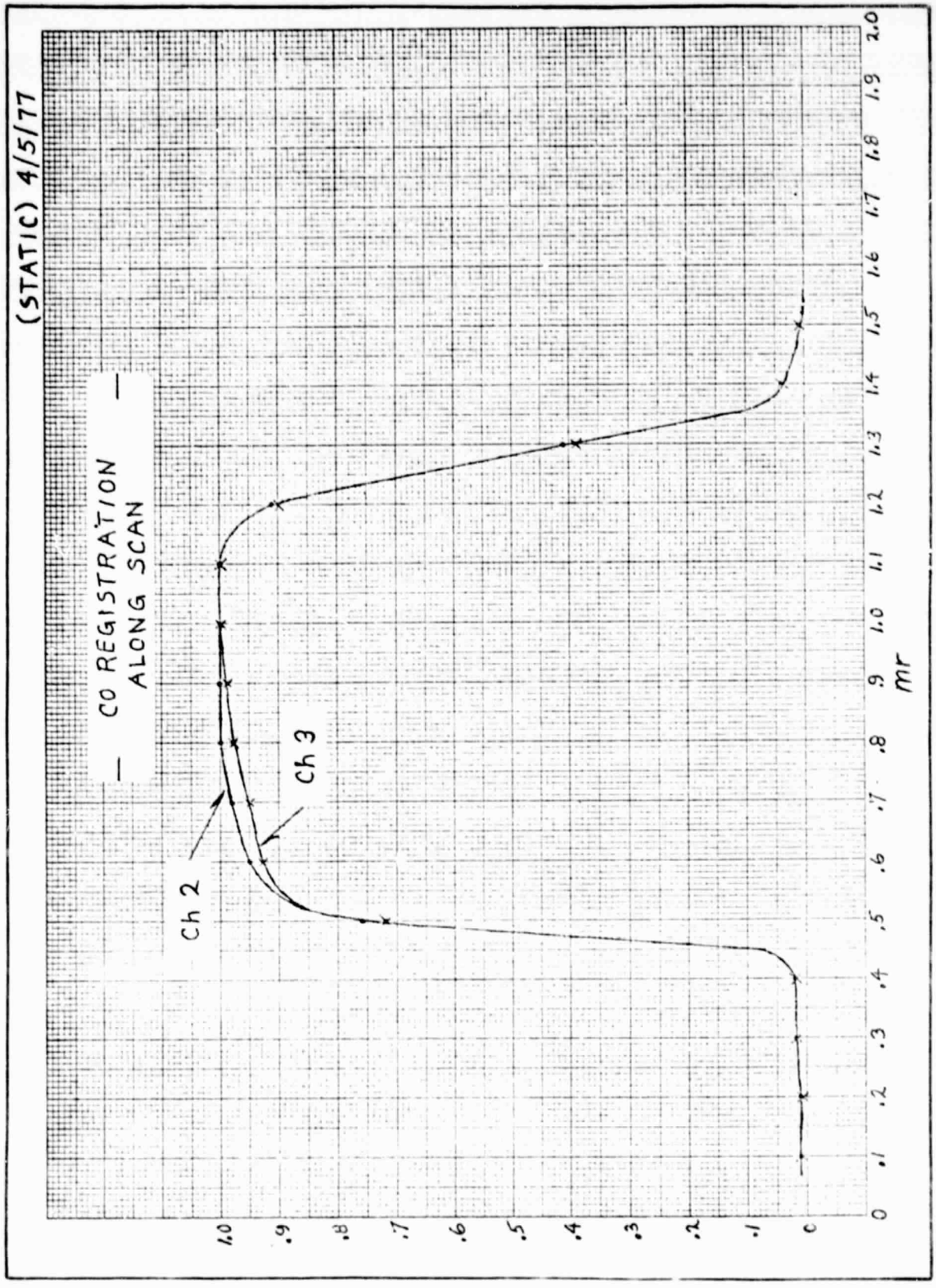

Figure 2-35 CO-REGISTRATION ALONG SCAN

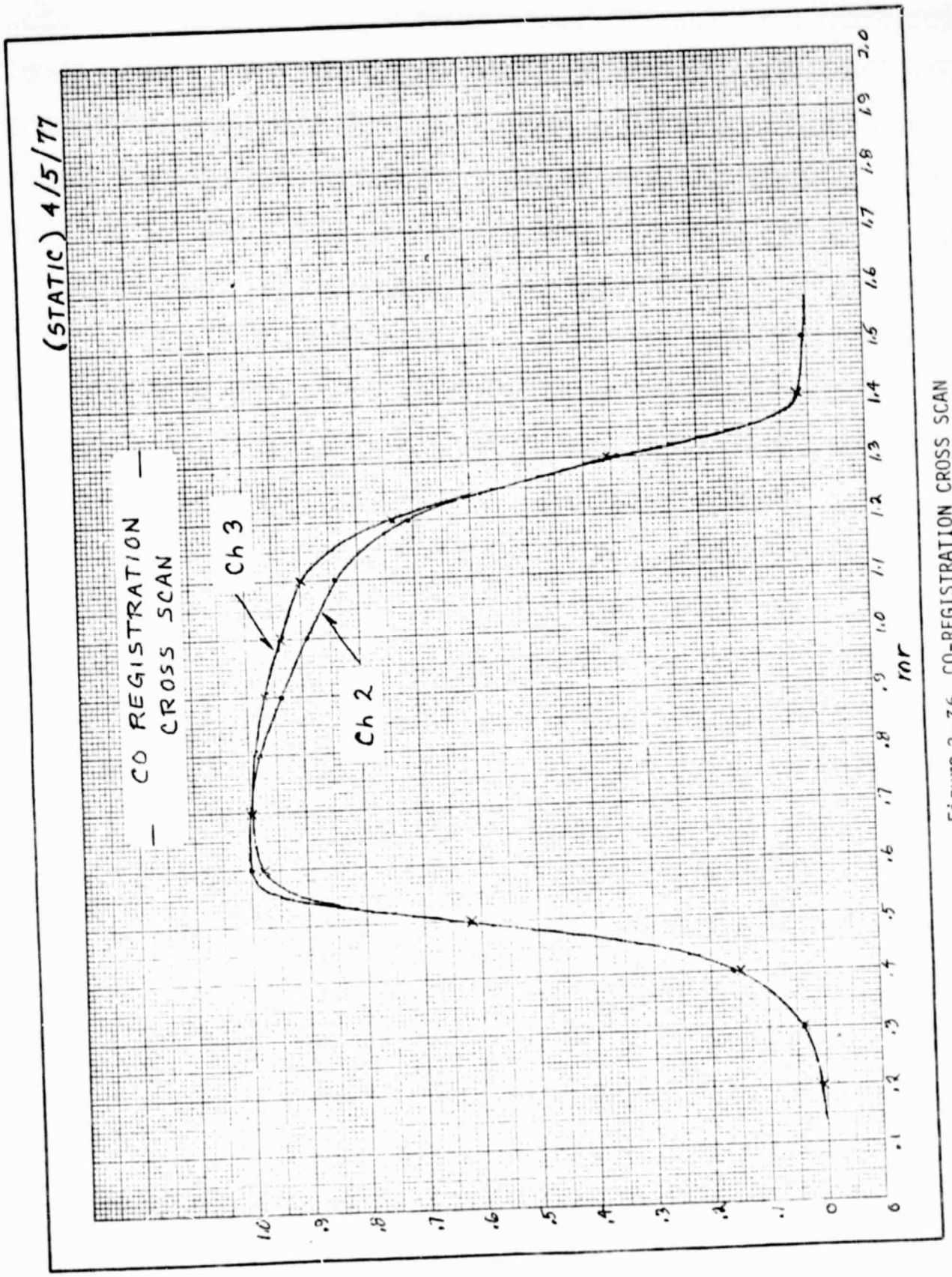

Figure 2-36 CO-REGISTRATION CROSS SCAN

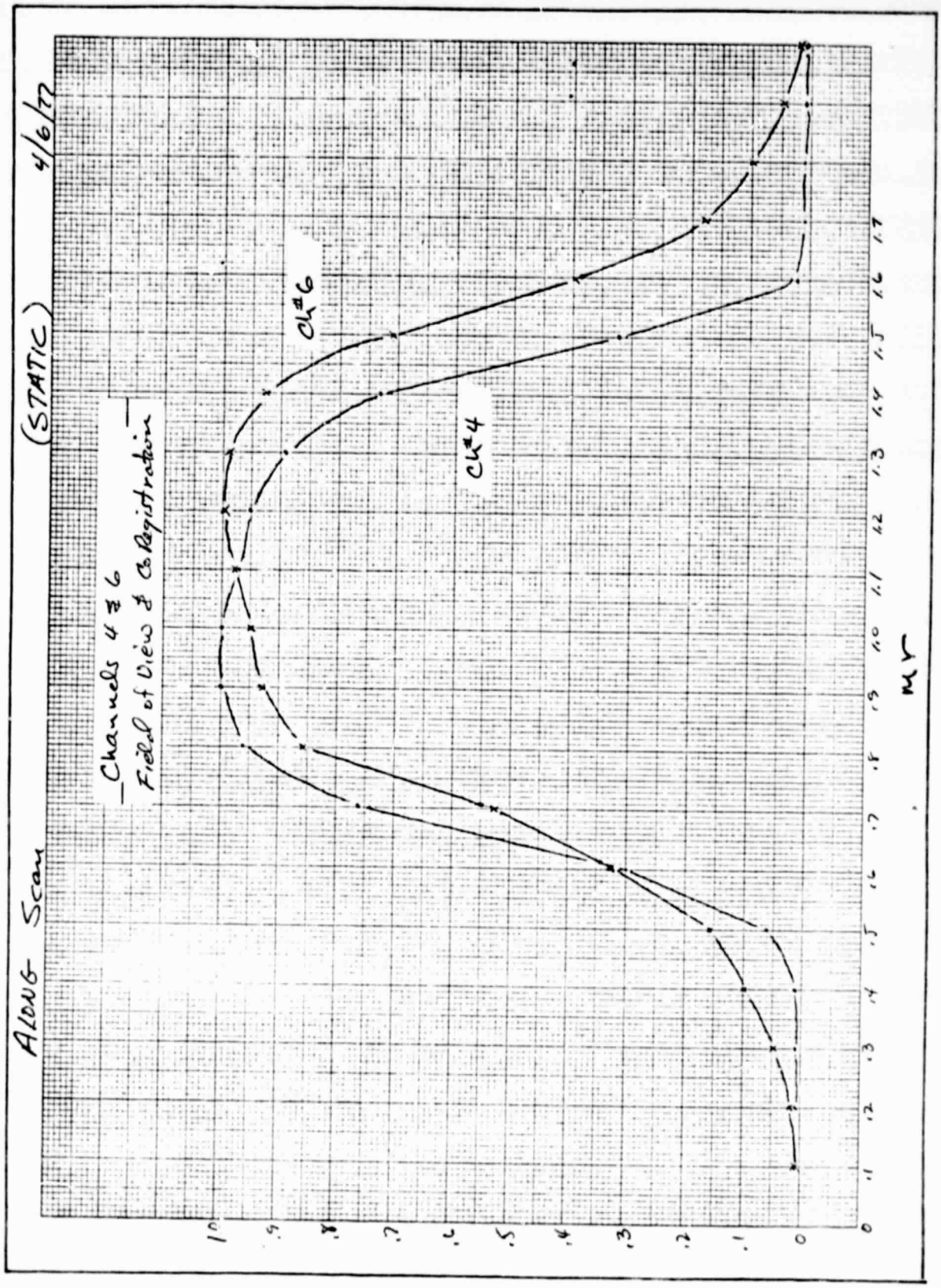

Figure 2-37 CHANNELS 4 & 6 FIELD OF VIEW & CO-REGISTRATION

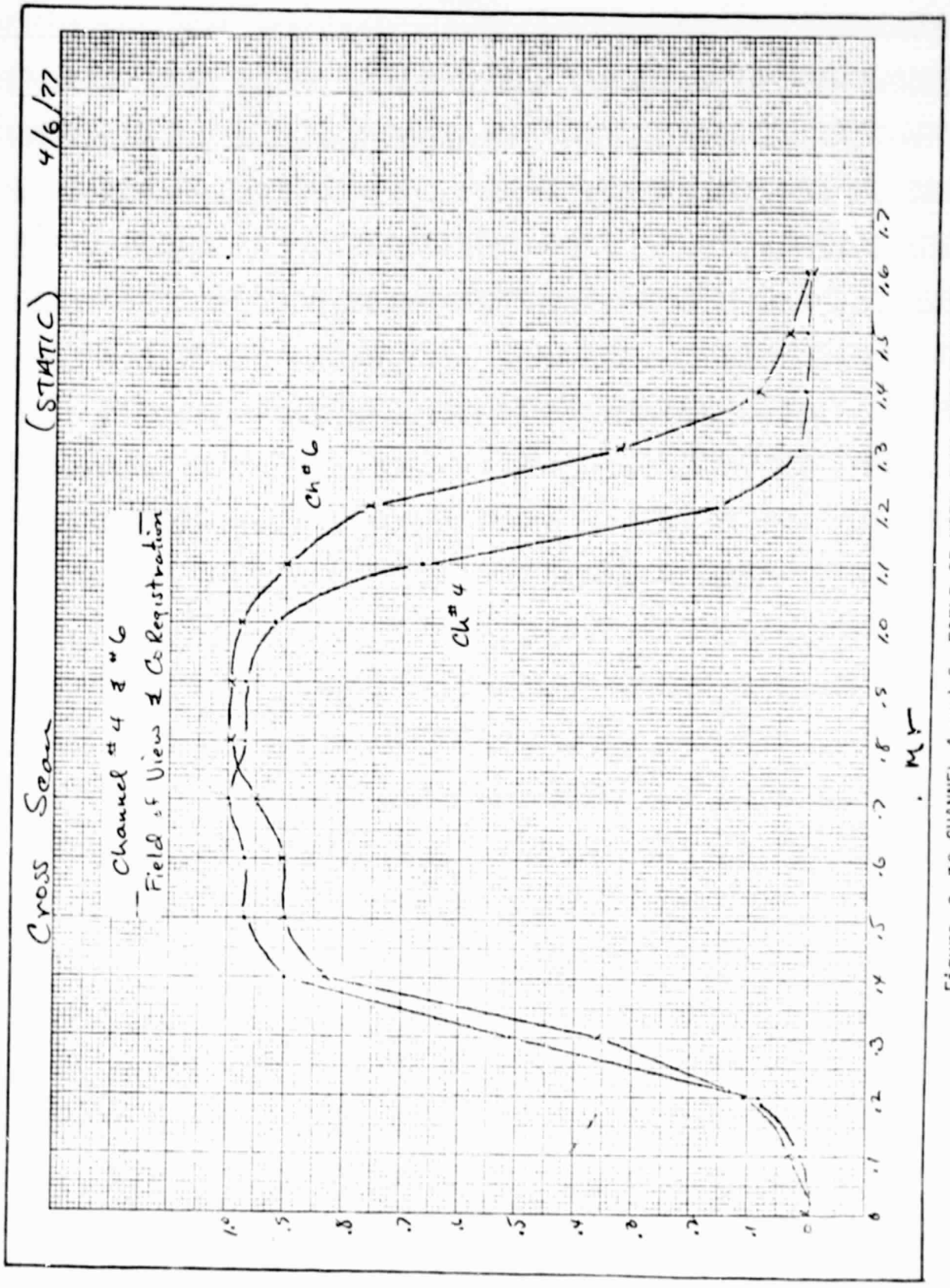

Figure 2-38 CHANNEL 4 and 6 FIELD OF VIEW & CO-REGISTRATION

2.1.6 Orbital Sequence Tests

It was previously stated in Section 2.1 that 117 Orbital Sequence Tests (OSTs) have been performed on the CZCS Protoflight. There are four types of OST's, designated A, B, C and D. The OST-A and OST-D tests are nearly identical and are performed at a line voltage of 24.5V. OST's B and C are identical to an OST-D except they are run at line voltages of 24.0 and 25.0 volts respectively. The OST-A differs from the others in that it includes channel 6 tests. The OST includes checks of electrical gain, signal to noise ratio, modulation transfer function, scan jitter, radiance response, response to inflight targets, and commands and telemetry. For OST-A tests, the channel 6 detector is cooled either by the bench cooler or, in the case of thermal vacuum, by a space simulation target.

The electrical gain check is the system level response to a 16 level staircase signal inserted at the front-end amplifier. The responses to steps 3, 8, and 13 were recorded for all OSTs and compared to previous levels. These levels have remained fairly constant except during high temperature excursions in vacuum. The problem was subsequently identified as a design problem in the d.c. restorer circuit and corrected prior to OST No. 110. Figure 2-39 shows the responses of channels 1-5 to step 13 under low gain, threshold off conditions. The baseline shift due to the d.c. restorer problem is particularly evident in channels 2 and 3 for high temperature OSTs (28-33, 37-42, 49-63 and 87-90). Also noticeable are the gain adjustments made to channels 1, 2 and 3 after the spectrometer was readjusted at OST No. 98 (see Section 2.1.2).

Radiance response measurements were made during OSTs using the MSS collimator as a source. A neutral density filter wheel was used to vary the source brightness without changing the spectral characteristics of the source. Imperfect repetition of alignment provides some output variability while lamp aging and contamination of collimator optics are the causes of other changes. A histogram of the responses of the various channels to this source is provided by Figure 2-40. Evident also in this figure are the thermally induced offsets identified in the Thermal Vacuum Test. Channel 6 response was also checked in OST-A's at a collimator blackbody temperature of 92°C. The signal to noise

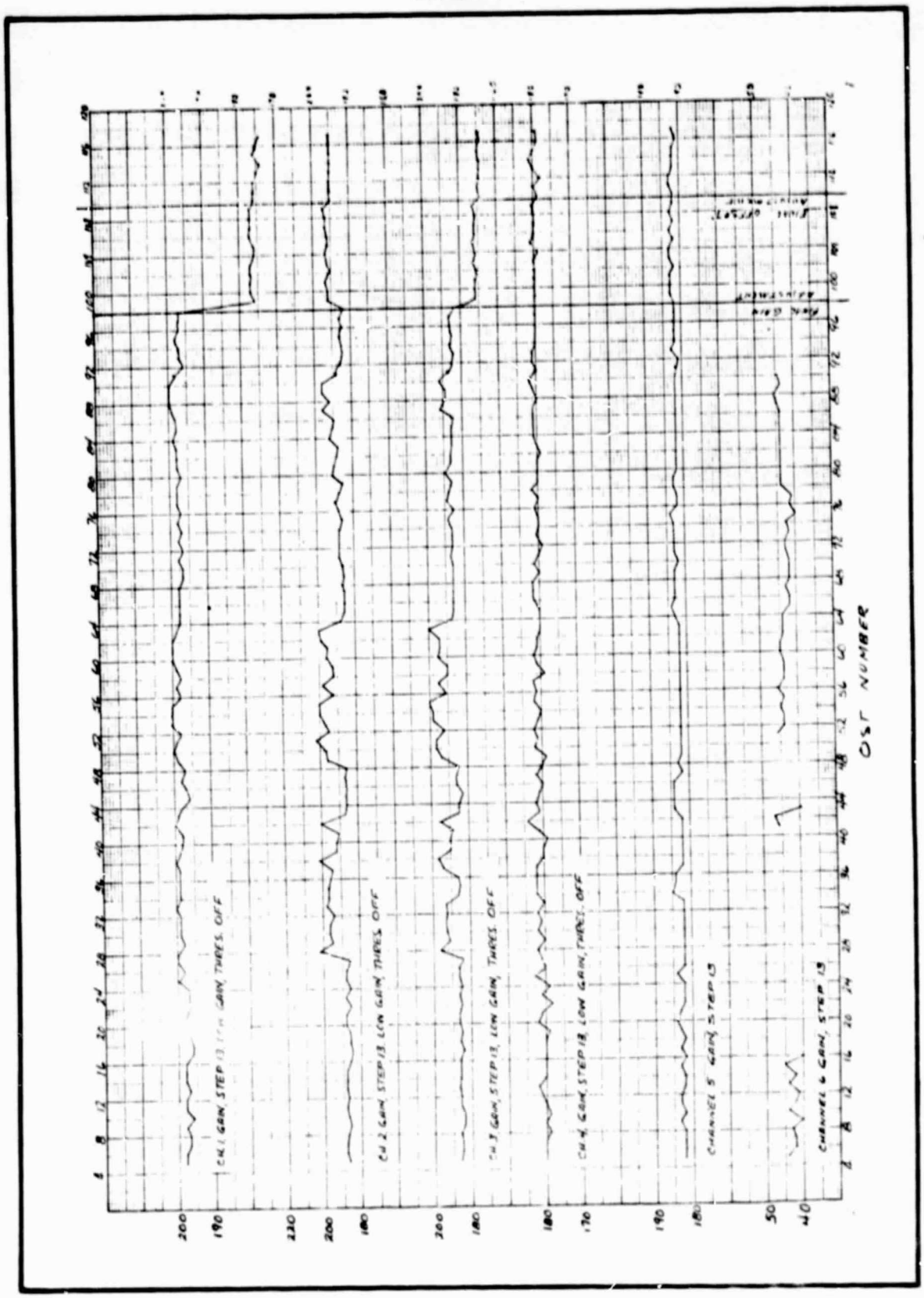

FIGURE 2-39 HISTOGRAM OF ELECTRICAL GAIN, CHANNELS 1-6

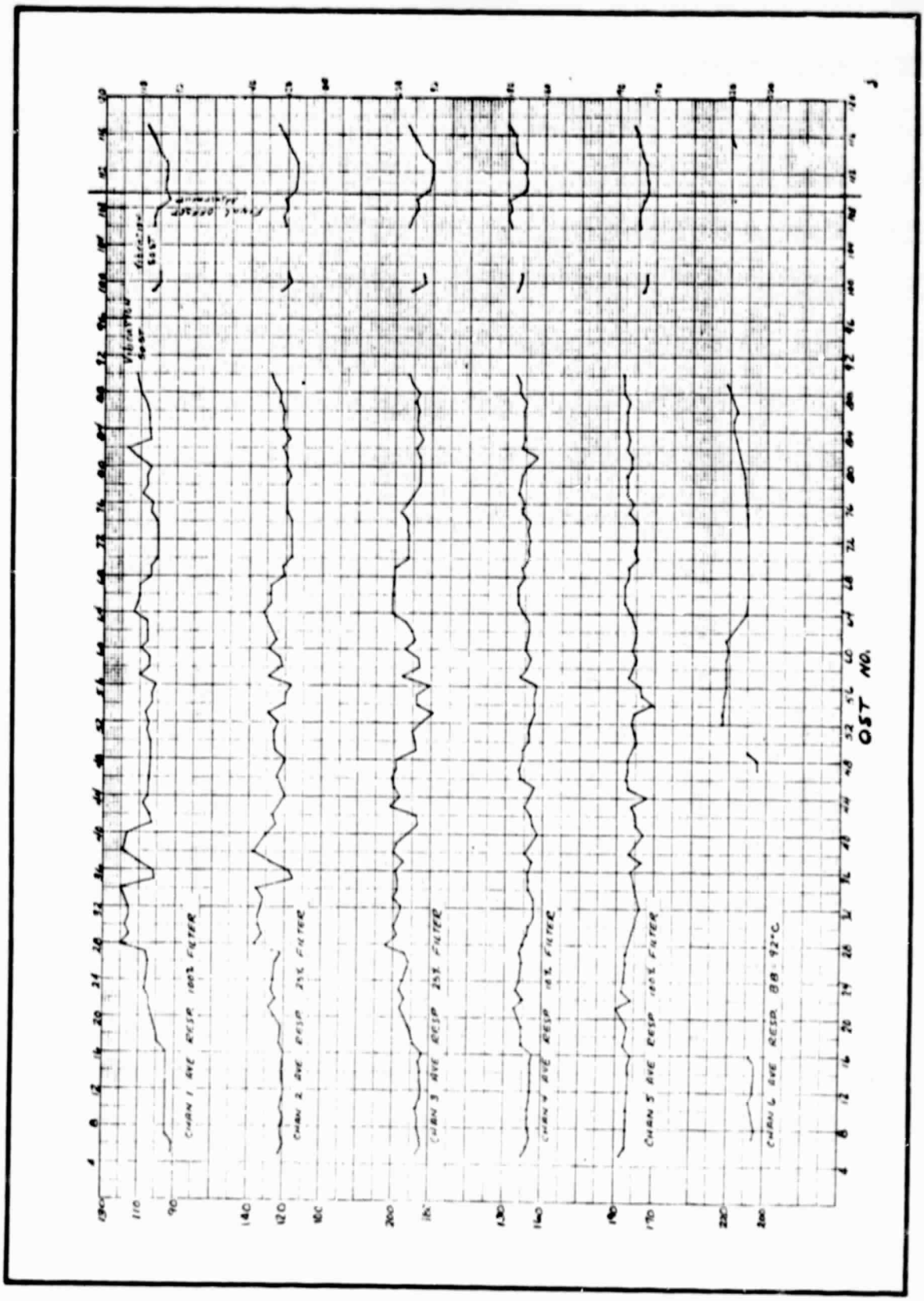

FIGURE 2-40 HISTOGRAM OF RADIANCE RESPONSE, CHANNELS 1-6

ratio was also checked at the same neutral density filter settings. Histograms of channel signal to noise ratios are found in Figure 2-41.

Here the variability is somewhat more random due, in large part, to the gaussian nature of the noise. The MSS collimator neutral density wheel would not stop at the 25 percent filter position after OST No. 76 and the ten percent N.D. position was used for channel 2 and 3 measurements until completion of the Thermal Vacuum test. Because of the variations in noise, the thermal offset is not readily apparent in these data.

Since MTF computations are based on measurement ratios, thermal offsets do not affect the results. Figure 2-42 is a histogram of 577 cycles/rad MTF's for the six channels. The variability is within the limits expected for the statistics involved.

The last of the histograms shows the responses of channels 1-5 to the internal visible calibration source and is designated as Figure 2-43. The thermal offset effects in channels 2 and 3 are sharply defined. The falloff in response, particularly at OST 97, is attributable to a problem in the visible calibration assembly (see Section 2.1.1). Particles from a black passivated steel spacer in the visible calibration assembly were loosened by vibration and coated a portion of the visible calibration optics. This reduced the output of that assembly much like a neutral density filter. The problem was solved by a small redesign and the gains of channels 1, 2 and 3 were adjusted after OST No. 98 accounting for the level changes after that point. The offsets were readjusted to remove the thermal sensitivity before OST 110 causing but minor output changes. This output from the BCU is a single, unaveraged sample, allowing the channel noise to affect the reading. As expected, channel 4, with its higher peak to peak noise, exhibits the greatest variability under normal circumstances. Also shown in Figure 2-43 is the temperature exposure history of the CZCS Protoflight and the sequence of the types of OSTs performed.

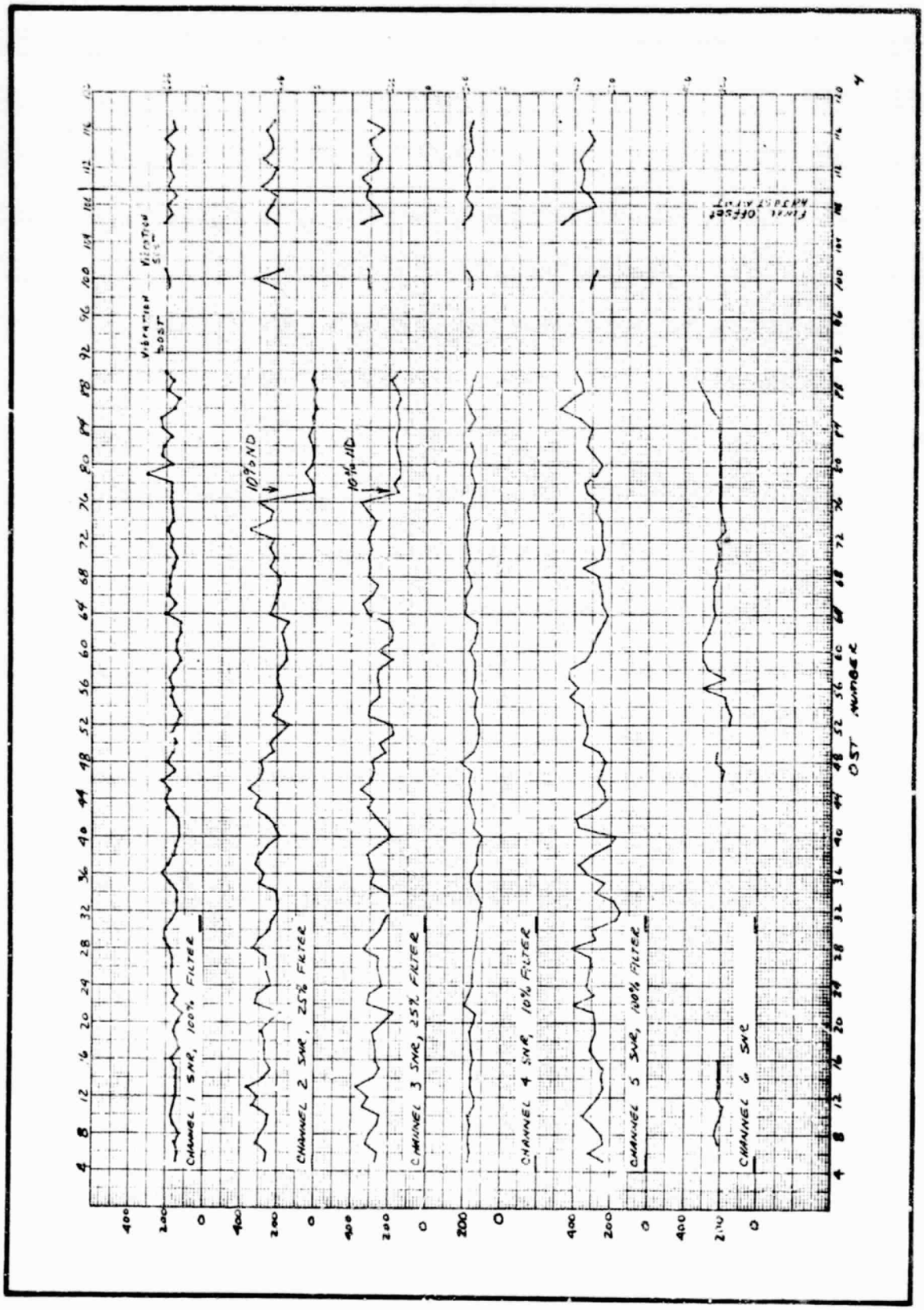

FIGURE 2-41 HISTOGRAM OF SIGNAL TO NOISE RATIOS, CHANNELS 1-6

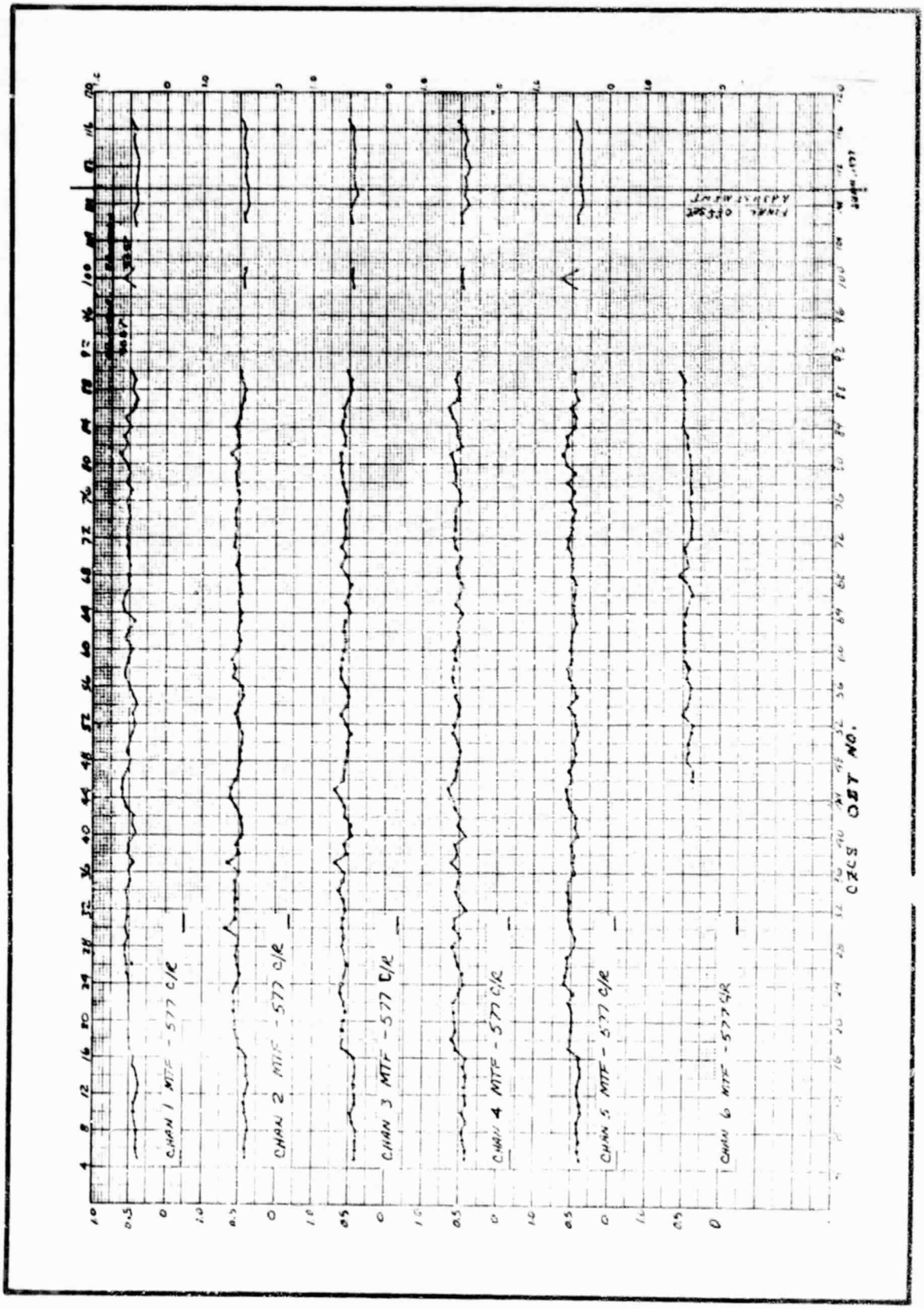

FIGURE 2-42 HISTOGRAM OF MTF AT 577 C/R FOR CHANNELS 1-6

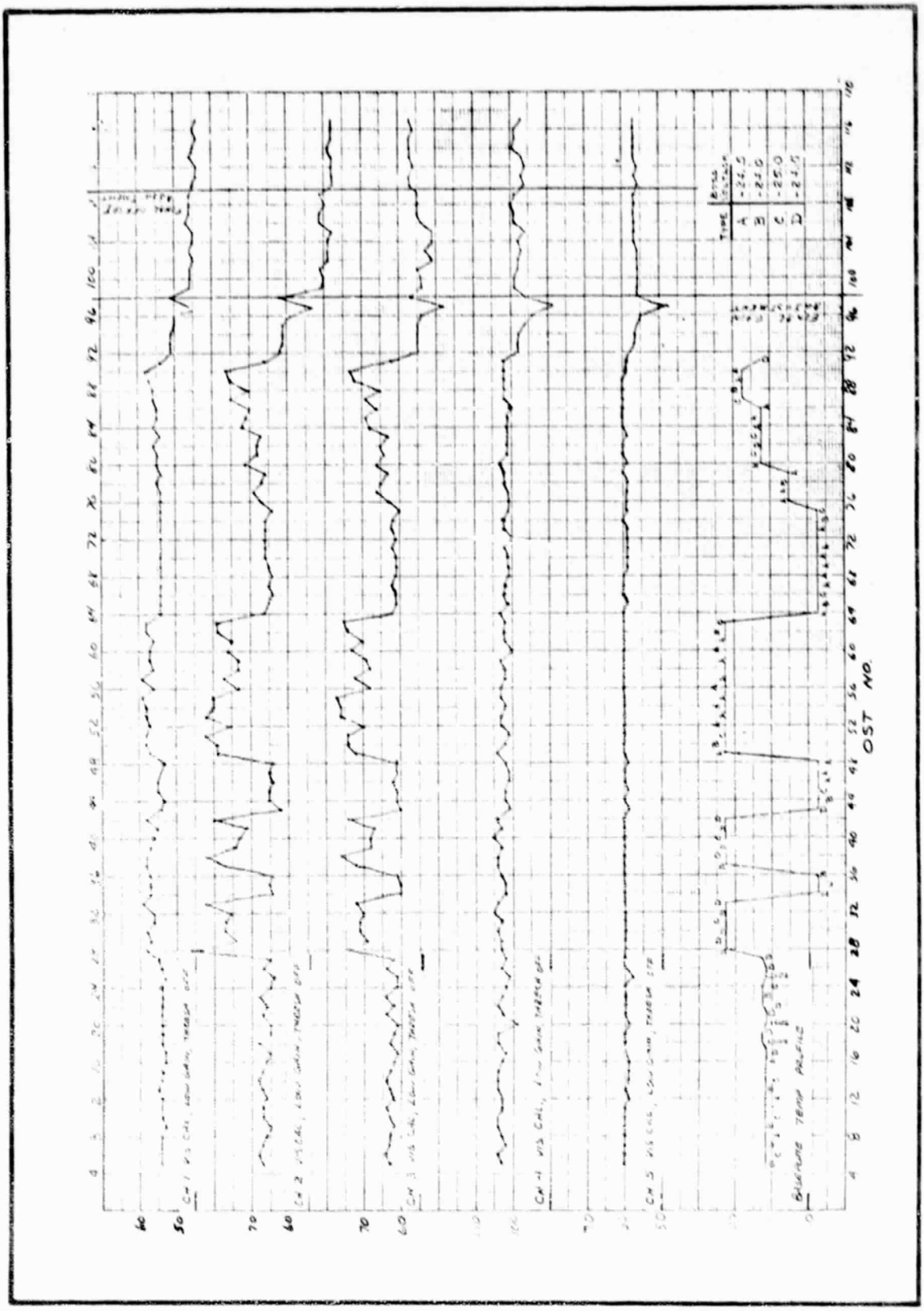

FIGURE 2-43 HISTOGRAM OF RESPONSE TO IN-FLIGHT CALIBRATION

2.2 PERFORMANCE EVALUATION

System and component level designs for the CZCS considered requirements as a primary driver. Calculations were made at the start of the program and, indeed, during the proposal phase to see if requirements could theoretically be met. Signal to noise ratios for channels 1-5, NETD for Channel 6 and MTF's for all channels were considered and analyzed at that time. A comparison of the theoretical results with the measured data for these parameters is provided in this section. In addition, a comparison of the measured Channel 6 spectral response against a theoretical composite using test data is presented. Where there are differences between the expected and the measured performance, these differences are discussed and, if possible, explained.

2.2.1 Signal to Noise Ratio, Channels 1-5

The peaking preamplification used in Channels 1-4 to achieve the required signal to noise ratios (see Volume 1) makes the noise characterization for those channels unique. There are seven noise terms in the signal to noise equation for Channels 1-4 not including photon fluctuation and quantization noise contributions. It can be shown that the noise current in these channels is:

$$I_n = \Delta f_n^{\frac{1}{2}} \left[2e(I_d + I_s) + \frac{4KT(R_1 + R_0)}{R_1 R_0} + I_{AN}^2 + \frac{Vn^2\ (R_1 + R_0)}{R_1 R_0} + \frac{[2\pi\ V_n(C_0 + C_1)\ \Delta f_n]^2}{3} \right]^{\frac{1}{2}}$$

where
- Δf_n = the system electronic noise bandwidth
- e = charge on an electron (1.6×10^{-19}C).
- I_d = photodiode dark current in A/ Hz
- I_s = $N_\lambda A\Omega\varepsilon\Delta\lambda S\alpha$ = signal current
- N_λ = radiance incident on the optical aperture
- A = area of the optical aperture
- Ω = the small angle field of view

ε = the optical efficiency

$\Delta\lambda$ = the spectral bandpass

S = the detector responsivity

α = an arbitrary degradation factor

K = Boltzmann constant (1.38×10^{-23} J/K)

T = Photodiode and preamplifier temperature

R_0 = Photodiode output resistance

R_1 = Feedback Resistance

I_{AN} = Preamplifier input noise current = 1×10^{-15}

V_n = Preamplifier (FET) noise voltage = 2×10^{-9}

C_0 = Photodiode and FET capacitance

C_1 = Feedback capacitance = 1×10^{-12} f.

The signal to noise ratio for these channels due to electrical noise is the signal current, i.e., $N_\lambda A\Omega\varepsilon\Delta\lambda S\alpha$, divided by the noise term above. Two other noise contributors are significant. These are the noise due to uncertainties in the quantization level and noise due to fluctuations in the number of photons in the scene. Analog to digital convertion or quantization produces a noise, the RMS value of which is the least significant bit divided by the square root of 12. ([1]) If the signal is 120 counts or DN, the signal to noise limit imposed by the A/D converter is $120 \times \sqrt{12}$ or 416.

At these wavelengths, photon fluctuations impose a limitation on the signal to noise ratio equal to the number of photons incident in the detector in one integration period. ([2]) Since there are λ/hc photons per watt second at wavelength λ, where h is Planck's constant and c is the speed of light, we can say there are hc/λ watts per photon per second incident on the detector. The power incident on the detector is merely $N_\lambda A\Omega\varepsilon\Delta\lambda$ and the integration period is $1/2\Delta f$. The number of photons incident on a detector at wavelength λ is then:

([1]) M. Schwartz, Information Transmission and Noise, p. 329.

([2]) W. Wolfe, et.al., Handbook of Military Infrared Technology, NRL, GPO, 1965, p. 513.

$$\frac{N_\lambda A\Omega\varepsilon\Delta\lambda}{(hc/\lambda_0)(2\Delta f)}$$

and the signal to noise ratio is the square root of that number. A composite or net signal to noise ratio can then be calculated from the three effects as:

$$S/N_{NET} = [S/N_E^{-2} + S/N_Q^{-2} + S/N_P^{-2}]^{-\frac{1}{2}}$$

Table 2-2 summarizes the values for the parameters contributing to the electronic noise. The noise current for Channel 5, which does not use or need peaking preamplification is:

$$I_N = 2\Delta f_n^{\frac{1}{2}}[2eN_\lambda A\Omega\varepsilon\Delta\lambda S\alpha + 2eI_d + \frac{4kT}{R_1}]^{\frac{1}{2}}$$

A summary of the signal to noise ratios for electrical, quantization, and photon fluctuation noises is provided by Table 2-3. These values are calculated at four spectral radiance levels for each channel. The net values are compared to measured values in the last two columns.

The most predictable thing about noise models is their unpredictability. While the calculated data have the same general characteristics shown by the measured data of Figures 2-8 through 2-12, only Channel 4 shows good agreement between measured and calculated values. This channel also has the highest electrical noise, making it more predictable than the other four channels. Fortunately, signal to noise ratios measured at the specified spectral radiance levels exceed the calculated values except in Channel 5. The measured signal to noise ratios are calculated from the ratio of the average of 100 samples to the standard deviation of those 100 samples. Channel 5 has frequently generated a sample set for which the standard deviation is zero and the SNR is, therefore, infinite. These data are not used in the compilation of data for reported SNR characteristics for Channel 5 and may be a factor in the reduced (although acceptable) SNR levels of that channel. It should also be noted that Channel 5 is quantization noise limited and photon noise has little, if any effect.

Table 2-2

Noise Influence Parameters, Channels 1-5

Channel	1	2	3	4	5
λ_0 (μm)	.442	.5205	.5506	.6691	.7488
Ω (SR)	6.6×10^{-7}	6.4×10^{-7}	6.44×10^{-7}	6.47×10^{-7}	6.64×10^{-7}
$\Delta\lambda$ (μm)	0.022	0.0206	0.020	0.019	.1005
Δf_n (Hz)	2.909×10^{4}	2.82×10^{4}	2.98×10^{4}	2.84×10^{4}	2.61×10^{4}
R_1 (ohms)	2×10^{8}	2×10^{8}	2×10^{8}	2×10^{8}	1×10^{6}
R_0 (ohms)	1×10^{9}	3.13×10^{8}	5.56×10^{8}	8.33×10^{8}	--
C_o (farads)	15.7×10^{-12}	15.3×10^{-12}	15.7×10^{-12}	15.3×10^{-12}	--
I_d (A.)	2.4×10^{-10}	2.8×10^{-10}	2.3×10^{-10}	1.8×10^{-10}	7.8×10^{-9}
S (A/W)	0.289	0.33	0.34	0.47	.454
N_λ ($Wcm^{-2}SR^{-1}\mu m^{-1}$)	5.4×10^{-3}	3.5×10^{-3}	2.86×10^{-3}	1.34×10^{-3}	1.08×10^{-2}
ε	0.35	0.41	0.42	0.34	0.27
Signal at N_λ (counts)	122	112	116	117	114

Table 2-3

Signal to Noise Ratio Summary for Channels 1-5

Channel	Signal N_λ $Wcm^{-2}sr^{-1}\mu^{-1}$	Calculated S/N Electronic	Calculated S/N Quanitzation	Calculated S/N Photon	Calculated S/N Net	Measured S/N Net
1	1×10^{-3}	113	80	209	62	53
1	2×10^{-1}	194	156	296	112	105
1	3×10^{-3}	258	232	362	156	154
1	* 5.41×10^{-3}	380	423	486	244	260
2	1×10^{-3}	125	111	238	78	89
2	2×10^{-3}	215	223	336	141	168
2	3×10^{-3}	287	334	412	192	238
2	* 3.5×10^{-3}	319	388	445	216	260
3	$.5 \times 10^{-3}$	74	69	158	48	72
3	1.25×10^{-3}	157	177	266	107	156
3	2.0×10^{-3}	222	281	336	154	200
3	* 2.86×10^{-3}	285	402	402	201	233
4	$.5 \times 10^{-3}$	84	154	167	67	61
4	1×10^{-3}	148	303	236	116	114
4	* 1.3×10^{-3}	185	405	273	143	144
4	2×10^{-3}	246	606	334	188	182
5	6×10^{-3}	454	218	1325	194	162
5	8×10^{-3}	591	293	1530	262	206
5	* 10×10^{-3}	771	395	--	352	265
5	12×10^{-3}	845	440	--	390	290

*specified level

Data sets with a greater number of samples would probably provide improved correlation between calculated and measured data assuming variations in target radiance would not add a fourth, spurious term to the system noise.

While Channels 1 and 4 show fairly good agreement between measured and calculated SNR's, Channels 2 and 3 show the greatest disparity, with the measured values consistently higher. There are no good explanations for this and we can merely conjecture about the cause. Errors in optical and detector component measurements, overstatement of quantization or photon fluctuation effects or uncertainties in the target calibration are all possibilities. We feel that the quantization noise contribution, while properly calculated, may be level dependent or require more samples for statistical accuracy.

2.2.2 Channel 6 NETD

The Noise Equivalent Temperature Difference (NETD) of Channel 6 is required to be 0.25K at a 270K scene on target. The NETD is the Noise Equivalent Radiance (NEN) divided by the slope of the radiance curve with temperatures at 270°K. That is,

$$\text{NETD} = \frac{\text{NEN}}{dN/dT} \text{ at } T = 270\text{K}.$$

Based on measured component values for transmission, detector D*, field of view, etc., and calculated values of preamplifier noise and quantization noise, we would expect a NETD of 0.106K. Measured NETDs for the Engineering and Protoflight Models place the NETD at 0.25K, however. The possible sources of additional noise are:

1. Excess amplifier noise
2. Line to line d.c. resistor drift
3. Detector temperature drift
4. Target temperature drift

To assess the excess amplifier noise contribution, the other three terms were analyzed for worst case contributions. The D.C. restorer was designed to place no more than a 10 millivolt drift in the output from line to line. This has an RMS value of 0.091 DN which is nearly insignificant. The detector is temperature controlled to have no more than a 0.1°C temperature excursion. This causes a slight change in the detector responsivity which has a temperature coefficient of 3.6% per °C at 120K. The resulting error has a RMS value of 0.288 DN. Due to its thermal mass and control, the Full Aperture Infrared (FAIR) target is not expected to change more than 0.1°C in a sample period of slightly more than 12 seconds (100 samples = 12.375 seconds). This small change has a RMS value corresponding to 0.139 D.N.

The expected noise, from which the 0.106K NETD was calculated, corresponds to 0.416 DN. To get to a noise level of 0.981 DN which was measured during the Thermal Vacuum tests, the excess amplifier noise at a minimim is:

$$[.981^2 - .416^2 - .091^2 - .288^2 - .139^2]^{\frac{1}{2}} = .824 \text{ DN.}$$

The noise levels of the various modules which make up the Channel 6 amplifier were separately measured and found to be in the range of expectation. No test was made on the overall amplifier as final gain and offset adjustments are made at the system level. Because of this, the most suspect source of potential noise are the ±12 volt regulators used in this channel.

2.2.3 Channel 6 Spectral Response

The measured spectral response of Channel 6 at the system level correlates quite well with a composite curve made up from vendor supplied data. Suppliers of the Channel 6 field lens, cooler window, aplanatic lens and focussing lens/interference filter provided transmission curves for each component. While reflectance measurements were also provided for the various mirrors and the dichoic beam splitter, the responses were quite flat over the wavelengths of interest and the composite response combines the transmission characteristics with the detector spectral response. Figure 2-44 shows the comparison between the calculated composite and the measured system response.

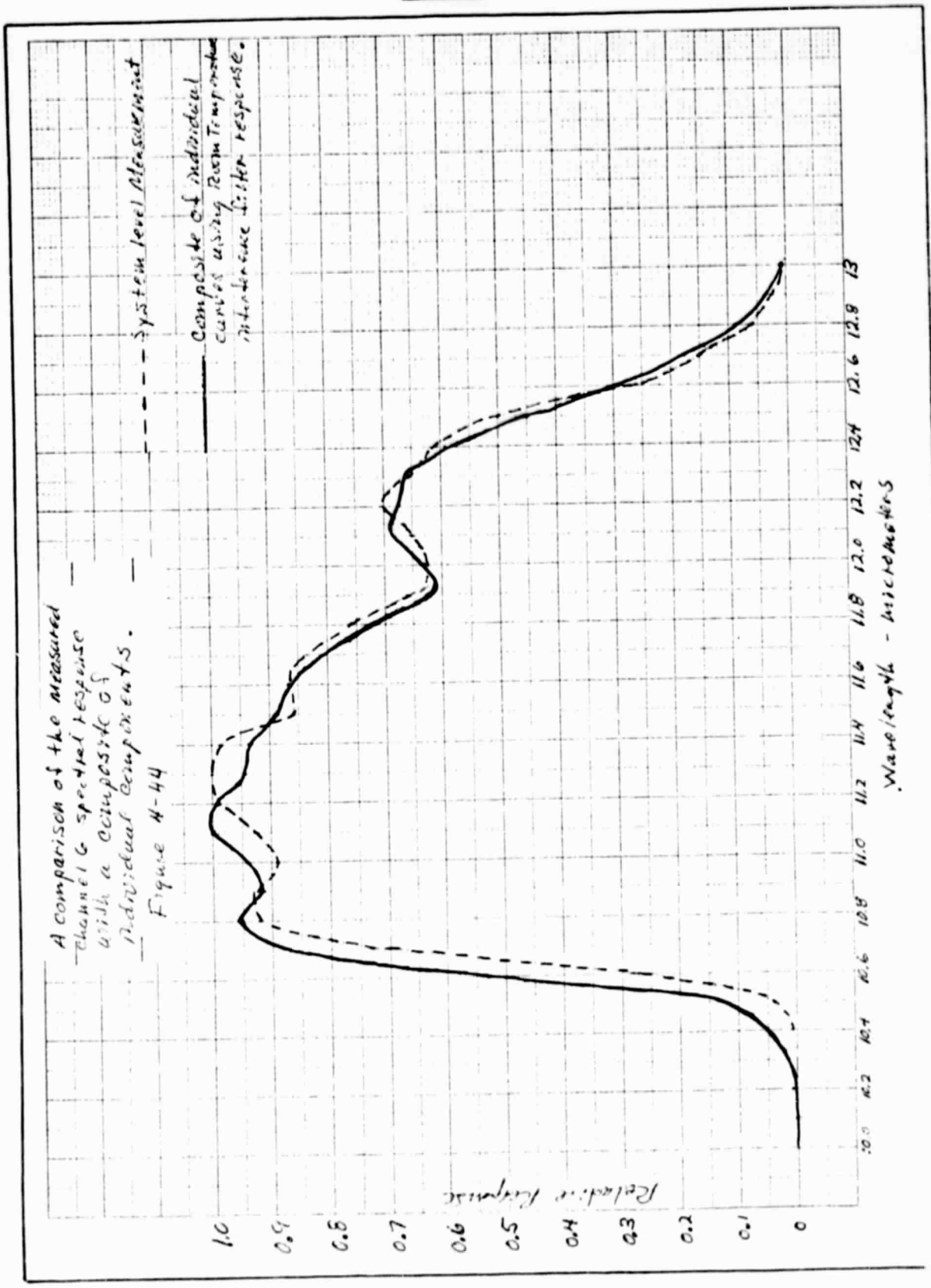

Figure 2-44 A COMPARISON OF THE MEASURED CHANNEL 6 SPECTRAL RESPONSE WITH A COMPOSITE OF INDIVIDUAL COMPONENTS.

It should be noted that ince the measured response is made on the bench with the bench cooler cooling the Channel 6 detector, the cooler outer stage and therefore the filter/focussing lens is at room temperature. Accordingly, the comparison is made using the vendor supplied room temperature characteristic response of the filter. Under orbital conditions the outer stage will operate at approximately 200K or -73°C. The lower 50% wavelength will decrease by approximately 1.1×10^{-3} micrometers per °C as it cools. The lower 50% wavelength will shift from the measured 10.65 micrometers to approximately 10.55 micrometers in operation under normal orbital conditions. The upper 50% wavelength will decrease by about 5.8×10^{-4} micrometers per °C and should decrease to about 12.45 micrometers from the measured 12.5 micrometers when in orbit.

The measured 50% response wavelengths are 10.65 and 12.5 micrometers as shown while the composite indicates 10.59 and 12.47 micrometers. Considering the potential for error inherent in both the vendor measurements and the system level measurement, the correlation is quite acceptable. The most critical components are the interference filter and the detector. The former has the greatest effect on the 50% response parts while the letter affects the peak response wavelength the most. Small errors in either component measurement could cause the differences shown. The accuracy of the system level measurements are also not beyond question. The McPherson Model 218 monochromator outputs unwanted orders which contaminate the spectral purity. Because of this, the response of a known filter was measured with the monochromator and correlation factors generated for each wavelength. While there are potential inaccuracies associated with this arrangement, it should be noted that the inaccuracy of the lower 50% wavelength measurement from the composite is less than 0.6%.

2.2.4 Modulation Transfer Function Evaluation

The components of the system Modulation Transfer Function (MTF) are discussed in Volume 1. An analysis based on the measured fields of view was made which also included the effects of the optics, presampling filter, and sampling. A field of view of 0.815 mrad was used for Channel 6. A comparison of measured and calculated results is presented in Table 2-4.

TABLE 2-4

Measured vs. Calculated MTFs at Three Spatial Frequencies

Channel	578 cycles/rad		385 cycles/rad		289 cycles/rad	
	Measured	Calculated	*Measured	Calculated	Measured	Calculated
1	.383	.461	.735	.813	.91	.965
2	.378	.461	.715	.813	.886	.965
3	.464	.461	.805	.813	.974	.965
4	.444	.461	.755	.813	.991	.965
5	.402	.461	.745	.813	.918	.965
6	.368	.380	.722	.748	.900	.903

*Interpolated from 578 cycles/rad and 289 cycles/rad measurements.

The variance in the measured results is primarily a sampling problem. Measurements at 578 cycles/rad were based on three cycles at that frequency while measurements at 385 cycles/rad and 289 cycles/rad had but two cycles and 1.5 cycles respectively. This was due to the collimation field angle being limited geometrically to 0.3°. Figure 2-42 in Section 2.1.6 is a histogram of repetitive measurements of the MTFs of the six channels at 577 cycles/rad. This shows that the MTFs of Channels 1 through 5 average approximately 0.5 while the Channel 6 MTF averages approximately 0.45.

Section 3
IN-ORBIT PERFORMANCE

Since its launch on October 24, 1978, the Coastal Zone Color Scanner has returned data, upon command, without any problems. This data can be divided into two categories. First and most important is the science or radiometric data. This data is reduced by the scientists on the Nimbus Experiment Team (NET) to obtain the desired data products showing the chlorophyll and sediment concentrations and sea surface temperatures. The second class of data is the housekeeping or diagnostic data. This is provided for engineering use only and provides information on the day to day health or status of the instrument.

3.1 RADIOMETRIC DATA

The radiometric or science data consists of an eight bit word for each of the six spectral bands for each picture element or data sample. Each data word is proportional to the radiance within its spectral band. The spectral bands are shown for reference in Table 3-1.

Table 3-1
CZCS Spectral Bands

Channel No.	Center Wavelength, μm	Wavelength Range, μm
1	0.443	0.433 - 0.453
2	0.520	0.510 - 0.530
3	0.550	0.540 - 0.560
4	0.670	0.660 - 0.680
5	0.750	0.700 - 0.800
6	11.5	10.5 - 12.5

The final data products, maps showing both chlorophyll and sediment concentrations as well as sea surface temperatures, are the responsibility of NOAA-NESS and NASA-Goddard. Figure 3-1 shows the present flow in the data processing to arrive at the final derived data products.

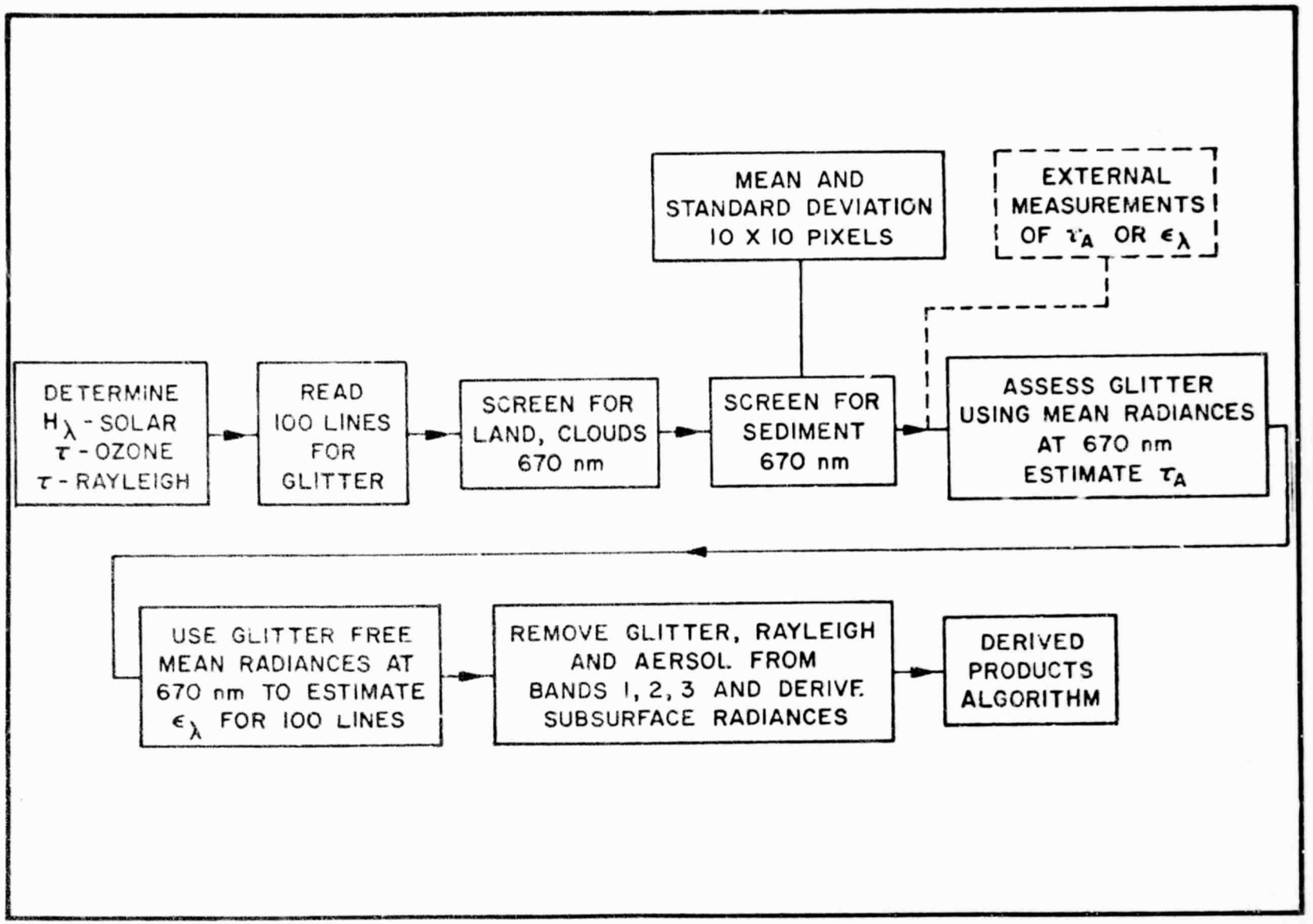

FIGURE 3-1 CZCS ATMOSPHERIC CORRECTION ALGORITHM FLOW

Before the derived products algorithms can be used, the radiances at the surface of the water for Channels 1, 2 and 3 must be determined. These are calculated by subtracting the Rayleigh scattering and aerosol scattering components from the radiances in each band as measured at the satellite. The Rayleigh component for each channel is calculated as a function of sun angle and path length to the surface. The aerosol scattering components are determined using the measured response in Channel 4. The scene is scanned for a cloud free, sediment free area of 10 x 10 pixels over water. The mean and standard deviation of the 100 pixels is calculated. If the standard deviation is less than a predetermined value, that portion of the scene is considered glitter free and the measurement totally due to aerosol scattering. The aerosol scattering component in channels 1, 2 and 3 is then calculated from the mean of the 10 x 10 pixel area and the ratio of the solar spectral content in the respective channels. Expressed mathmatically for Channel 1,

$$L_{A443} = L_{A670} \left(\frac{L_{S443}}{L_{S670}}\right)$$

where

L_{A443} is the aerosol scattering component in Channel 1

L_{A670} is the mean of the 10 x 10 pixel area for Channel 4 and therefore is the measured aerosol component in Channel 4.

L_{S443} and L_{S670} are the relative amounts of radiant power in each of the respective spectral bands due to the solar spectral response.

These three aerosol components, for Channels 1, 2 and 3, are used to correct 100 lines of data before a new 10 x 10 pixel area is examined and new correction factors calculated.

In summary, the glitter free, scatter free data is determined from the following expressions:

$$L_{W443} = L_{M443} - L_{R443} - L_{A443}$$

$$L_{W520} = L_{M520} - L_{R520} - L_{A520}$$

$$L_{W550} \quad L_{M550} - L_{R550} - L_{A550}$$

where

L_W = estimate of the radiance at the surface of the water in the specified spectral bond.

L_M = measured radiance at the satellite in the specified spectral band.

L_R = Rayleigh scattering component in the specified band calculated from the sun angle and path length to the surface.

L_A = Aerosol scattering component in the specified spectral band based on a glitter free 10 x 10 pixel sample in the 670 nm band.

The final data products are calculated from the ratios of the radiances in certain channels. Scientists on the Nimbus Experiment Team have tried various ratio combinations and have found that the following equations produce the best correlation to surface truth measurements.

$$\text{chlorophyll plus phaeophytin concentration} = a \left(\frac{L_{W443}}{L_{W550}}\right)^b$$

$$\text{suspended matter (sediment) concentration} = c \left(\frac{L_{W443}}{L_{W520}}\right)^d$$

Final data products using these algorithms should be available from IPD at Goddard in mid 1979.

Figures 3-2 through 3-5 are some examples of the raw science data being returned by CZCS. Several things should be noted with regard to this data.

- The gains in Channels 1 through 4 are scaled for the expected reflected radiances from water. Therefore land areas, especially in Channels 3 and 4, will be very saturated.

- Channel 5 detects vegetation and shows the best contrast over land. It is also good for detecting clouds.
- All of the data is uncorrected, with no subtraction of scattering or ratios of channels.
- Channel 6 was turned off at the time all of the data was taken.

The photographs in Figure 3-2 are from the laserfax quick-look data from the Nimbus ground station showing the western part of the Gulf of Mexico, the Gulf coast of Texas and parts of Mexico. This data was taken on October 30, 1978. A couple of points to note in the data are the apparent plumes of unknown origin off the shore of Tampico, Mexico and in the Laguna de Tamiahua, south of Tampico.

The photographs in Figure 3-3 show the southern part of the Mediterranean Sea and northern Africa, including the mouth of the Nile River and the Suez Canal. These photographs were produced from the raw science data by IPD of GSFC. Note the increased annotation on these photographs.

Figures 3-4 and 3-5 are additional photographs showing the Gulf of Mexico around the Florida coast and the areas around Monterey Bay, California.

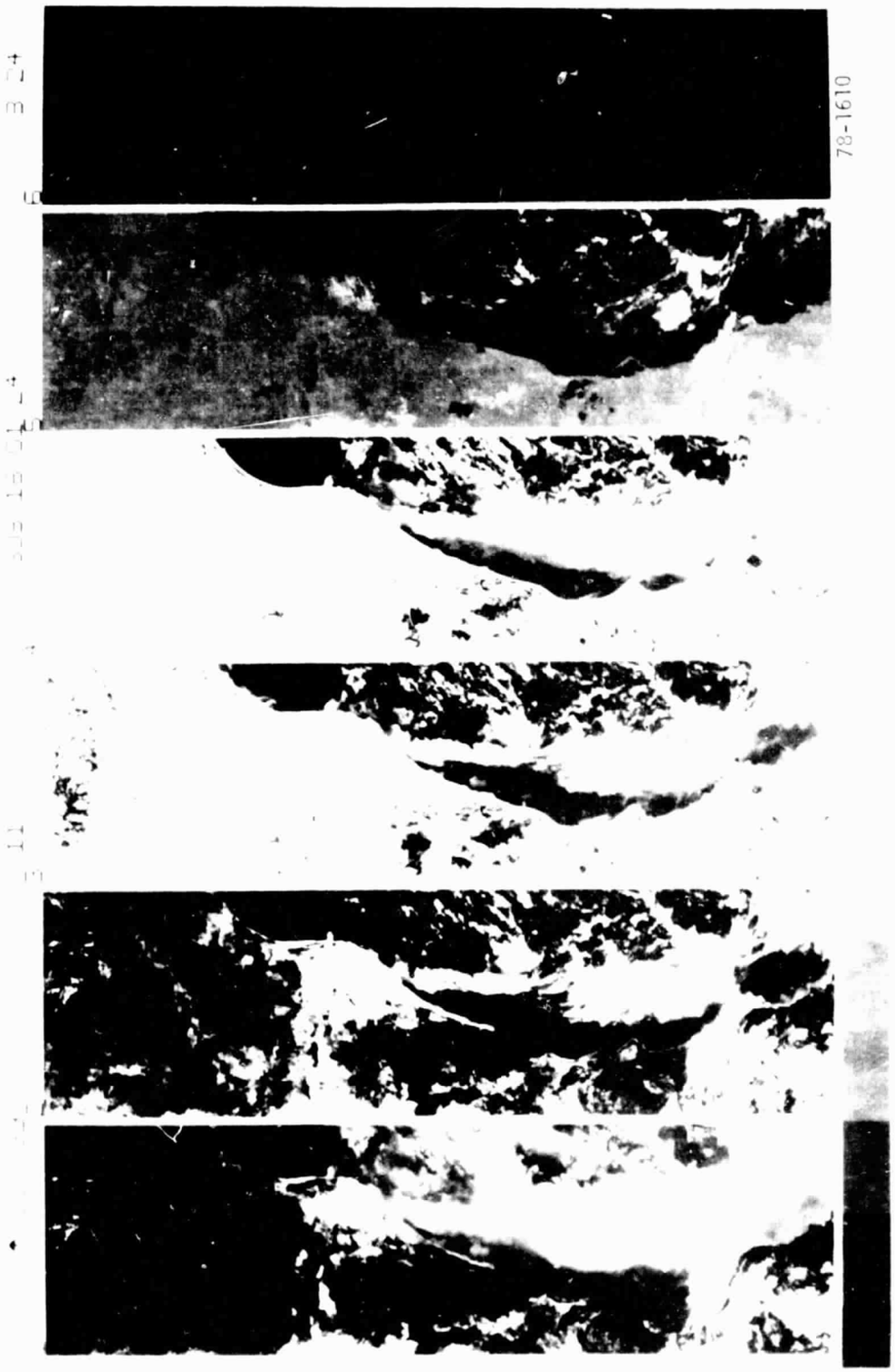

Fig. 3-2 (a) QUICK LOOK DATA FOR CHANNELS 1 THROUGH 5 OVER THE GULF OF MEXICO

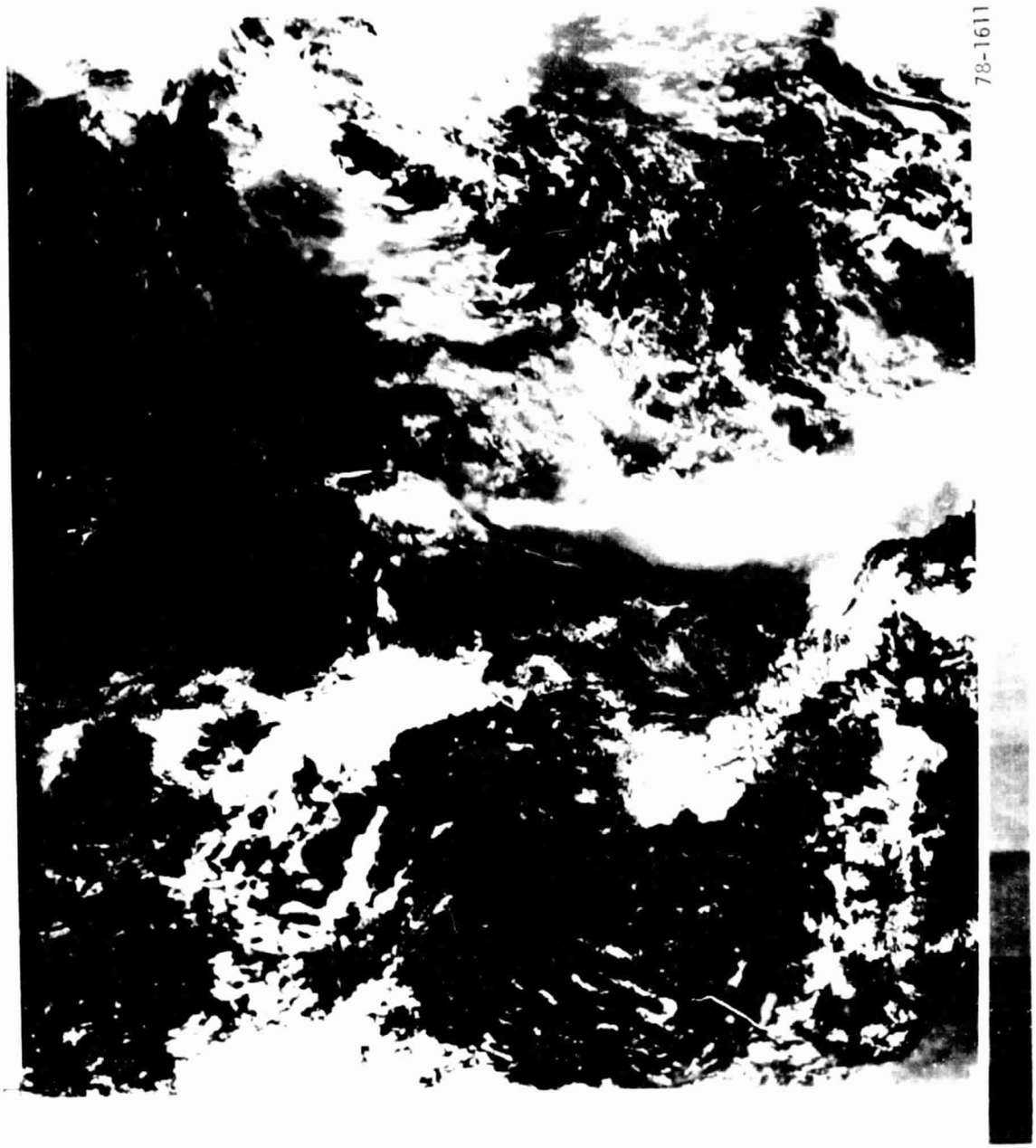

Fig. 3-2 (b) CHANNEL DATA

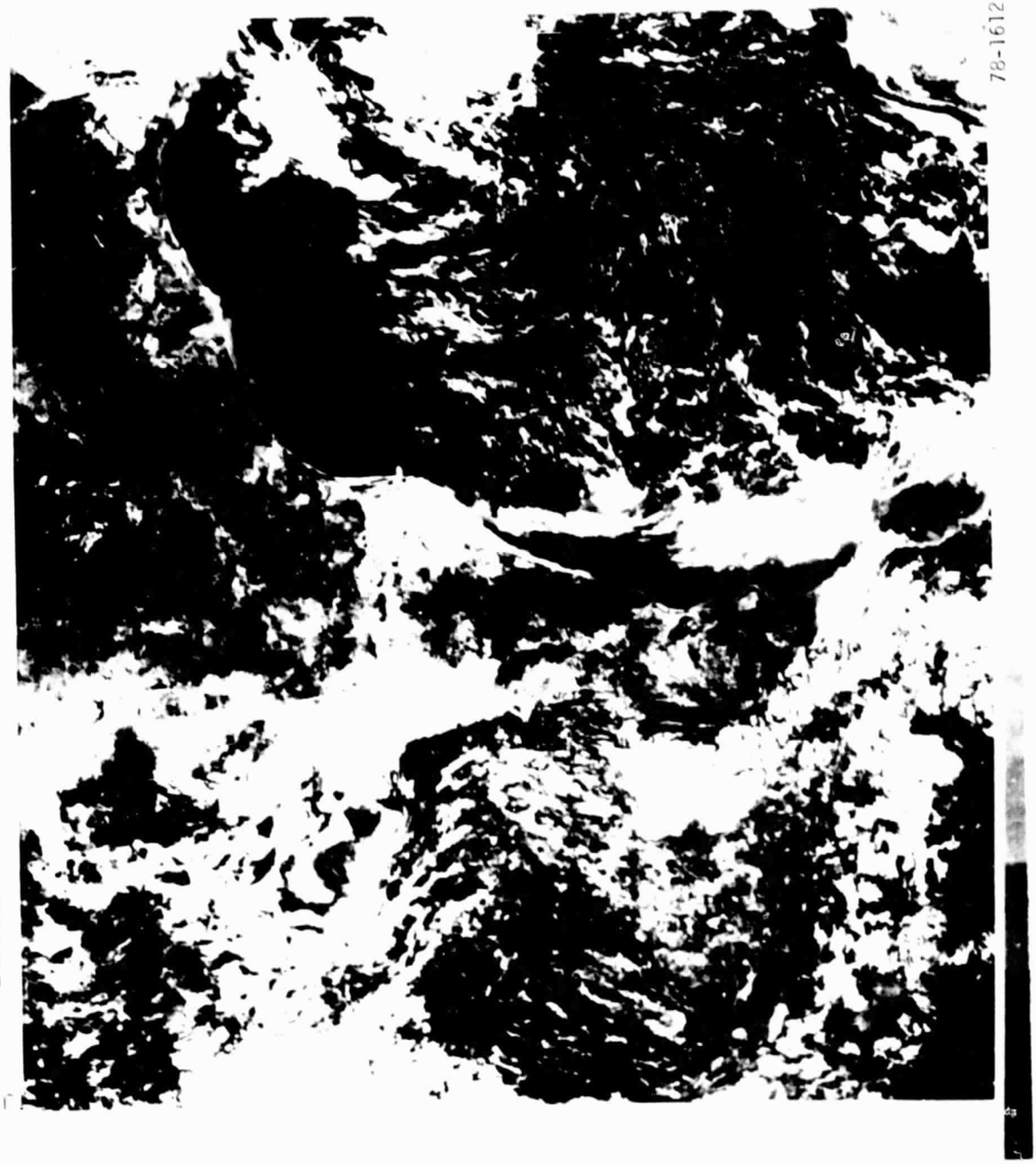

Fig. 3-2 (c) CHANNEL 2 DATA

Fig. 3-2 (d) CHANNEL 3 DATA

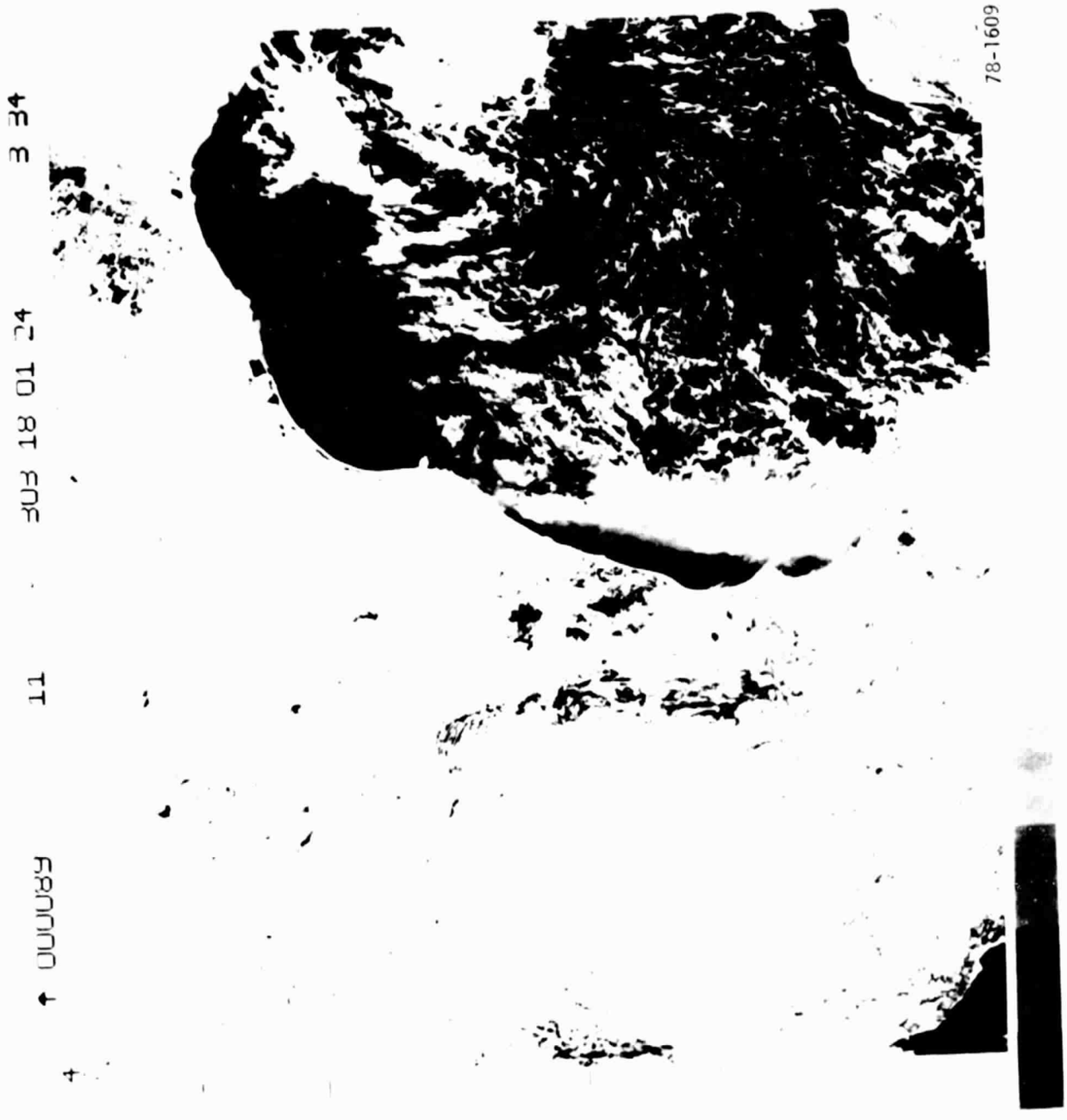

Fig. 3-2 (e) CHANNEL 4 DATA

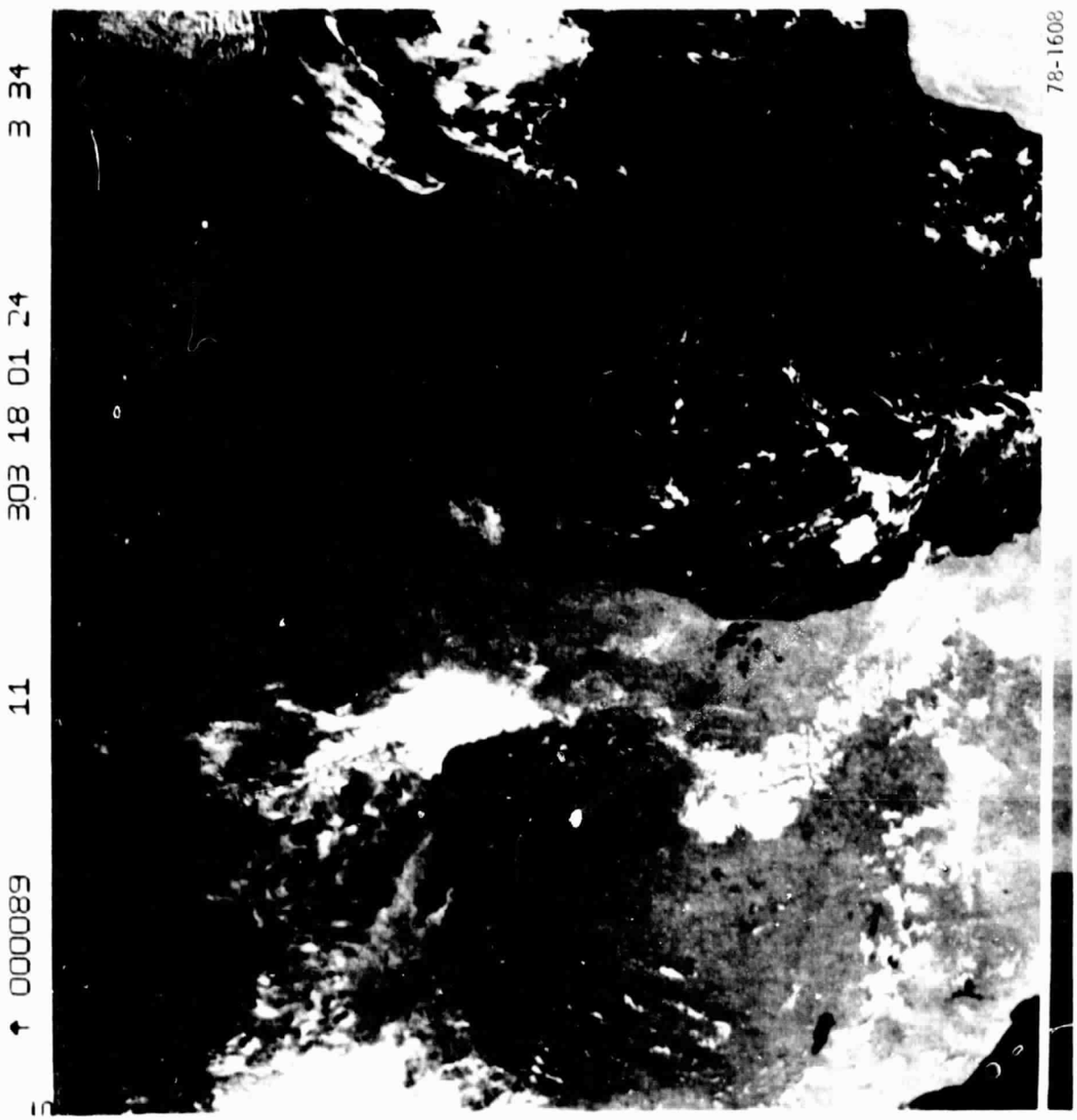

Fig. 3-2 (f) CHANNEL 5 DATA

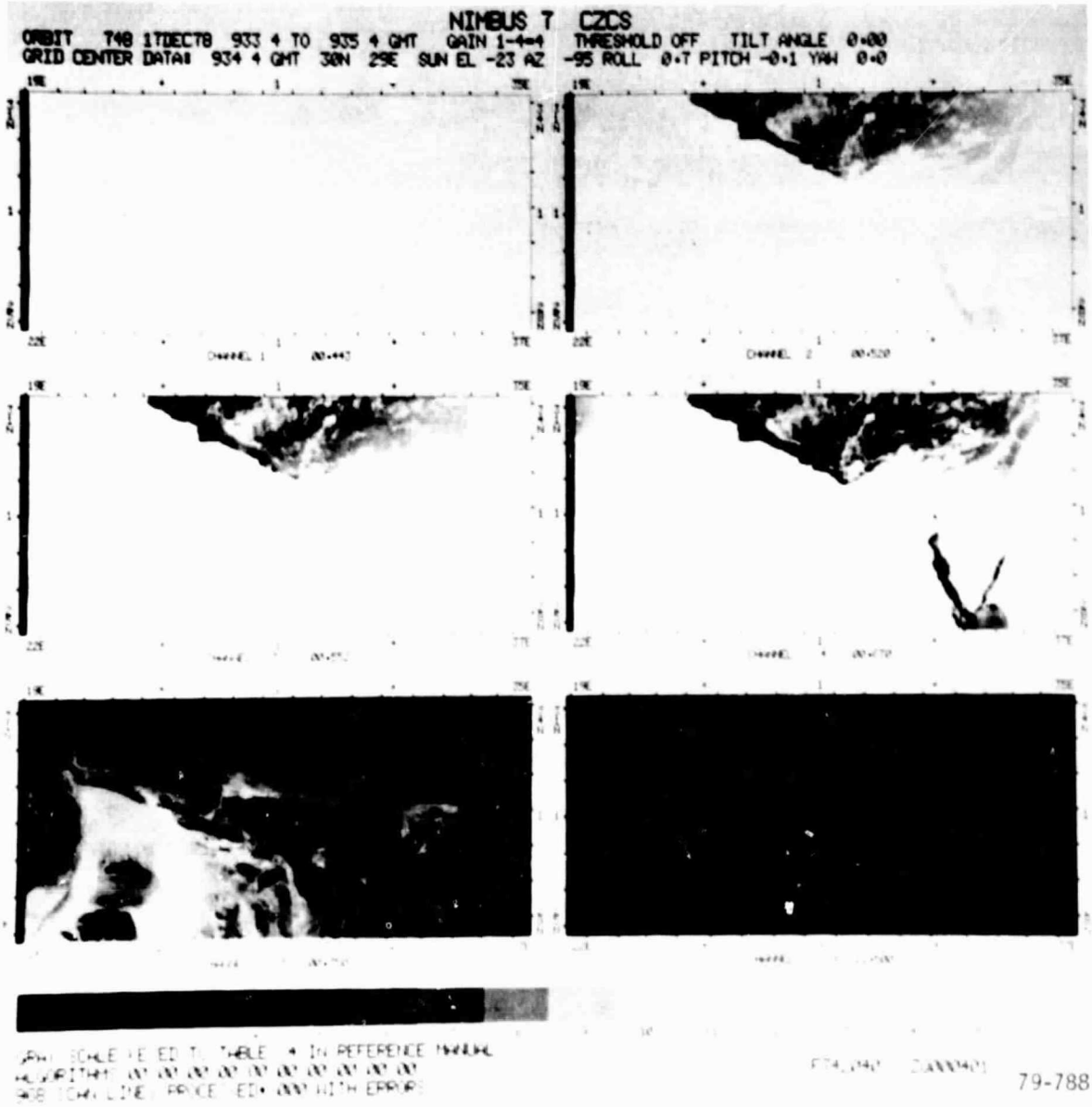

Fig. 3-3 (a) PORTION OF THE MEDITERRANEAN SEA AND NORTHERN AFRICA

79-793

Fig. 3-3 (b) CHANNEL 5 DATA

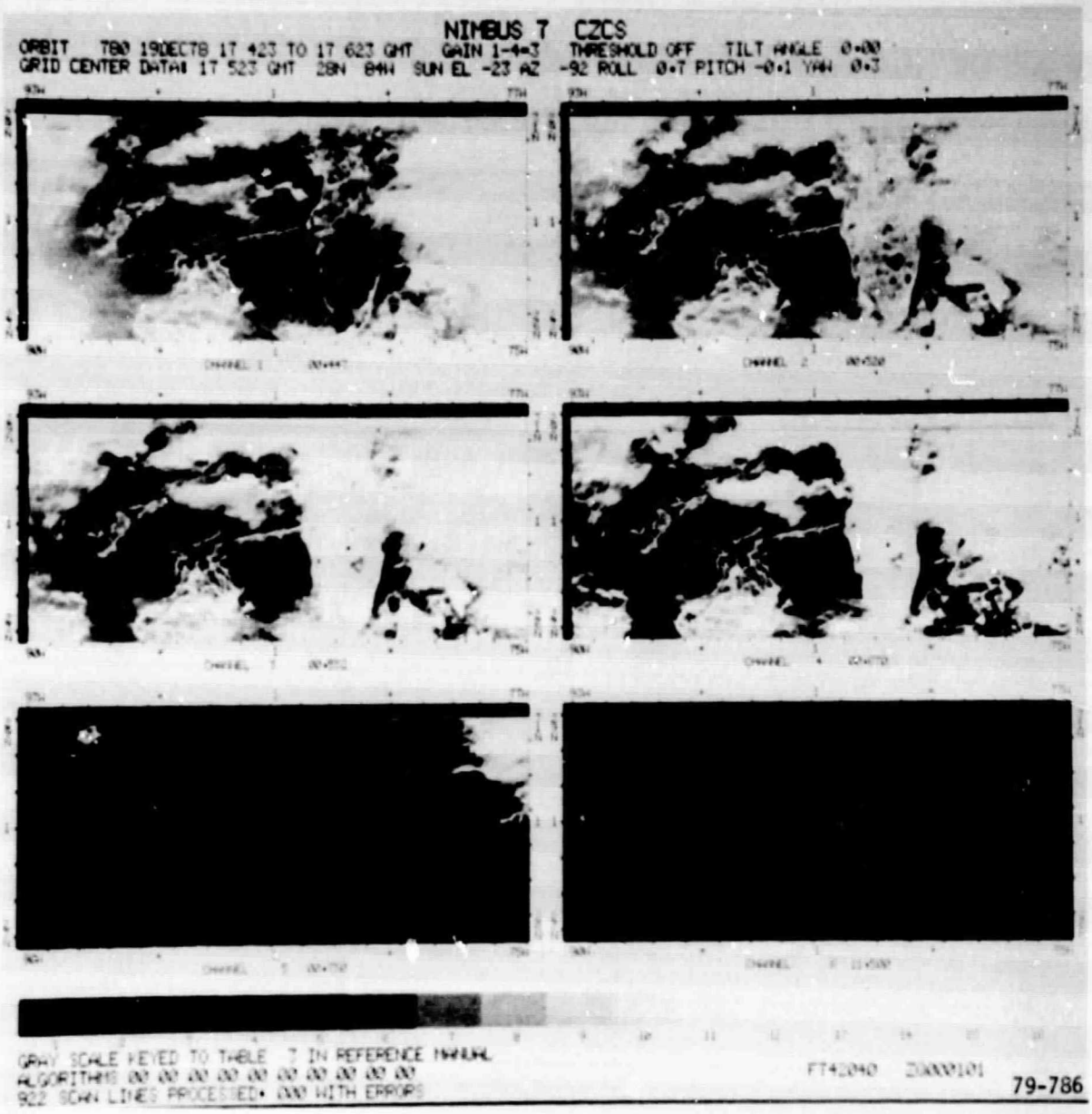

Fig. 3-4 (a) GULF COAST AND FLORIDA

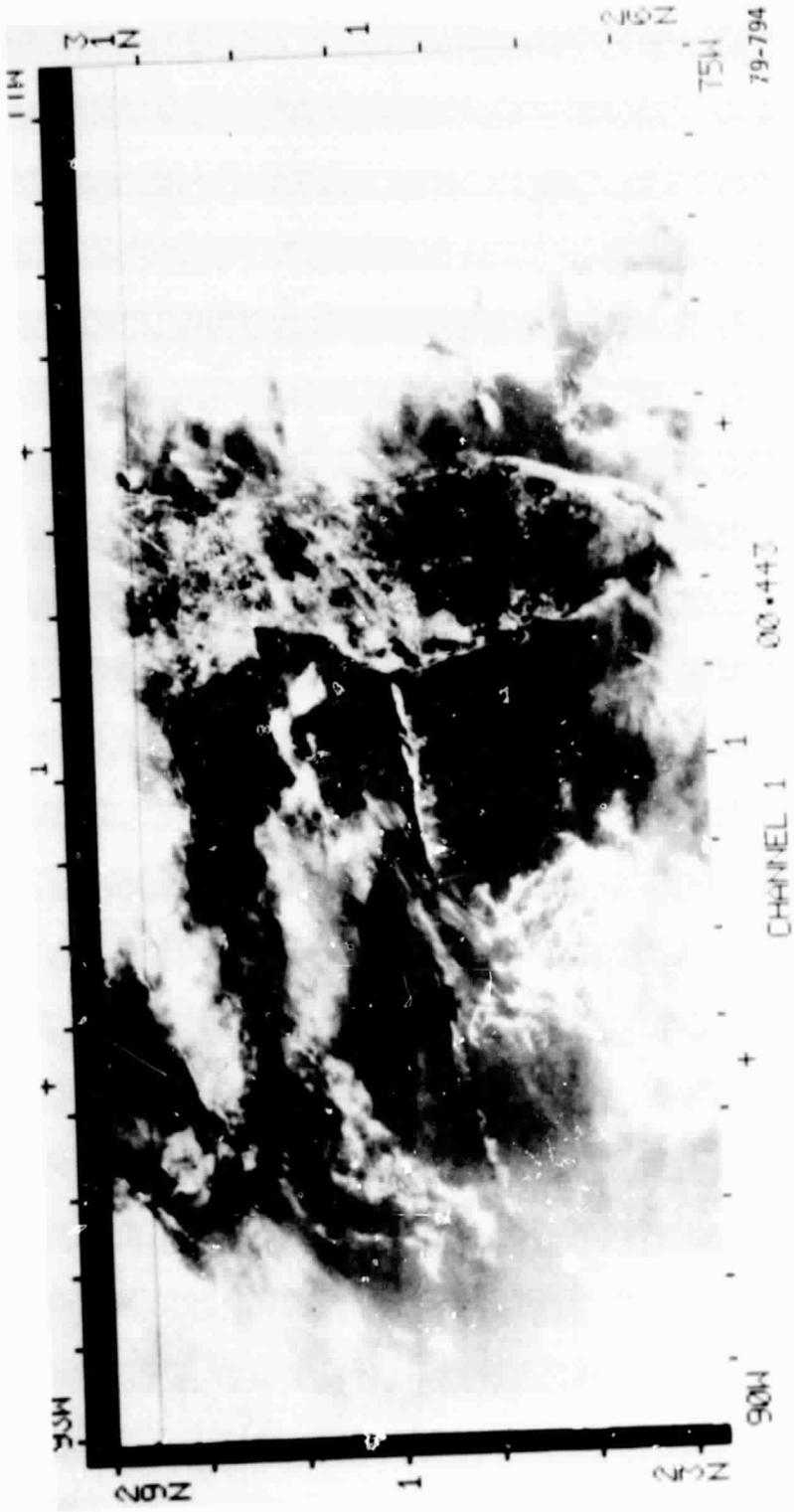

Fig. 3-4 (b) CHANNEL 1 DATA

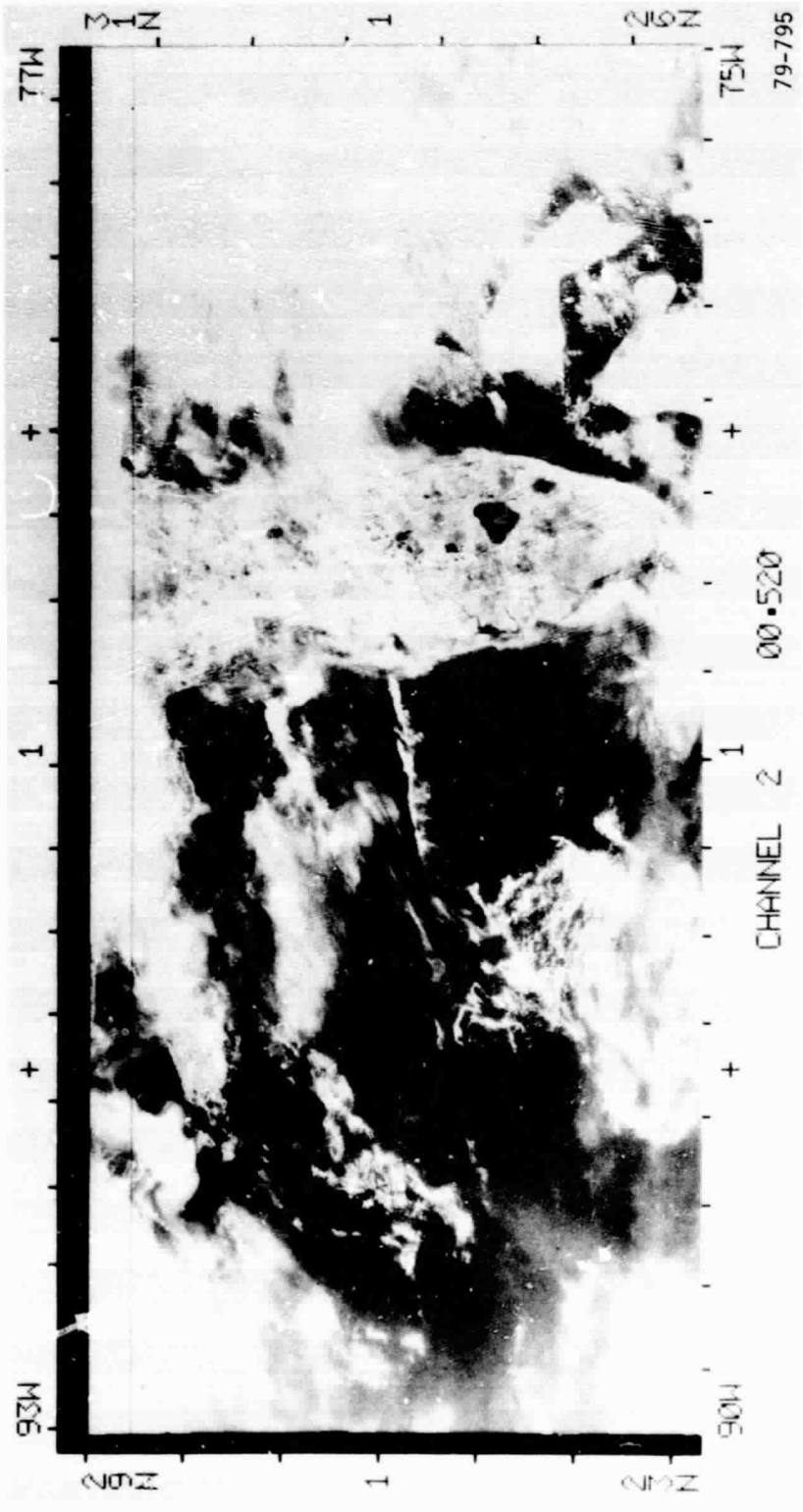

Fig. 3-4 (c) CHANNEL 2 DATA

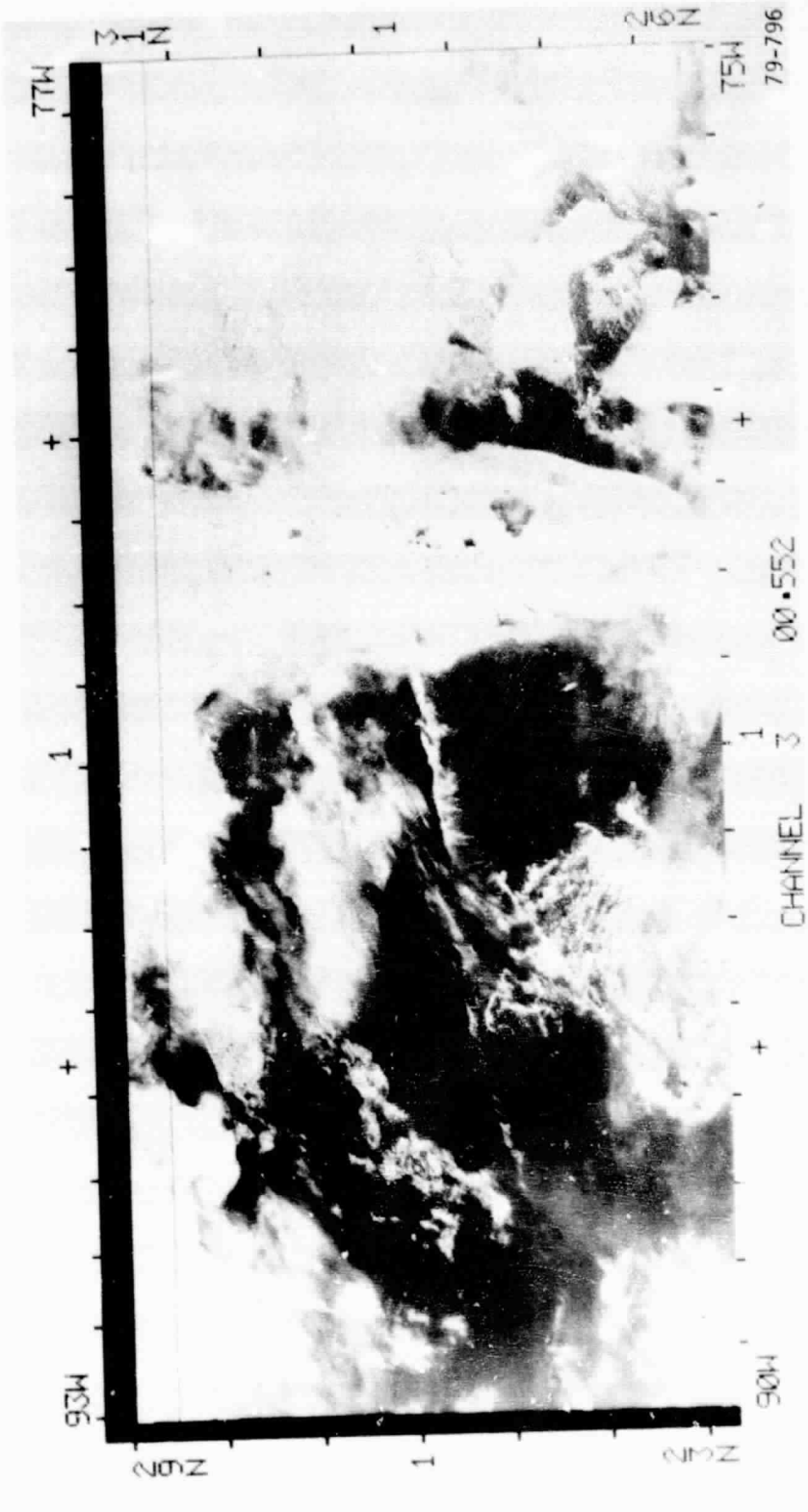

Fig. 3-4 (d) CHANNEL 3 DATA

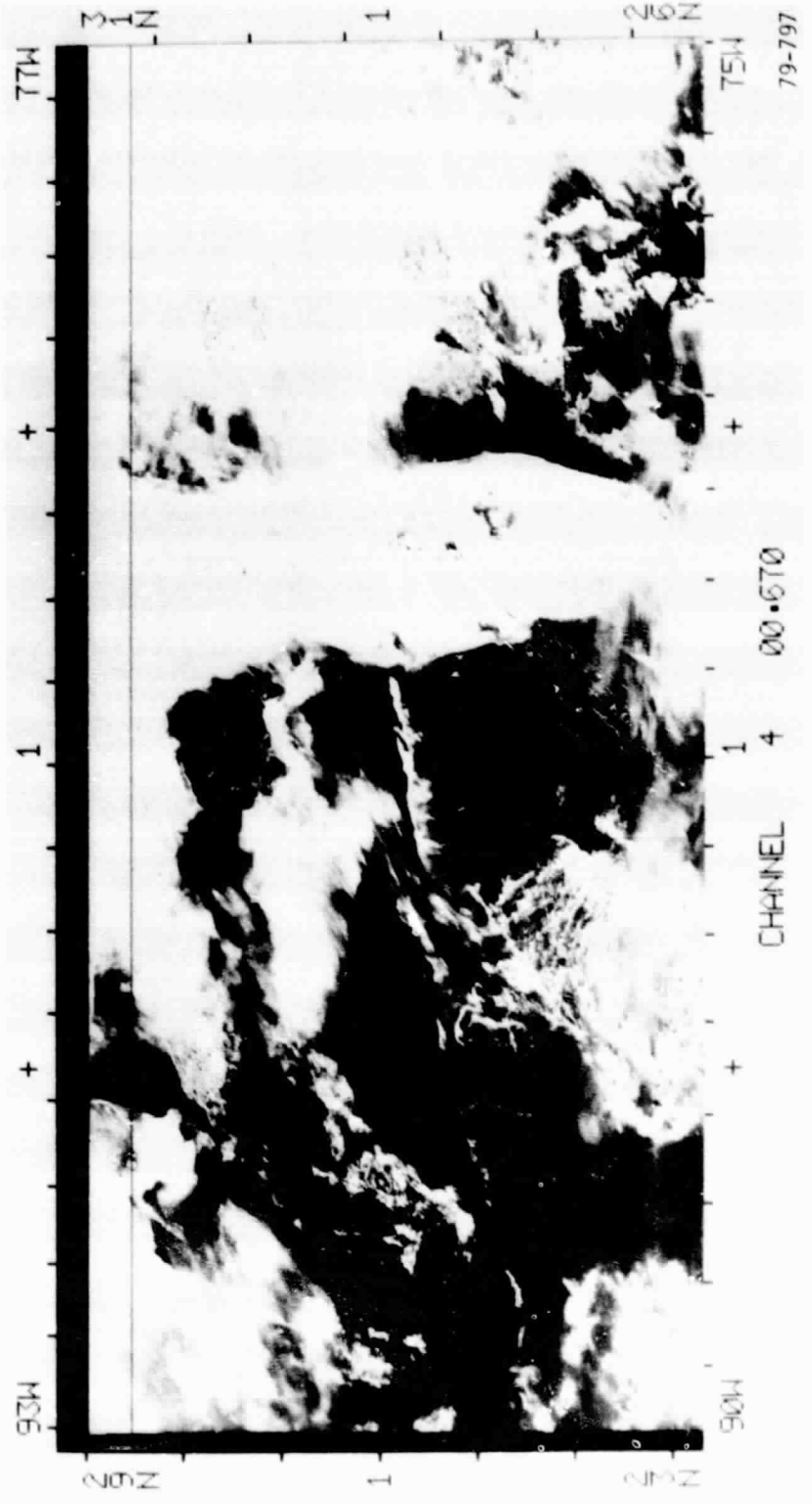

Fig. 3-4 (e) CHANNEL 3 DATA

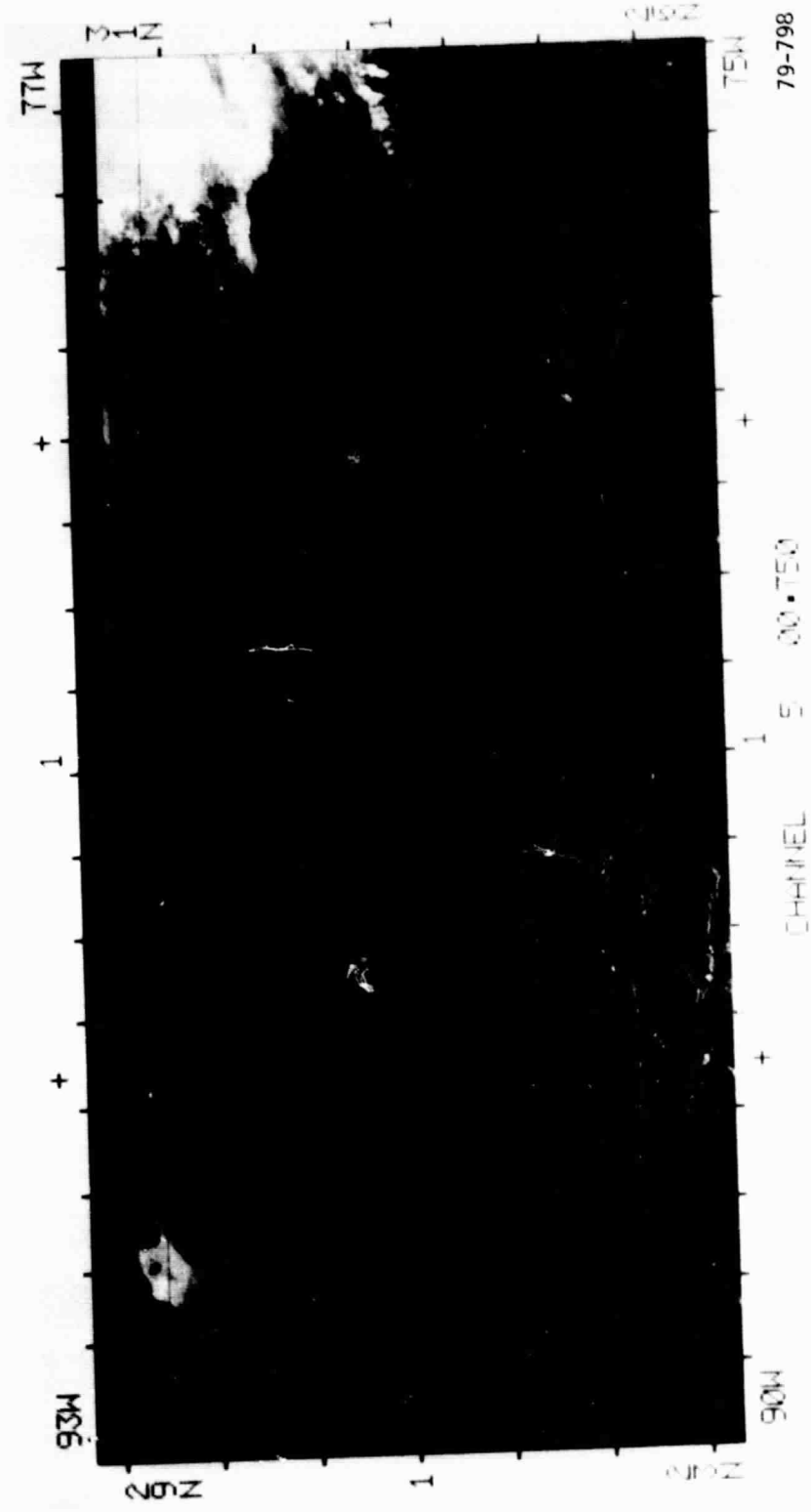

Fig. 3-4 (f) CHANNEL 5 DATA

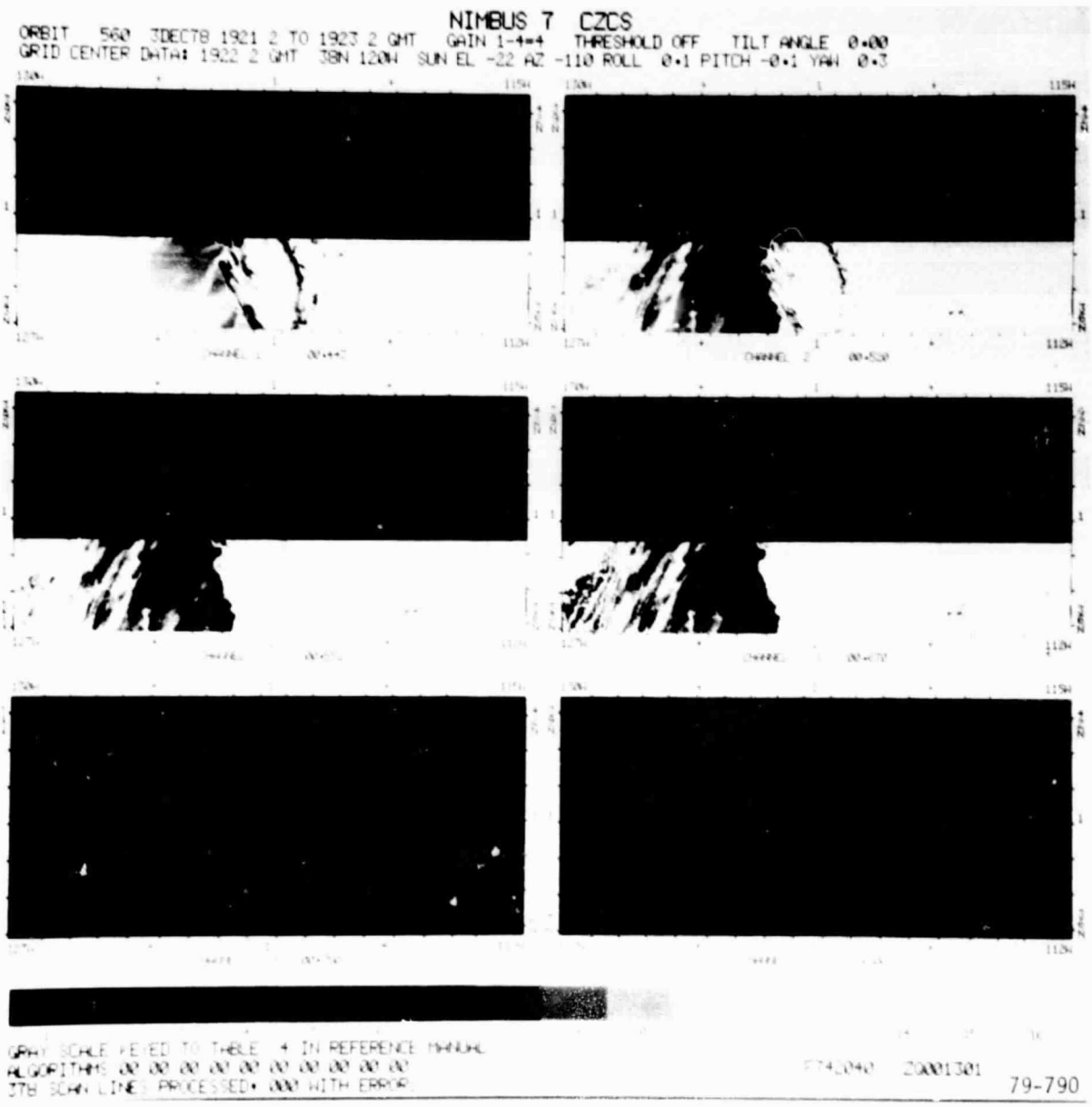

Fig. 3-5 (a) MONTEREY BAY AREA IN CALIFORNIA

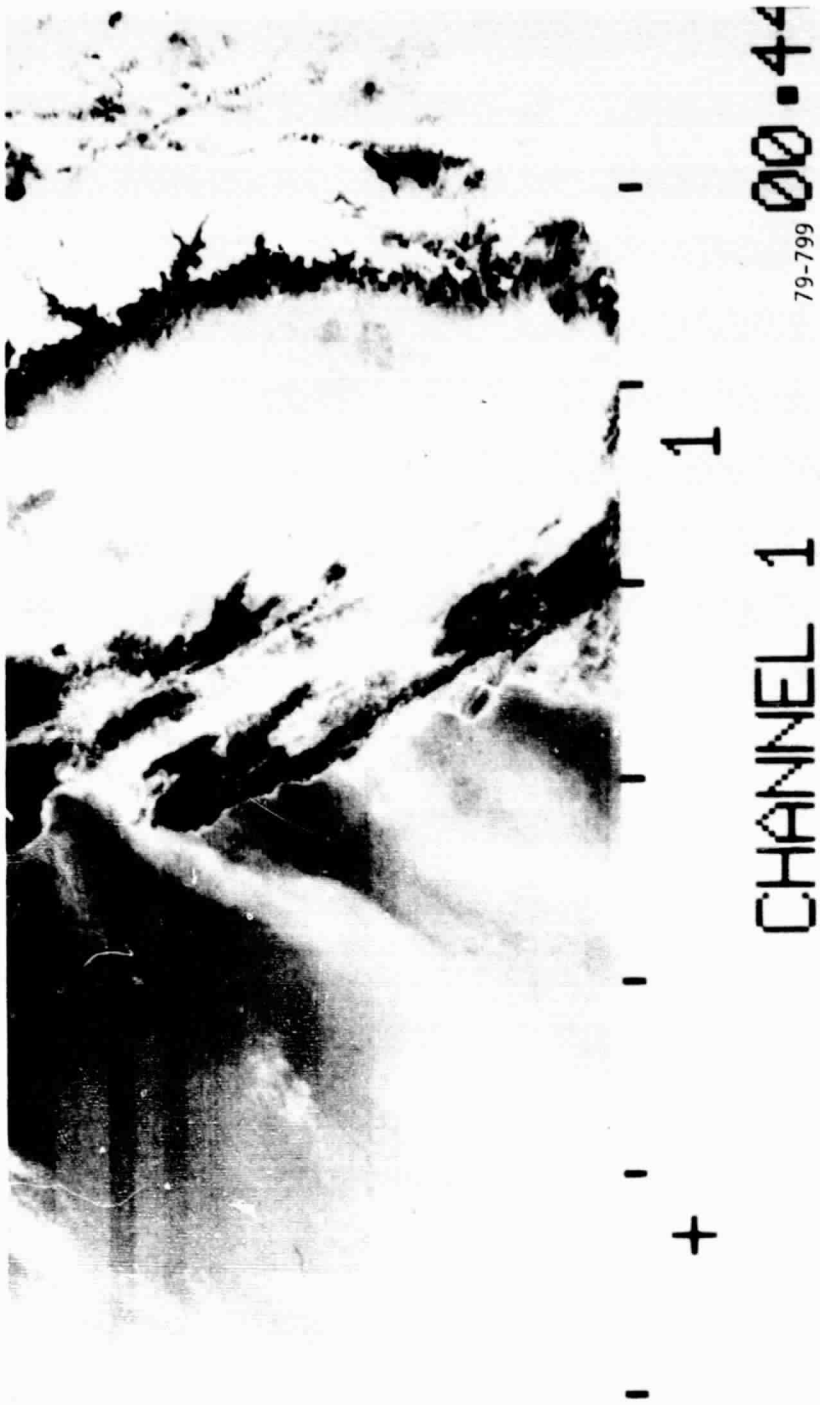

Fig. 3-5 (b) CHANNEL 1 DATA

Fig. 3-5 (c) CHANNEL 2 DATA

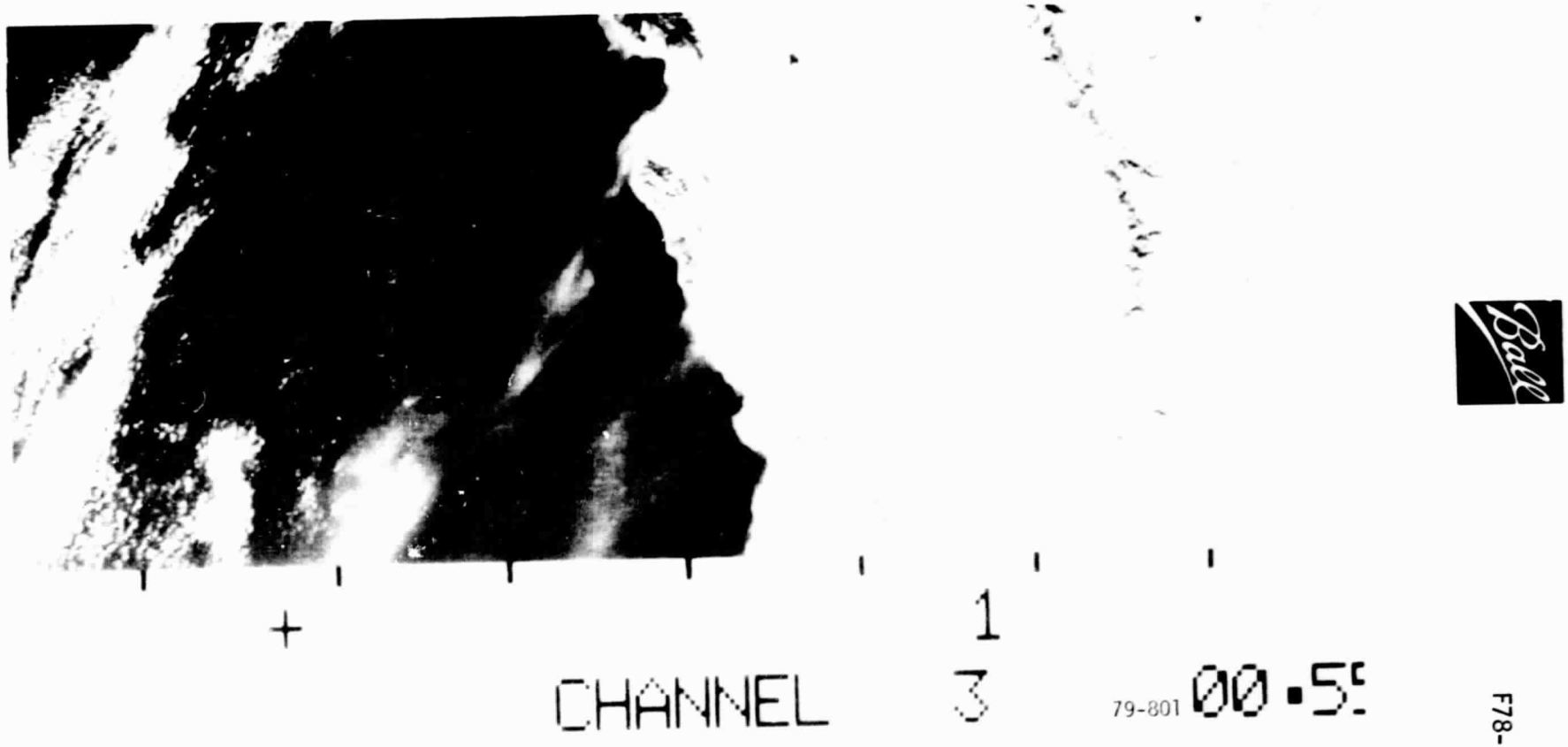

Fig. 3-5 (d) CHANNEL 3 DATA

Fig. 3-5 (e) CHANNEL 4 DATA

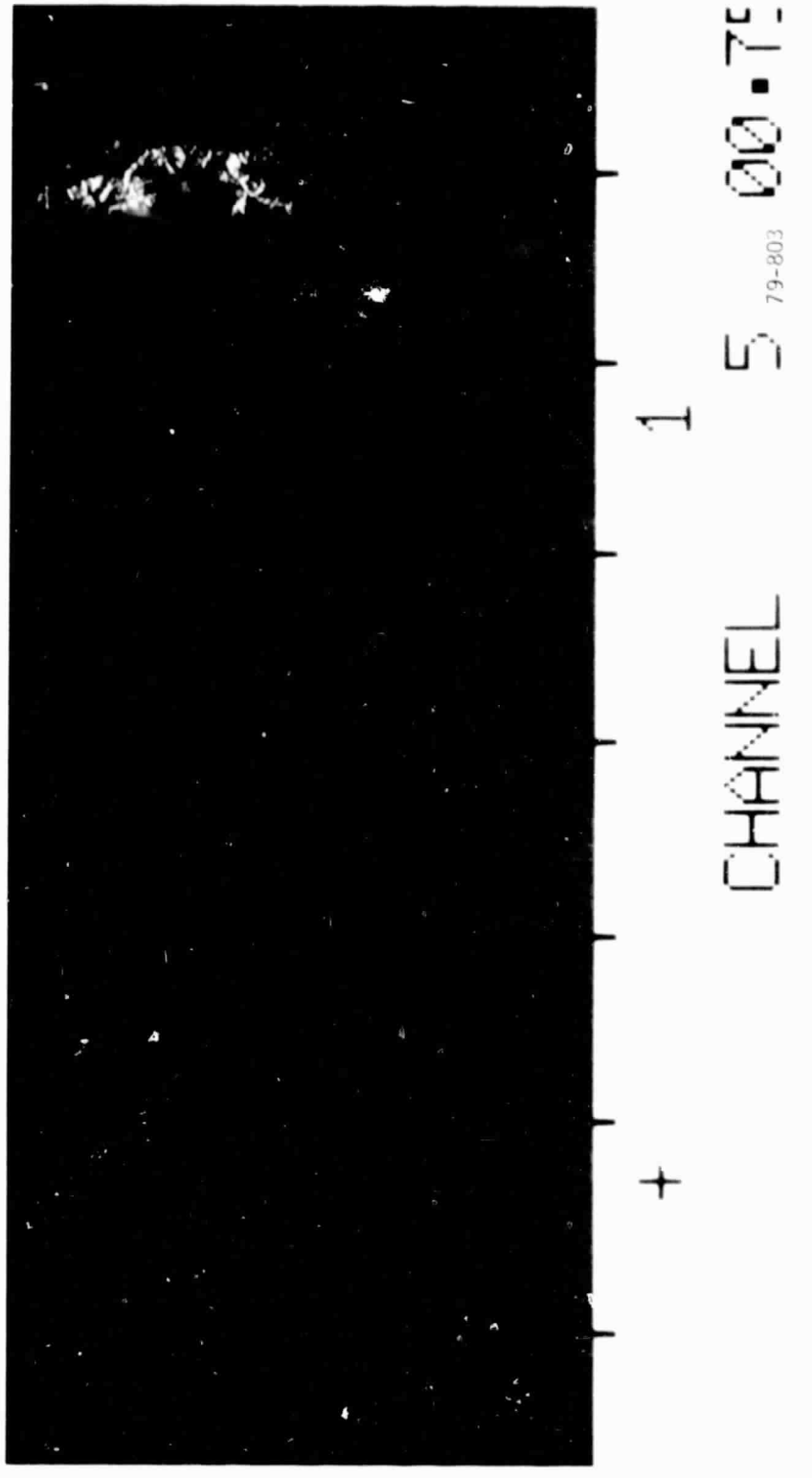

Fig. 3-5 (f) CHANNEL 5 DATA

3.2 HOUSEKEEPING DATA & TRENDS IN INSTRUMENT PERFORMANCE

In addition to the science data, some of the housekeeping data is of engineering interest. It is used to reaffirm design analysis and predict instrument lifetime. Some of this data is presented in the following paragraphs.

3.2.1 Radiative Cooler Performance

Twenty-one days after launch, the radiative cooler door was opened and the final post-launch decontamination sequence started prior to cooldown. The decontamination procedure called for the door heater to be turned on for 8 hours while the cooler outer stage heater was duty cycled to maintain its temperature warm but below the cooler mounting ring interface temperature. However it was soon noticed that the door temperature was at +70°C and rising rather than leveling off at 40-50°C as expected. Therefore it was decided to terminate the decontamination cycle and start the cooldown.

As Figure 3-6 shows, the inner stage or patch stabilized at 115.3K. This is below the controlled operating point of 120K but above the expected value of 100-112K based on the thermal/vacuum system test at General Electric. The outer stage temperature of 224.5K is also about 20 degrees higher than anticipated. The coupling coefficient between the inner stage and the outer stage,

$$\frac{\Delta T_{is}}{\Delta T_{os}},$$

is 0.24K/K. Therefore, if the outer stage temperature was 20 degrees low, the inner stage temperature would be approximately 110.5K.

It is difficult at this point to determine exactly why the cooler is running warmer than predicted. The more probable causes are 1) degraded surface finishes due to contaminants outgassed from the spacecraft and 2) view factors from the cooler radiating surfaces to the spacecraft and fiberglass thermal shields that are different than modeled. A complete decontamination sequence

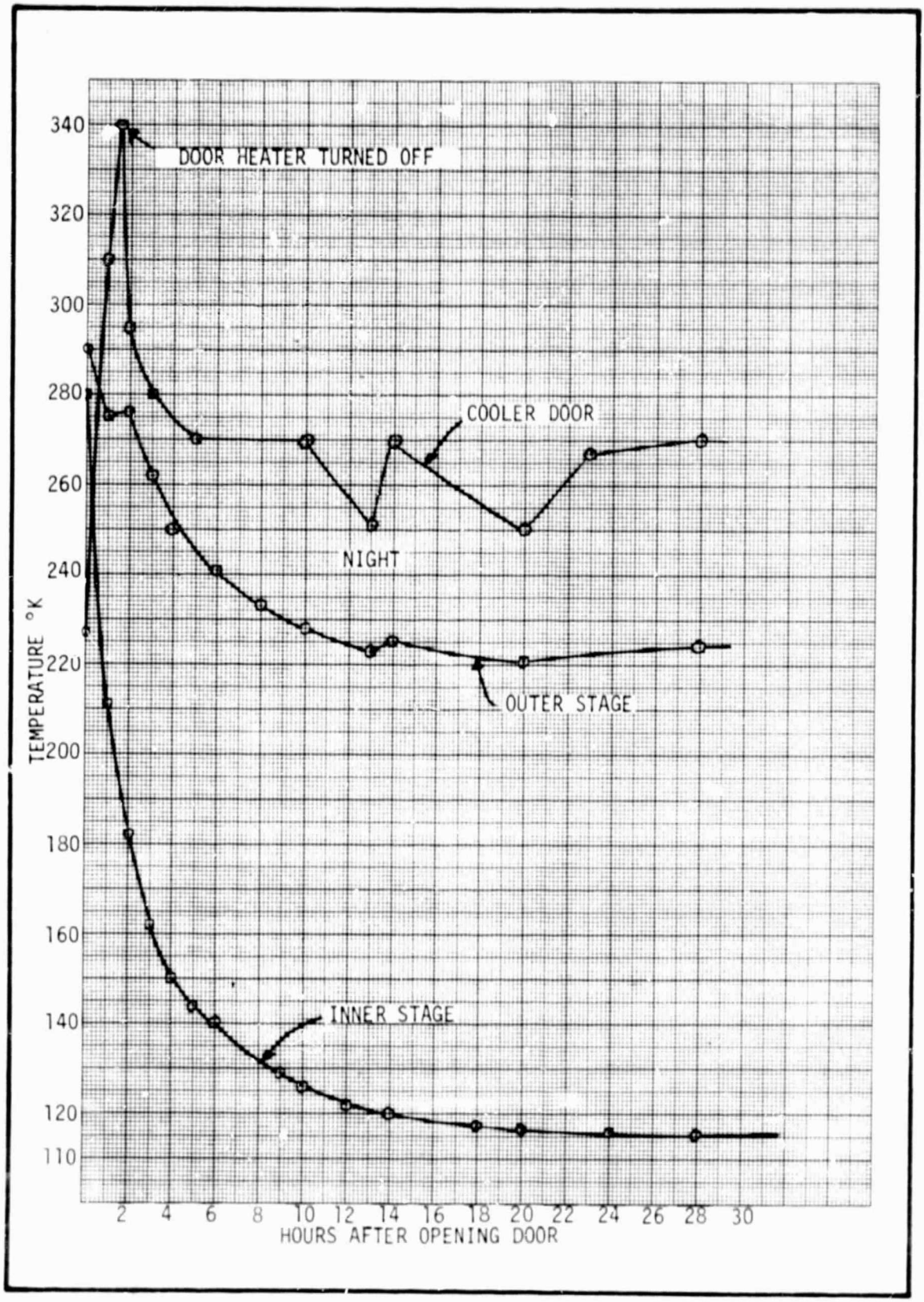

Figure 3-6 CZCS Radiative Cooler Performance After Opening the Door

was not performed since Channel 6 was performing normally, even though the temperature margin was less than desired. And there is general reluctance to warm the cooler/detector any more than necessary due to the detector anomaly discussed in Section 3.2.2.

3.2.2 Channel 6 (HgCdTe) Detector Impedance

While running tests during sensor integration onto the spacecraft, it was noticed that the resistance of the HgCdTe detector in Channel 6 was increasing slowly with time. The resistance changes from 24 ohms at 120K in April, 1976 to 34 ohms in December, 1977. This caused the DC restorer circuitry to reach its control limit and the Channel 6 electronics saturated.

Mr. Harold Goldburg, et.al., of Goddard Space Flight Center determined the phenomenon to be caused by an intermetallic growth taking place between the gold lead bond wire and the deposited Indium conductor on the HgCdTe chip into which the gold lead was wedge bonded. The intermetalic growth is apparently lifting the gold lead from the Indium conductor. It was concluded that most if not all of the electrical conduction was through the intermetalic and/or the platinum paste placed over the bond. This would account for the increase in detector resistance with no corresponding increase in responsivity.

It was further concluded that the growth could be encouraged by modest heat - perhaps 50 to 100°C. Therefore, two procedural changes were implemented after the DC restorer was re-biased to accommodate the new resistance and its dynamic range doubled. First, the Channel 6 electronics would be turned on, putting the bias current through the detector, only when the detector temperature was below 120K. This would minimize the chance of any microscopic localized heating in the area of the wire bond. Second, the cooler would undergo a complete decontamination cycle only when the cooler temperature rose above the 120K control point. This would minimize the opportunity for operator error causing detector overheating.

From February, 1978 when the DC restorer was readjusted until launch, the detector resistance increased about 0.5 ohms. From launch in October, 1978

until April, 1979, the resistance increased another 1.44 ohms. This rate of change is relatively slow compared to the rate prior to observing the problem, as illustrated in the resistance history plot in Figure 3-7. At the present rate of change, the total resistance will not reach 63 ohms and saturate the DC restorer for another seven to nine years (late 1980's).

3.2.3 Scan Mirror Drive Mechanism

In order to get any science data from the CZCS, the scan mirror and its momentum compensator must both operate properly. And as expected their performance since launch has been flawless. The scan motor and momentum compensation currents are monitored via telemetry as any significant increase in these currents could indicate bearing and/or lubrication problems. Since launch there has been no change in these currents and in fact they have been 10 to 20 percent lower than during thermal/vacuum tests. The phase detector error signal from the scanner phase locked loop electronics, another indicator of scan mechanism changes, also has not changes since launch.

3.2.4 CZCS Instrument Temperature

There are numerous temperature sensors located on different subassemblies in the instrument. All orbital temperatures have been nominal with minor deviations from orbit to orbit. Table 3-2 summarizes some of the temperature data taken during the daytime part of the orbit.

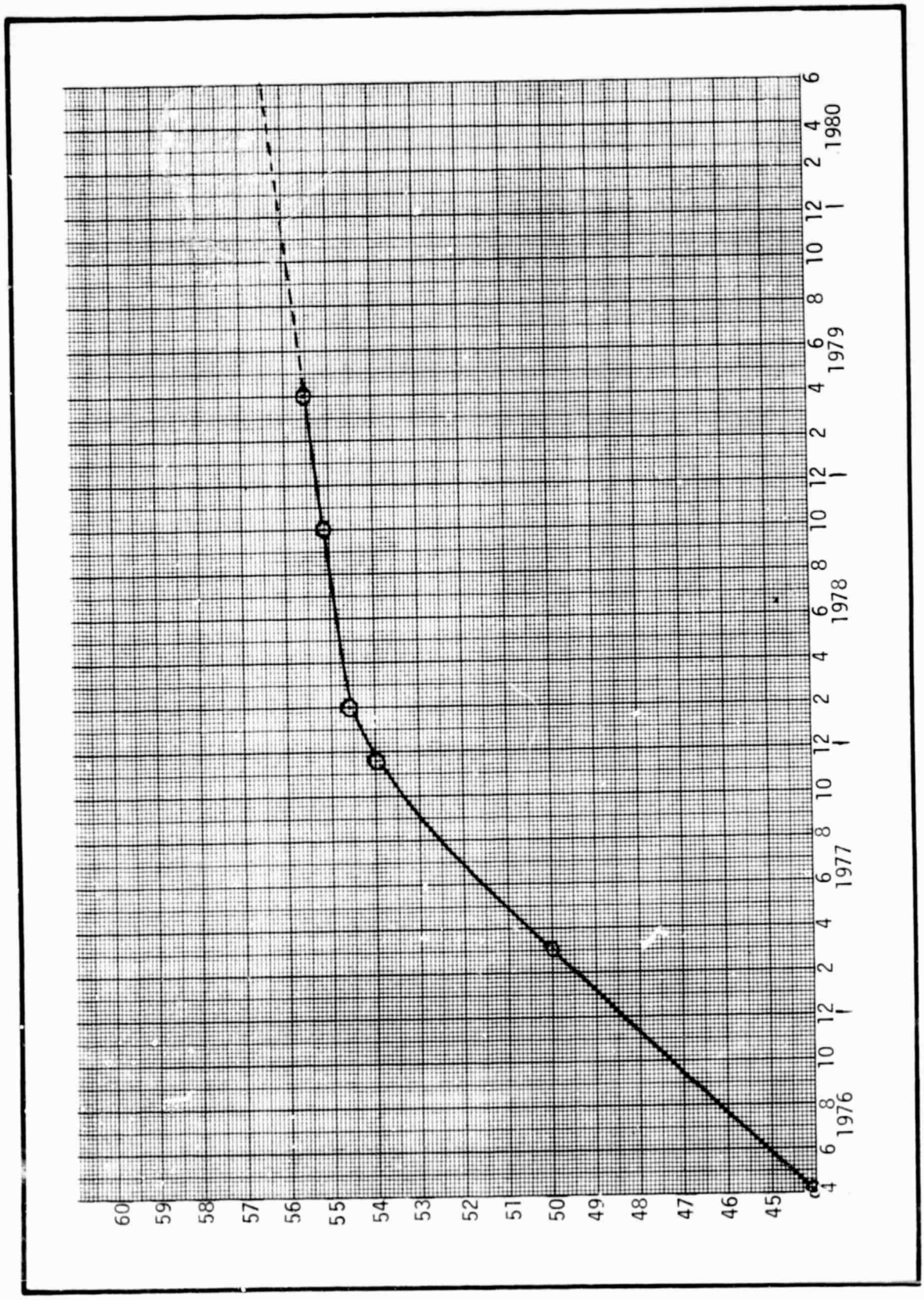

Figure 3-7 CZCS Hg CdTe Detector Resistance Measured at 120K and Including Cooler Wiring

C-2

Table 3-2

CZCS Orbital Temperatures

Temperature Monitor Point	Nominal °C	Range, °C
Baseplate	18.5	17.5 - 20.0
Radiative Cooler Interface	16.5	15.0 - 19.0
Telescope	17.5	16.3 - 19.2
Blackbody Target	18.0	16.4 - 19.6
Spectrometer	17.0	15.5 - 18.9
Main Electronics	30.0	24.0 - 39.8
Analog Electronics	21.0	19.6 - 24.0
Scan Motor	17.0	14.4 - 19.5
Momentum Compensator Motor	15.0	13.5 - 16.4